



## CLOSED-FORM EXPRESSION FOR GROUND RETURN ADMITTANCE AND ASSESSMENT OF SOIL MODELING IN UNDERGROUND CABLE SYSTEMS

João Pedro Lopes Salvador

Tese de Doutorado apresentada ao Programa de Pós-graduação em Engenharia Elétrica, COPPE, da Universidade Federal do Rio de Janeiro, como parte dos requisitos necessários à obtenção do título de Doutor em Engenharia Elétrica.

Orientador: Antonio Carlos Siqueira de Lima

Rio de Janeiro  
Julho de 2019

CLOSED-FORM EXPRESSION FOR GROUND RETURN ADMITTANCE AND  
ASSESSMENT OF SOIL MODELING IN UNDERGROUND CABLE SYSTEMS

João Pedro Lopes Salvador

TESE SUBMETIDA AO CORPO DOCENTE DO INSTITUTO ALBERTO LUIZ  
COIMBRA DE PÓS-GRADUAÇÃO E PESQUISA DE ENGENHARIA (COPPE)  
DA UNIVERSIDADE FEDERAL DO RIO DE JANEIRO COMO PARTE DOS  
REQUISITOS NECESSÁRIOS PARA A OBTENÇÃO DO GRAU DE DOUTOR  
EM CIÊNCIAS EM ENGENHARIA ELÉTRICA.

Examinada por:

---

Prof. Antonio Carlos Siqueira de Lima, D.Sc.

---

Prof. Robson Francisco da Silva Dias, D.Sc.

---

Prof. Alberto Resende De Conti, D.Sc.

---

Prof. Marco Aurélio de Oliveira Schroeder, D.Sc.

---

Prof. Rafael Silva Alípio, D.Sc.

RIO DE JANEIRO, RJ – BRASIL  
JULHO DE 2019

Salvador, João Pedro Lopes

Closed-Form Expression for Ground Return Admittance and Assessment of Soil Modeling in Underground Cable Systems/João Pedro Lopes Salvador. – Rio de Janeiro: UFRJ/COPPE, 2019.

XIX, 100 p.: il.; 29,7 cm.

Orientador: Antonio Carlos Siqueira de Lima

Tese (doutorado) – UFRJ/COPPE/Programa de Engenharia Elétrica, 2019.

Referências Bibliográficas: p. 75 – 81.

1. Closed-Form Solutions. 2. Rational Modeling. 3. Sensitivity Analysis. 4. Soil Parameters. 5. Transient Behavior. 6. Underground Cable Systems. I. Lima, Antonio Carlos Siqueira de. II. Universidade Federal do Rio de Janeiro, COPPE, Programa de Engenharia Elétrica. III. Título.

*Para Thaís e Joana.*

# Agradecimentos

Embora a Tese de Doutorado seja um trabalho muitas vezes solitário, o suporte que recebi ao longo dos anos de desenvolvimento desta pesquisa foi de valor incalculável. Neste primeiro contato direto com o leitor, gostaria de destacar alguns agradecimentos.

A Deus por tornar tudo isso possível. À minha esposa Thaís e à minha filha Joana por estarem ao meu lado em todos os momentos, ainda que muitas vezes minha presença não tenha sido integral. A toda minha família, em especial meus pais Pedro Paulo e Elaine, meu irmão Luiz Gustavo, minha cunhada Bianca e minha sobrinha Manuela, meus sogros Carlos Alberto e Simone e minha cunhada Nathália, por todo o suporte e confiança ao longo desta fase que por vezes pareceu interminável. A todos os amigos de fora do mundo acadêmico por todo encorajamento, amizade e alegria.

Ao amigo e orientador Professor Antonio Carlos Siqueira de Lima não só pelo meu desenvolvimento acadêmico e profissional na última década, mas também por todo incentivo em buscar mais de um sonho simultaneamente. À Professora Maria Teresa Correia de Barros (IST, Portugal) e ao amigo Dr. Antônio Paulo Cardillo Magalhães pelas ideias, discussões e parceria durante o desenvolvimento desta Tese. Ao Professor Rafael Alípio (CEFET/MG) pela grande ajuda na compreensão dos modelos de solo e pela fundamental contribuição na elaboração dos modelos racionais de solos variantes na frequência, determinante para a conclusão da Tese. À amiga Tálita Valentini pelo aconselhamento.

À Universidade Federal do Rio de Janeiro e seus Professores por estes longos anos de aprendizado desde o início da Graduação, lá em 2007. Também aos amigos que fiz e contribuíram diretamente ao longo desta caminhada: Beatriz Coitia, Camilo Rosero, Felipe Camara, Flávio Martins, Gustavo Viana, Isabela Natal, Jardel Cunha, Leonardo Santos, Márcio Silva, Renan Fernandes, Thiago Gomes e aos colegas do LASPOT/COPPE/UFRJ.

A todos do *campus* Angra dos Reis do CEFET/RJ pela vivência e pelo suporte que têm sido imprescindíveis para meu desenvolvimento como docente e pesquisador. A Camila Fernandes, Cintia Carraro e Raphael Poubel (hoje no CEFET/MG), pela parceria desde a primeira hora do curso de Engenharia Elétrica e importantíssima

até hoje; Ezequiel da Silva pelo apoio, incentivo e organização fundamentais; José Rafael Lebre que já era uma referência para mim desde os tempos da Eletrotécnica no CEFET/RJ Maracanã, lá em 2004, e que hoje em dia tenho a satisfação de debater os mais diversos assuntos em altíssimo nível, sempre respeitando as diferenças de ideias e crenças; Carlos Henrique Oliveira pela experiência transmitida; e Alessandro Oliveira por ser quase um irmão desde o meu início no *campus*. A todos os colegas da sala 1D pela torcida e companheirismo.

Ao Conselho Nacional de Desenvolvimento Científico e Tecnológico (CNPq) pelo apoio financeiro.

Resumo da Tese apresentada à COPPE/UFRJ como parte dos requisitos necessários para a obtenção do grau de Doutor em Ciências (D.Sc.)

## EXPRESSÃO FECHADA PARA ADMITÂNCIA DE RETORNO E AVALIAÇÃO DA MODELAGEM DO SOLO EM SISTEMAS DE CABOS SUBTERRÂNEOS

João Pedro Lopes Salvador

Julho/2019

Orientador: Antonio Carlos Siqueira de Lima

Programa: Engenharia Elétrica

Com a evolução dos sistemas de potência, é crescente o aumento do interesse em sistemas de cabos subterrâneos para a transmissão de energia elétrica, principalmente devido ao aumento da densidade populacional nas cidades, ao aproveitamento de fontes renováveis de energia e à exploração de petróleo, apenas para dar alguns exemplos. Uma característica comum nesses sistemas é a dificuldade de inspeção e manutenção, o que aumenta a importância de estudos relacionados a simulações computacionais. Além disso, a diversidade de tipos de solos devido a condições ambientais, geológicas e variações climáticas traz incertezas aos parâmetros do solo, nomeadamente, à resistividade e à permissividade.

Esta pesquisa se propõe a estudar a influência desses parâmetros no comportamento transitório dos sistemas de cabos subterrâneos. É conveniente considerar a resistividade e a permissividade do solo como uma admitância que possui três possíveis definições: (a) um valor fixo de condutividade igual ao inverso de uma resistividade aparente, i.e., medida ou arbitrada; (b) uma combinação de valores fixos de condutividade e permissividade; e (c) tanto a condutividade quanto a permissividade são funções dependentes da frequência.

As principais contribuições desta Tese são: a representação de modelos de solo dependentes de frequência por funções racionais; uma expressão fechada para a admitância de retorno pelo solo computacionalmente eficiente; e a utilização dessas ferramentas para a avaliação dos efeitos associados à modelagem do solo no desempenho transitório dos sistemas de cabos subterrâneos. Para isso, são apresentados resultados referentes a análises de sensibilidade, comportamento dos modos de propagação e sobretensões devido a diferentes esquemas de energização.

Abstract of Thesis presented to COPPE/UFRJ as a partial fulfillment of the requirements for the degree of Doctor of Science (D.Sc.)

## CLOSED-FORM EXPRESSION FOR GROUND RETURN ADMITTANCE AND ASSESSMENT OF SOIL MODELING IN UNDERGROUND CABLE SYSTEMS

João Pedro Lopes Salvador

July/2019

Advisor: Antonio Carlos Siqueira de Lima

Department: Electrical Engineering

As power systems evolve, there is a new interest for underground cable systems due to the increase of densely populated cities, the harnessing of renewable energy sources and oil and gas exploitation, just to give a few examples. A common characteristic of these systems lies on the inspection and maintenance difficulty, which increases the importance of computational simulation studies. The diversity of soil types with different environmental, geological and climate conditions bring uncertainties to soil parameters, namely, resistivity and permittivity.

This research proposes to study the influence of these parameters on transient behavior of underground cable systems. It is convenient to consider soil resistivity and permittivity as an immittance that has three possible definitions: (a) a fixed value of conductivity given by the inverse of an apparent resistivity, i.e., measured or chosen; (b) a combination of the fixed conductivity with a fixed value of permittivity; and (c) both conductivity and permittivity are treated as frequency-dependent functions.

The main contributions of this Thesis are: the representation of frequency-dependent soil models by rational functions; one closed-form expression for ground return admittance computationally efficient; and the combined usage of these tools to assess the soil models effects in underground cable systems transient performance. For that, results are presented regarding sensitivity analyses, propagation modes behavior and overvoltages due to different energization schemes.

# Contents

|  |            |
|--|------------|
| <b>List of Figures</b>   | <b>xi</b>  |
| <b>List of Tables</b>  | <b>xv</b>  |
| <b>List of Symbols</b>   | <b>xvi</b> |
| <b>List of Abbreviations</b>                                     | <b>xix</b> |
| <b>1 Introduction</b>  | <b>1</b>   |
| 1.1 Motivation . . . . .   | 2          |
| 1.2 Problem Description . . . . .                                | 3          |
| 1.3 Objectives . . . . .   | 4          |
| 1.4 Thesis Outline . . . . .                                     | 6          |
| 1.5 Published Research . . . . .                                 | 6          |
| <b>2 Soil Modeling</b>   | <b>8</b>   |
| 2.1 General Background . . . . .                                 | 8          |
| 2.2 Probabilistic Modeling . . . . .                             | 9          |
| 2.3 Soil Frequency Dependence . . . . .                          | 13         |
| 2.4 Rational Approximation of Soil Models . . . . .              | 19         |
| 2.5 Discussion . . . . .   | 24         |
| <b>3 Cable System Modeling</b>                                   | <b>27</b>  |
| 3.1 Assembly of Matrices $\mathbf{Z}$ and $\mathbf{Y}$ . . . . . | 28         |
| 3.2 Typical Cable Systems Configurations . . . . .               | 31         |
| 3.3 Voltage and Current Relations . . . . .                      | 33         |
| 3.4 Novel Expression for Ground Admittance . . . . .             | 34         |
| 3.5 Natural Modes of Propagation . . . . .                       | 40         |
| 3.6 Discussion . . . . .   | 44         |
| <b>4 Uncertainties Assessment</b>                                | <b>46</b>  |
| 4.1 Sensitivity Analysis . . . . .                               | 46         |
| 4.2 Test Cases . . . . .   | 61         |

|          |   |           |
|----------|---|-----------|
| 4.2.1    | Case 1 . . . . .  | 61        |
| 4.2.2    | Case 2 . . . . .  | 66        |
| 4.3      | Discussion . . . . .  | 71        |
| <b>5</b> | <b>Conclusions</b>  | <b>72</b> |
| 5.1      | Future Work . . . . .   | 74        |
|          | <b>References</b>   | <b>75</b> |
| <b>A</b> | <b>Review on Smith-Longmire and Alipio-Visacro Models</b>                 | <b>82</b> |
| A.1      | Smith-Longmire . . . . .  | 82        |
| A.2      | Alipio-Visacro . . . . .  | 84        |
| <b>B</b> | <b>Further Expressions for Z and Y</b>                                    | <b>86</b> |
| B.1      | Impedances per-unit-length . . . . .                                      | 86        |
| B.2      | Admittance per-unit-length . . . . .                                      | 88        |
| <b>C</b> | <b>Additional Graphics: Sensitivity of Ground Return Series Impedance</b> | <b>89</b> |
| <b>D</b> | <b>Additional Graphics: Sensitivity of Ground Return Shunt Impedance</b>  | <b>95</b> |

# List of Figures

|      |  |    |
|------|--|----|
| 1.1  | Research even tree. . . . .  | 5  |
| 2.1  | Normalized $P_\rho(\rho)$ obtained from actual measurements in [23]. . . . .   | 11 |
| 2.2  | Normalized PDFs for pipe-type cable ground return impedance and admittance. . . . .  | 12 |
| 2.3  | Variations of $\sigma$ and $\omega\varepsilon$ with frequency for different soil models. . . . .   | 18 |
| 2.4  | Comparison of absolute values of $\kappa$ regarding different soil models. . . . .   | 19 |
| 2.5  | Rational Approximation of Smith-Longmire model. . . . .  | 21 |
| 2.6  | Rational Approximation of Alipio-Visacro model. . . . .  | 22 |
| 3.1  | Radii of SC-cable layers. . . . .  | 28 |
| 3.2  | Configurations of cables systems. . . . .  | 32 |
| 3.3  | Nodes considered for typical cable systems. . . . .  | 33 |
| 3.4  | Conductance and capacitance of cable system. . . . .   | 37 |
| 3.5  | Modal propagation function and characteristic admittance. . . . .  | 38 |
| 3.6  | Excitation schemes. . . . .  | 38 |
| 3.7  | Cross-bonding inter-sheath excitation scheme. . . . .  | 38 |
| 3.8  | Voltage at terminal 7 – excitation of intersheath mode. . . . .  | 39 |
| 3.9  | Voltage at terminal 7 – excitation of ground mode. . . . .   | 39 |
| 3.10 | Voltage at terminal 31 – cross-bonded cable system. . . . .  | 40 |
| 3.11 | Comparison of modes attenuation and velocity regarding frequency dependence. $\kappa_1 = \sigma_0 = 1/\rho_0$ , $\kappa_2 = \sigma_0 + j\omega\varepsilon_\infty$ , $\kappa_{3_{SL}}$ considers Smith-Longmire model, and $\kappa_{3_{AV}}$ considers Alipio-Visacro model. . . . .                    | 42 |
| 3.12 | Numerical issues related to modes propagation calculation above 1.6 MHz. $\kappa_1 = \sigma_0 = 1/\rho_0$ , $\kappa_2 = \sigma_0 + j\omega\varepsilon_\infty$ , $\kappa_{3_{SL}}$ considers Smith-Longmire model, and $\kappa_{3_{AV}}$ considers Alipio-Visacro model. . . . .                        | 43 |
| 3.13 | Modes propagation between 1 MHz and 10 MHz. Series expansion approach of Bessel functions [69]. $\kappa_1 = \sigma_0 = 1/\rho_0$ , $\kappa_2 = \sigma_0 + j\omega\varepsilon_\infty$ , $\kappa_{3_{SL}}$ considers Smith-Longmire model, and $\kappa_{3_{AV}}$ considers Alipio-Visacro model. . . . . | 44 |

|      |  |    |
|------|--|----|
| 4.1  | Sensitivities of series impedance for pipe-type cable configuration. Figures (a): $\kappa = \sigma_0 = 1/\rho_0$ ; (b): $\kappa = \sigma_0 + j\omega\varepsilon_r\varepsilon_0$ ; (c): Smith-Longmire; and (d): Alipio-Visacro. . . . .                                      | 51 |
| 4.2  | Sensitivities of series impedance for flat horizontal configuration. Figures (a)–(c): $\kappa = \sigma_0 = 1/\rho_0$ ; (d)–(f): $\kappa = \sigma_0 + j\omega\varepsilon_r\varepsilon_0$ ; (g)–(i): Smith-Longmire; and (j)–(l): Alipio-Visacro. . . . .                      | 52 |
| 4.3  | Sensitivities of series impedance for trefoil configuration. Figures (a)–(c): $\kappa = \sigma_0 = 1/\rho_0$ ; (d)–(f): $\kappa = \sigma_0 + j\omega\varepsilon_r\varepsilon_0$ ; (g)–(i): Smith-Longmire; and (j)–(l): Alipio-Visacro. . . . .                              | 53 |
| 4.4  | Sensitivities of series self impedance for flat vertical configuration. Figures (a)–(c): $\kappa = \sigma_0 = 1/\rho_0$ ; (d)–(f): $\kappa = \sigma_0 + j\omega\varepsilon_r\varepsilon_0$ ; (g)–(i): Smith-Longmire; and (j)–(l): Alipio-Visacro. . . . .                   | 54 |
| 4.5  | Sensitivities of series mutual impedance for flat vertical configuration. Figures (a) and (b): $\kappa = \sigma_0 = 1/\rho_0$ ; (c) and (d): $\kappa = \sigma_0 + j\omega\varepsilon_r\varepsilon_0$ ; (e) and (f): Smith-Longmire; and (g) and (h): Alipio-Visacro. . . . . | 55 |
| 4.6  | Sensitivities of shunt impedance for pipe-type cable configuration. Figures (a): $\kappa = \sigma_0 = 1/\rho_0$ ; (b): $\kappa = \sigma_0 + j\omega\varepsilon_r\varepsilon_0$ ; (c): Smith-Longmire; and (d): Alipio-Visacro. . . . .                                       | 56 |
| 4.7  | Sensitivities of shunt impedance for flat horizontal configuration. Figures (a)–(c): $\kappa = \sigma_0 = 1/\rho_0$ ; (d)–(f): $\kappa = \sigma_0 + j\omega\varepsilon_r\varepsilon_0$ ; (g)–(i): Smith-Longmire; and (j)–(l): Alipio-Visacro. . . . .                       | 57 |
| 4.8  | Sensitivities of shunt impedance for trefoil configuration. Figures (a)–(c): $\kappa = \sigma_0 = 1/\rho_0$ ; (d)–(f): $\kappa = \sigma_0 + j\omega\varepsilon_r\varepsilon_0$ ; (g)–(i): Smith-Longmire; and (j)–(l): Alipio-Visacro. . . . .                               | 58 |
| 4.9  | Sensitivities of shunt self impedance for flat vertical configuration. Figures (a)–(c): $\kappa = \sigma_0 = 1/\rho_0$ ; (d)–(f): $\kappa = \sigma_0 + j\omega\varepsilon_r\varepsilon_0$ ; (g)–(i): Smith-Longmire; and (j)–(l): Alipio-Visacro. . . . .                    | 59 |
| 4.10 | Sensitivities of shunt mutual impedance for flat vertical configuration. Figures (a) and (b): $\kappa = \sigma_0 = 1/\rho_0$ ; (c) and (d): $\kappa = \sigma_0 + j\omega\varepsilon_r\varepsilon_0$ ; (e) and (f): Smith-Longmire; and (g) and (h): Alipio-Visacro. . . . .  | 60 |
| 4.11 | Energization scheme of Case 1. . . . .   | 61 |
| 4.12 | Case 1 – soil resistivity $100 \Omega\cdot\text{m}$ . $\kappa_1 = \sigma_0 = 1/\rho_0$ , $\kappa_2 = \sigma_0 + j\omega\varepsilon_\infty$ , $\kappa_{SL}$ considers Smith-Longmire model, and $\kappa_{AV}$ considers Alipio-Visacro model. . . . .                         | 63 |
| 4.13 | Case 1 – soil resistivity $3000 \Omega\cdot\text{m}$ . $\kappa_1 = \sigma_0 = 1/\rho_0$ , $\kappa_2 = \sigma_0 + j\omega\varepsilon_\infty$ , $\kappa_{SL}$ considers Smith-Longmire model, and $\kappa_{AV}$ considers Alipio-Visacro model. . . . .                        | 64 |

|      |  |    |
|------|--|----|
| 4.14 | Case 1 – soil resistivity 120 k $\Omega$ ·m. $\kappa_1 = \sigma_0 = 1/\rho_0$ , $\kappa_2 = \sigma_0 + j\omega\varepsilon_\infty$ , $\kappa_{SL}$ considers Smith-Longmire model, and $\kappa_{AV}$ considers Alipio-Visacro model. . . . .                                  | 65 |
| 4.15 | Energization scheme of Case 2. . . . .   | 66 |
| 4.16 | Case 2 – soil resistivity 100 $\Omega$ ·m. $\kappa_1 = \sigma_0 = 1/\rho_0$ , $\kappa_2 = \sigma_0 + j\omega\varepsilon_\infty$ , $\kappa_{SL}$ considers Smith-Longmire model, and $\kappa_{AV}$ considers Alipio-Visacro model. . . . .                                    | 68 |
| 4.17 | Case 2 – soil resistivity 3000 $\Omega$ ·m. $\kappa_1 = \sigma_0 = 1/\rho_0$ , $\kappa_2 = \sigma_0 + j\omega\varepsilon_\infty$ , $\kappa_{SL}$ considers Smith-Longmire model, and $\kappa_{AV}$ considers Alipio-Visacro model. . . . .                                   | 69 |
| 4.18 | Case 2 – soil resistivity 120 k $\Omega$ ·m. $\kappa_1 = \sigma_0 = 1/\rho_0$ , $\kappa_2 = \sigma_0 + j\omega\varepsilon_\infty$ , $\kappa_{SL}$ considers Smith-Longmire model, and $\kappa_{AV}$ considers Alipio-Visacro model. . . . .                                  | 70 |
| C.1  | Sensitivities of series impedance for pipe-type cable configuration. Figures (a): $\kappa = \sigma_0 = 1/\rho_0$ ; (b): $\kappa = \sigma_0 + j\omega\varepsilon_r\varepsilon_0$ ; (c): Smith-Longmire; and (d): Alipio-Visacro. . . . .                                      | 90 |
| C.2  | Sensitivities of series impedance for flat horizontal configuration. Figures (a)–(c): $\kappa = \sigma_0 = 1/\rho_0$ ; (d)–(f): $\kappa = \sigma_0 + j\omega\varepsilon_r\varepsilon_0$ ; (g)–(i): Smith-Longmire; and (j)–(l): Alipio-Visacro. . . . .                      | 91 |
| C.3  | Sensitivities of series impedance for trefoil configuration. Figures (a)–(c): $\kappa = \sigma_0 = 1/\rho_0$ ; (d)–(f): $\kappa = \sigma_0 + j\omega\varepsilon_r\varepsilon_0$ ; (g)–(i): Smith-Longmire; and (j)–(l): Alipio-Visacro. . . . .                              | 92 |
| C.4  | Sensitivities of series self impedance for flat vertical configuration. Figures (a)–(c): $\kappa = \sigma_0 = 1/\rho_0$ ; (d)–(f): $\kappa = \sigma_0 + j\omega\varepsilon_r\varepsilon_0$ ; (g)–(i): Smith-Longmire; and (j)–(l): Alipio-Visacro. . . . .                   | 93 |
| C.5  | Sensitivities of series mutual impedance for flat vertical configuration. Figures (a) and (b): $\kappa = \sigma_0 = 1/\rho_0$ ; (c) and (d): $\kappa = \sigma_0 + j\omega\varepsilon_r\varepsilon_0$ ; (e) and (f): Smith-Longmire; and (g) and (h): Alipio-Visacro. . . . . | 94 |
| D.1  | Sensitivities of shunt impedance for pipe-type cable configuration. Figures (a): $\kappa = \sigma_0 = 1/\rho_0$ ; (b): $\kappa = \sigma_0 + j\omega\varepsilon_r\varepsilon_0$ ; (c): Smith-Longmire; and (d): Alipio-Visacro. . . . .                                       | 96 |
| D.2  | Sensitivities of shunt impedance for flat horizontal configuration. Figures (a)–(c): $\kappa = \sigma_0 = 1/\rho_0$ ; (d)–(f): $\kappa = \sigma_0 + j\omega\varepsilon_r\varepsilon_0$ ; (g)–(i): Smith-Longmire; and (j)–(l): Alipio-Visacro. . . . .                       | 97 |
| D.3  | Sensitivities of shunt impedance for trefoil configuration. Figures (a)–(c): $\kappa = \sigma_0 = 1/\rho_0$ ; (d)–(f): $\kappa = \sigma_0 + j\omega\varepsilon_r\varepsilon_0$ ; (g)–(i): Smith-Longmire; and (j)–(l): Alipio-Visacro. . . . .                               | 98 |

|     |   |     |
|-----|---|-----|
| D.4 | Sensitivities of shunt self impedance for flat vertical configuration.<br>Figures (a)–(c): $\kappa = \sigma_0 = 1/\rho_0$ ; (d)–(f): $\kappa = \sigma_0 + j\omega\varepsilon_r\varepsilon_0$ ; (g)–<br>(i): Smith-Longmire; and (j)–(l): Alipio-Visacro. . . . .                  | 99  |
| D.5 | Sensitivities of shunt mutual impedance for flat vertical configuration.<br>Figures (a) and (b): $\kappa = \sigma_0 = 1/\rho_0$ ; (c) and (d): $\kappa = \sigma_0 + j\omega\varepsilon_r\varepsilon_0$ ;<br>(e) and (f): Smith-Longmire; and (g) and (h): Alipio-Visacro. . . . . | 100 |

# List of Tables

|     |  |    |
|-----|--|----|
| 2.1 | Statistical Analysis of Soil Apparent Resistivity. Adapted from [23]. . .  | 10 |
| 2.2 | Example of Weibull Distribution data for identified soils. . . . .         | 10 |
| 2.3 | Rational model of Smith-Longmire Soil. . . . .                             | 23 |
| 2.4 | Rational model of Alipio-Visacro Soil. . . . .                             | 25 |
| 4.1 | Maximum voltage at terminal 11 for Case 1, in [pu]. . . . .                | 66 |
| 4.2 | Maximum overvoltage for Case 2, in [pu]. . . . .                           | 67 |
| A.1 | Coefficients for Smith-Longmire Model. . . . .                             | 83 |
| C.1 | Results for sensitivity analysis plotted against ground resistivity. . . . | 89 |
| D.1 | Results for sensitivity analysis plotted against ground resistivity. . . . | 95 |

# List of Symbols

|                         |   |
|-------------------------|---|
| $C$                     | Capacitance [F]   |
| $\vec{E}$               | Electric field vector in frequency domain [V/m]   |
| $f$                     | Frequency [Hz]  |
| $G$                     | Conductance [S]   |
| $h_i$                   | Depth in which cable $i$ is buried [m]  |
| $\mathbf{H}_c$          | Propagation function, voltage deformation matrix  |
| $\vec{H}$               | Magnetic field vector in frequency domain [A/m]   |
| $I_\nu(\cdot)$          | Bessel function $I$ of order $\nu$  |
| $j$                     | The imaginary number, $\sqrt{-1}$   |
| $\vec{J}$               | Current density [A/m <sup>2</sup> ]   |
| $K_\nu(\cdot)$          | Bessel function $K$ of order $\nu$  |
| $L$                     | Inductance [H]  |
| $P_A(B)$                | Probability of $A$ due to variable $B$  |
| $r$                     | Radius of a cable and its layers [m]  |
| $R$                     | Resistance [ $\Omega$ ]   |
| $\mathbf{T}_\mathbf{I}$ | Current eigenvectors; current transformation matrix                                       |
| $\mathbf{T}_\mathbf{V}$ | Voltage eigenvectors; voltage transformation matrix                                       |
| $x_{ij}$                | Horizontal distance between cables $i$ and $j$ [m]  |
| $Y_{ij}$                | Term of the $i$ -th row and $j$ -th column of the per-unit-length admittance matrix [S/m] |
| $Y_{si}$                | Self per-unit-length admittance of cable $i$ [S/m]  |

|                      |   |
|----------------------|---|
| $Y_{mij}$            | Mutual per-unit-length admittance between cables $i$ and $j$ [S/m]  |
| $\mathbf{Y}_C$       | Characteristic admittance matrix [S]  |
| $\mathbf{Y}_g$       | Ground return per-unit-length admittance matrix [S/m]   |
| $\mathbf{Y}_n$       | Nodal admittance matrix [S]   |
| $Z_{ij}$             | Term of the $i$ -th row and $j$ -th column of the per-unit-length impedance matrix [ $\Omega$ /m]   |
| $Z_{si}$             | Self per-unit-length impedance of cable $i$ [ $\Omega$ /m]  |
| $Z_{mij}$            | Mutual per-unit-length impedance between cables $i$ and $j$ [ $\Omega$ /m]  |
| $\mathbf{Z}_g$       | Ground return per-unit-length impedance matrix [ $\Omega$ /m]   |
| $\gamma_k$           | Propagation constant of medium $k$ , $\gamma = \sqrt{j\omega\mu_k(\sigma_k + j\omega\varepsilon_k)}$ [ $\text{m}^{-1}$ ]  |
| $\varepsilon$        | Permittivity [F/m]  |
| $\varepsilon_0$      | Free space permittivity, $8.854 \times 10^{-12}$ [F/m]  |
| $\varepsilon_r$      | Fixed relative permittivity   |
| $\varepsilon_\infty$ | Fixed permittivity: $\varepsilon_\infty = \varepsilon_r\varepsilon_0$   |
| $\kappa$             | Soil immittance. The generic relation between current density $\vec{J}$ and the electric field $\vec{E}$ : $(\vec{J} = \kappa\vec{E})$ [S/m]  |
| $\kappa_1$           | In this Thesis, $\kappa_1 = \sigma_0 = 1/\rho_0$ , which is $\kappa$ that considers only the conductive component of $\vec{J}$ , with $\rho_0$ and $\sigma_0$ the medium apparent resistivity and conductivity, respectively, i.e., a fixed value measured or arbitrarily chosen[S/m] |
| $\kappa_2$           | In this Thesis, $\kappa_2 = \sigma_0 + j\omega\varepsilon_r\varepsilon_0$ , which is $\kappa$ that considers both the conductive and displacement components of $\vec{J}$ , with $\sigma_0$ the same as before, $\varepsilon_0$ and $\varepsilon_r$ defined below [S/m]               |
| $\kappa_3$           | In this Thesis, $\kappa_3 = \sigma(\omega) + j\omega\varepsilon(\omega)$ , which is $\kappa$ that considers the frequency-dependence of $\sigma$ and $\varepsilon$ [S/m]  |
| $\kappa_{AV}$        | $\kappa_3$ considering Alipio-Visacro model [S/m]   |

|               |  |
|---------------|--|
| $\kappa_{SL}$ | $\kappa_3$ considering Smith-Longmire model [S/m]    |
| $\mu$         | Permeability [H/m]                                   |
| $\mu_0$       | Free space permeability, $4\pi \times 10^{-7}$ [H/m] |
| $\mu_r$       | Relative permeability                                |
| $\rho$        | Resistivity [ $\Omega \cdot m$ ]                     |
| $\rho_0$      | Soil's apparent resistivity [ $\Omega \cdot m$ ]     |
| $\sigma$      | Conductivity [S/m]                                   |
| $\sigma_0$    | Soil's apparent Conductivity [S/m]                   |
| $\omega$      | Angular frequency, $2\pi f$ [rad/s]                  |

# List of Abbreviations

|          |                                    |
|----------|------------------------------------|
| AV       | Alipio-Visacro (Soil Model)        |
| EMT      | Electromagnetic Transients         |
| EMTP     | Electromagnetic Transients Program |
| NLT      | Numerical Laplace Transform        |
| PDF      | Probability Density Function       |
| PT-cable | Pipe-type three-phase cable        |
| SC-cable | Single-core coaxial cable          |
| SL       | Smith-Longmire (Soil Model)        |
| TEM      | Transverse Electromagnetic         |
| VF       | Vector Fitting                     |

# Chapter 1

## Introduction

Power systems and specifically transmission lines are strongly affected by its surroundings, be it overhead or underground. One key factor is the soil, which represents a natural return path for the energy flowing on the lines. When steady-state or transient stability studies are considered the transmission modeling is quite simplified, considering mostly only lumped positive-sequence parameters of the electrical network, once the interest lies in the operation at industrial frequency and at frequencies that represent the electric machinery dynamics. Thus, the poor knowledge of soil parameters should not impact the results.

Nevertheless, when dealing with electromagnetic transients, frequency range may reach several kHz or even MHz scale and the modeling ought to represent as accurate as possible the parameters behavior so that simulation can minimize project errors. For that sort of studies, power cables are modeled with distributed parameters that take into account geometric configuration between conductors and also the soil interaction with the conductor parts, e.g., core and sheath.

Computation of electromagnetic transients on buried – underground or undersea – cables have been performed at different levels of numerical accuracy. In most transient studies, however, the soil is assumed as a homogeneous single layer and with constant, i.e., fixed and frequency independent, soil resistivity. However, its unknown dynamics might bring some impact to the behavior of the propagation of the traveling waves in conductors and offer to soil several uncertainties. The question is how much of this interference is noteworthy or can be neglected.

There is a large number of variables that may affect the soil characterization, such as monsoons, weather conditions, water flow in deeper soil layers, environmental issues in the surrounding area and other seasonal changes. Furthermore, there is a considerably large variety of soil types that transmission lines pass (over or through), e.g., a flooded or an extremely dry soil.

From a geological perspective, soils are described by several components, such as water saturation, porosity, size and shape of particles, thickness and composition of

minerals, to give some examples. As it gathers this much of information, the electric resistivity is an important parameter for analyzing soil behavior due to its interaction with fluids. As for the electrical studies and how it may affect the performance of systems, one may resort to multilayer configurations for the soil to try and simulate the behavior of its actual composition.

The bottleneck of this approach is that, since soil composition is so diverse and dependent on so many factors as mentioned, for some applications it may be impossible to precise how is the best way to establish the layers, i.e., all horizontal or all vertical or even a mixed configuration. In fact, there is a growing number of aspects that impact on soil behavior due to seasonal changes and weather conditions. The same soil may result in several different values of measured resistivity, when different boundary conditions are considered, which in turn leads to different statistical behavior of fairly close soils.

## 1.1 Motivation

In recent years there has been an increase of interest and usage of underground and undersea power cable systems applications, mostly due to the growing necessity of harnessing renewable energies offshore and onshore, and also for transmitting electricity under densely populated cities, modernization of power systems including smart grid solutions, and submarine oil and gas exploitation. Although it represents an improvement on system compactness and insulation, the fact that these systems are buried into something may lead to unfeasible maintenance situations. For that reason, one has to resort to reliable projects and case studies to understand the system behavior during operation as well as energization, switching and surge performances.

Considering the uncertainties mentioned, and in order to understand how the transients of underground power cable systems are influenced by soil, there exists a necessity of either developing a model able to evaluate the soil electromagnetic parameters – for each and every soil type and regarding barely infinite variables concerning environmental and terrain issues – or investigating how these unknown dynamics inflict the system behavior.

One way to carry this investigation is by applying artificial intelligence techniques, e.g., neural networks, to predict the soil influence. However, this would demand a brute-force search among an enormous set of previously calculated scenarios and with no effectiveness guaranteed, once these algorithms should be fed with some sort of rules and boundary conditions that are equally unknown. Therefore, even if such techniques are to be considered, some prior work has to be done in order to include important nuances in the analysis.

To overcome the almost unachievable task of measuring all the soil area, maintaining a soil parameter database updated and adjusted to weather modifications and so forth, and instead of considering one mathematical model that covers all soil composition variations, the investigation of the possible impacts of soil modeling on EMT studies is the main motivation of this work.

## 1.2 Problem Description

As soil characteristics are influenced by its uncertainties, to avoid the unfeasible task of modeling the external characteristics of almost infinite variables one possibility is to obtain the statistical behavior of the soil resistivity by measuring it under different conditions and then obtain a probabilistic modeling. In the following, such model obtained for the measured resistivity should provide information regarding the ground return quantities, i.e., a respective probabilistic model for the ground interaction. The disadvantage of this approach relies on the amount of measurements needed in order to obtain the statistical behavior robust enough. Therefore, other approaches need to be investigated in order to take into account how does the system perform due to soil parameter variations.

One typical assumption made is to consider only fixed soil apparent resistivity (or conductivity), i.e., the measurable value, although it is well-known as a frequency-dependent parameter [1]. This leads to other very common assumption that the ground return admittance might be neglected. However, as frequency increases it is also necessary to consider soil permittivity. The ground return admittance should thus be of interest and not only the ground return impedance. Furthermore, it is necessary to include soil frequency-dependence into ground return impedance and admittance matrices, once soil influence is sensed in the transmission system by means of these matrices. For that, it is proposed to represent the soil immittance  $\kappa = \sigma + j\omega\varepsilon$  as a rational function based on approximation of existing frequency-dependent soil models, as accepted for publication in [2].

However, regardless of considering or not frequency-dependent soils, both ground return impedance and admittance matrix terms are determined by infinite integrals [3]. This implies on highly complex and computational heavy burden solutions, which are desirable to be avoided. For that, closed-form formulas have been used with great agreement with the integral responses. The ground return impedance closed-form expression has already been developed [4]. As for the ground return admittance, a closed-form expression is here developed and was accepted for publication in [5]. This approximation is proved to be suited for frequency and time-domain analysis of underground cable system transients and validated by comparing it with a quasi-TEM approximation of the infinite integrals.

Finally, the impact of the soil modeling on the cable systems is evaluated by combining the developed approaches. A frequency-domain analysis is considered to evaluate how the soil model impacts on the cable system natural modes of propagation. Further, a sensitivity analysis is performed in order to investigate how the ground return impedance and admittance respond to resistivity variations, combined with frequency variations. These analyses should provide information of how much each system configuration is affected by the soil model, which can be also assessed by carrying time-domain simulation and evaluating the responses.

### 1.3 Objectives

Initially, the main objective of this research was a quantitative analysis of the uncertainties regarding soil behavior and their impact on underground cable systems transient response. However, during research execution, the need for more accurate modeling of soil parameters, including its frequency dependence, was verified. Although there might exist several different approaches possible to assess the influence of soil, the contributions of this Thesis are in the sense of investigating characteristics that might later be used as reference information for further studies. Therefore, the objectives of this Doctorate Thesis are listed below, following the event tree depicted in Fig. 1.1.

1. To investigate the probabilistic model of ground return impedance and admittance, with respect to a probability density function of the soil apparent resistivity obtained from the literature.
2. To obtain a workable representation of frequency-dependent soil models, by means of rational modeling, i.e., a pole-residue representation.
3. To derive a closed-form expression for the ground return admittance, suitable for frequency- and time-domain EMT simulations.
4. To evaluate how soil parameters should affect the natural modes of propagation of the cable systems.
5. To perform a sensitivity analysis regarding several different cable systems configurations, in order to acknowledge how the cable systems respond to soil resistivity and frequency variation.
6. To investigate this influence on time-domain simulation results.

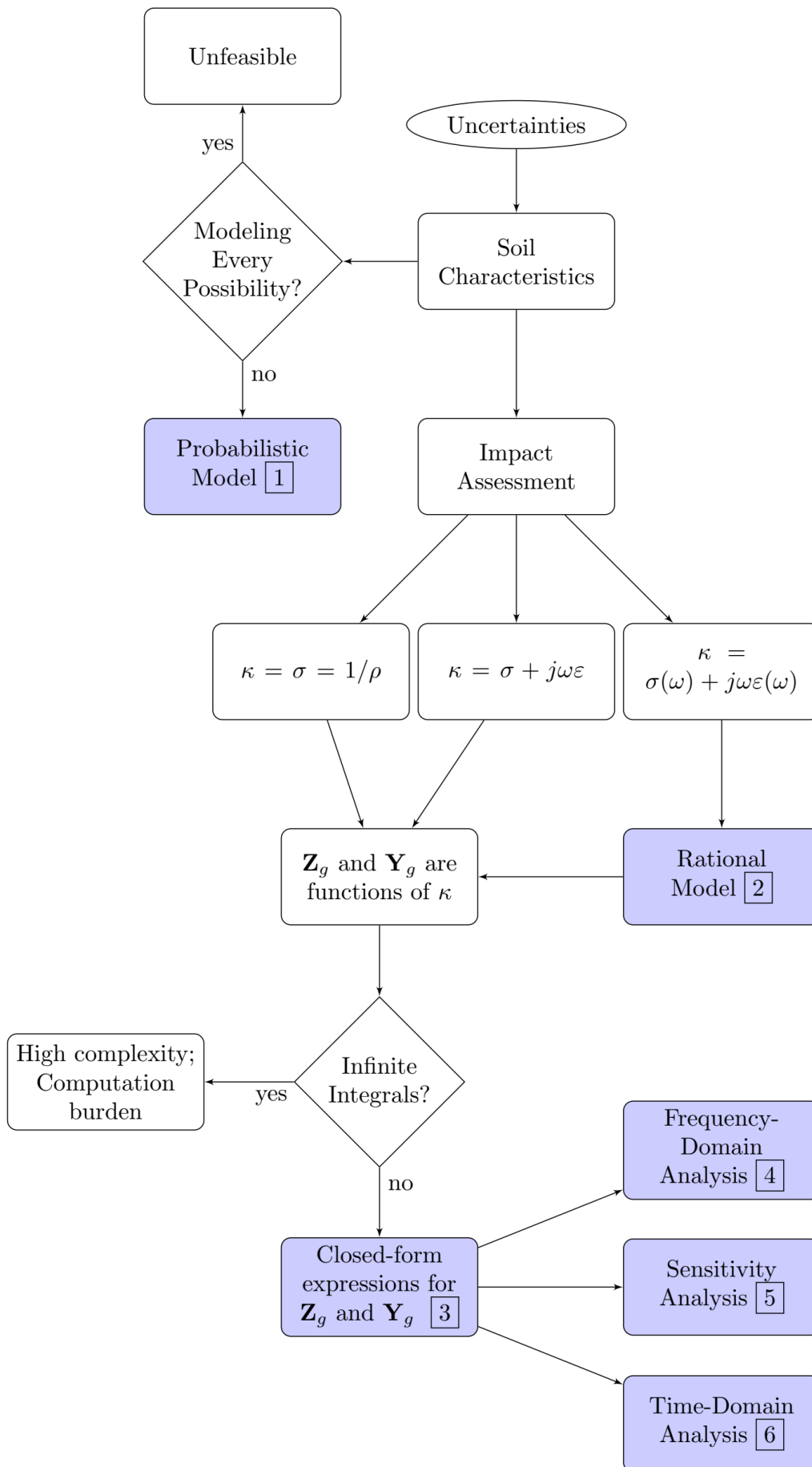


Figure 1.1: Research even tree.

## 1.4 Thesis Outline

This Chapter presented the context in which this research is inserted. In the following list, next chapters are described:

**Chapter 2** contains the general aspects of soil characteristics. The probabilistic approach is investigated. The inclusion of the soil as a frequency-dependent parameter is proposed by means of a rational model.

**Chapter 3** reviews important aspects on cable system modeling. It features a novel closed-form expression for the ground return admittance. The influence of soil frequency-dependence on the natural modes of propagation is also addressed.

**Chapter 4** presents an important contribution on the assessment of the impact of soil parameters on cable systems performance, by means of a sensitivity analysis realized for both ground return impedance and admittance. Furthermore, it presents test cases and results regarding some aspects given in the previous chapters, considering time-domain simulation.

**Chapter 5** draws the main conclusions and present future work propositions.

## 1.5 Published Research

During this doctorate research several studies were carried and some of the material was accepted for publication, as listed in the following.

- A. LIMA, **J. SALVADOR**, M. TOMASEVICH, M. T. CORREIA DE BARROS, “Lightning performance of overhead transmission lines considering distinct grounding system formulations”. In: *GROUND’2016 & 7th LPE – International Conference on Grounding and Earthing & 7th International Conference on Lightning Physics and Effects*, pp. 246–250, Porto de Galinhas, 2016.
- A. MAGALHÃES, **J. SALVADOR**, A. LIMA, M. T. CORREIA DE BARROS, “Identification of incipient faults in subsea HVDC systems”. In: *PSCC’2016 – Power Systems Computation Conference*, DOI: 10.1109/PSCC.2016.7540920, Genoa, 2016.
- V. CUNHA, **J. SALVADOR**, A. LIMA, “Estudo de sobretensões em linhas de transmissão com diferentes modelos de descarga atmosférica”. In: *CBA’2016 – Congresso Brasileiro de Automática*, Vitória, 2016.

- A. LIMA, R. DIAS, **J. SALVADOR**, A. MAGALHÃES, M. T. CORREIA DE BARROS; “Modeling of Long Feeders in Power Electronics Based Systems”. Chapter III of *COBEP 2017 Tutorials*, ISBN: 978-1-5090-6247-8, pp. 153–190, Juiz de Fora, 2017.
- **J. SALVADOR**, A. LIMA, M. T. CORREIA DE BARROS; “Underground cable systems ground return impedance sensitivity do soil resistivity uncertainties”. In: *PSCC'2018 – Power Systems Computation Conference*, DOI: 10.23919/PSCC.2018.8442598, Dublin, 2018.
- **J. SALVADOR**, A. MAGALHÃES, A. LIMA, M. T. CORREIA DE BARROS; “Closed-Form Expression for Ground Return Admittance in Underground Cables”. *IEEE Transactions on Power Delivery*. DOI: 10.1109/TPWRD.2019.2897257, Accepted in January 28th, 2019.
- **J. SALVADOR**, R. ALIPIO, A. LIMA, M. T. CORREIA DE BARROS; “A Concise Approach of Soil Models for Time-Domain Analysis”. *IEEE Transactions on Electromagnetic Compatibility*. DOI: 10.1109/TEMPC.2019.2927273, Accepted in June 29th, 2019.

# Chapter 2

## Soil Modeling

This chapter presents a study regarding the soil modeling to be included in electromagnetic transient simulation. In order to contextualize the determination of soil resistivity, some topics about the geological perspective and resistivity measurements are covered, although not being the main scope of this research. As EMT simulation regards frequencies up to several kHz or even MHz range, the frequency dependence of soil parameters is addressed. Furthermore, a rational modeling of frequency-dependent soil models is derived in order to improve its inclusion on simulations.

### 2.1 General Background

The soil plays a key role on the evaluation of electromagnetic transients, for it is a natural return path for the transmission systems. However, a numerous quantity of variables are associated with its characterization which leads to uncertainties and increases the difficulty of consistently consider all of the involved parameter. It is desirable, therefore, to try and understand the involved parameters so approximations should be given sense, i.e., so that it is possible to infer whether an approximation is valid or not.

From a geological perspective, soil characteristic is associated with different variables, being the concentrated amount of fluids one of the most important. The idea to use the electrical resistivity as parameter for soil characterization back to 1940s, with Archie's Equation, which states soil resistivity considering the current surface conduction through ion and particles [6]:

$$\rho = a \rho_w \Phi^{-m} S_w^{-n} \quad (2.1)$$

where  $\rho$  is the electrical resistivity,  $\rho_w$  is the resistivity of the pore water,  $\Phi$  is the porosity,  $S_w$  is the water saturation,  $a$  is a constant,  $m$  is the cementation exponent

and  $n$  is the water saturation exponent. This equation is used for its simplicity and has been applied for soil surveys [7], soil gas study [8, 9] and oil exploitation [10, 11].

The dependence of the soil resistivity with temperature must also be accounted for. This relation is given by [12]:

$$\rho_t = \frac{\rho_{18}}{1 + \alpha(t - 18)} \quad (2.2)$$

where  $\rho_t$  is the resistivity in  $\Omega\text{m}$ , corrected to temperature  $t$  in  $^\circ\text{C}$ ,  $\rho_{18}$  is the soil resistivity at  $18^\circ\text{C}$ , and  $\alpha$  is the material constant relative to soil [13].

Even though the combined usage of equations (2.1) and (2.2) should lead to fair results, they are not suitable from an electrical engineering point of view. This happens because power systems are submitted to a large combination of soils that are influenced by seasonal changes on its moisture composition [14] which makes barely unfeasible the task of applying the “geological approach” to include such information on the studies.

An adequate solution might be achieved by considering an apparent resistivity, i.e., taking a measured or the average of resistivity measurements, or even postulate a single value for the soil resistivity based on the approximate characteristics of the soil considered. This is the most common approach when dealing with any sort of power systems studies. Some standardized procedures [15, 16] indicate the way DC and low frequency resistivity should be measured which in turn provides the values that are reasonable to be assigned. Other way to approach the soil variety is to consider the soil divided in finite layers, i.e., multilayer soil [17, 18]. Either way, the basic hypothesis assumed is of a homogeneous soil (or a superposition of homogeneous finite parts of soils) with a fixed value of resistivity.

## 2.2 Probabilistic Modeling

As already stated before, the soil presents a highly non-uniform characteristic and, considering the diversity of aspects that may inflict its behavior, a probabilistic modeling ought to increase its knowledge. In the past, a Normal distribution was proposed [19], as soil conductivity is primarily electrolytic [6]. Further, some works [20, 21] have dealt with soil resistivity uncertainties effects on transmission lines parameters and protection considering probability modeling.

An extensive experimental campaign through Continental Portugal [22] collected some interesting data regarding soil resistivity measurements. In the remainder of this Thesis, the expression “apparent resistivity” is used in reference to a fixed resistivity value,  $\rho_0$ , either chosen or obtained via measurements. Simões Alves and Correia de Barros then obtained statistical description of 177 different identi-

fied soils [23]. Table 2.2 replicates some examples of the measured data and some remarkable features can be observed. In the measurements, soils presented large variation on its measured resistivity values, which can be noted by analyzing each soil's average, mean, minimum and maximum values. One of the identified soils provided measurements that ranged from around 200  $\Omega\cdot\text{m}$  to roughly 120  $\text{k}\Omega\cdot\text{m}$ .<sup>1</sup>

Table 2.1: Statistical Analysis of Soil Apparent Resistivity. Adapted from [23].

| Soil | Population Size | Resistivity |        |         |          |
|------|-----------------|-------------|--------|---------|----------|
|      |                 | Average     | Median | Minimum | Maximum  |
| A    | 33              | 3635.2      | 975.5  | 62.6    | 41202.2  |
| B    | 23              | 234.1       | 162.2  | 10.3    | 753.8    |
| C    | 17              | 14229.7     | 4801.8 | 541.4   | 51514.7  |
| D    | 39              | 10472.92    | 2286.3 | 202.2   | 121522.9 |
| E    | 15              | 136.72      | 80.8   | 12.2    | 459.7    |

In the following, when the whole set of data is analyzed, the probability density function (PDF) is not symmetrical and higher resistivity values should have lower probabilities. For that reasons, Gamma, Log-Normal, Exponential and Weibull distributions were tested, and the latter was proven to be the most adequately choice [23]. The Weibull distribution  $P_\rho(\rho)$  is given by:

$$P_\rho(\rho) = \frac{\beta_W}{\alpha_W} \left( \frac{\rho}{\alpha_W} \right)^{\beta_W - 1} \exp \left[ - \left( \frac{\rho}{\alpha_W} \right)^{\beta_W} \right] \quad (2.3)$$

where  $\alpha_W$  is the scale factor and  $\beta_W$  is the shape factor. As an example, consider the two soils presented in [23], with statistical data given in Tab. 2.2 and with Weibull data given in Tab. 2.2. The PDF of each soil is depicted in Fig. 2.1.

Table 2.2: Example of Weibull Distribution data for identified soils.

| Type of soil | $\alpha_W$ | $\beta_W$ |
|--------------|------------|-----------|
| A            | 0.94917    | 1337.882  |
| B            | 1.1705     | 247.092   |

This is an interesting feature because, once the PDF of the soil resistivity is known, one may use the relations between ground return immittances, i.e., impedance and admittance, and soil resistivity as a way to estimate the PDF of the immittances. In another chapter a review on cable systems modeling is presented and the relations between ground return quantities and soil resistivity are clarified. However, the definition of a probability distribution function for impedance or admittance is not straightforward since they are complex valued functions and one

<sup>1</sup>This is an extremely large value, enough to be considered as rock. However, the other data of the same soil attest the argument that the behavior is strongly affected by external conditions.

would have to rely on covariance matrices which can be cumbersome [24]. In the remainder of this document, whenever the terms “impedance” and “admittance” are used, they are related to per-unit-length quantities.

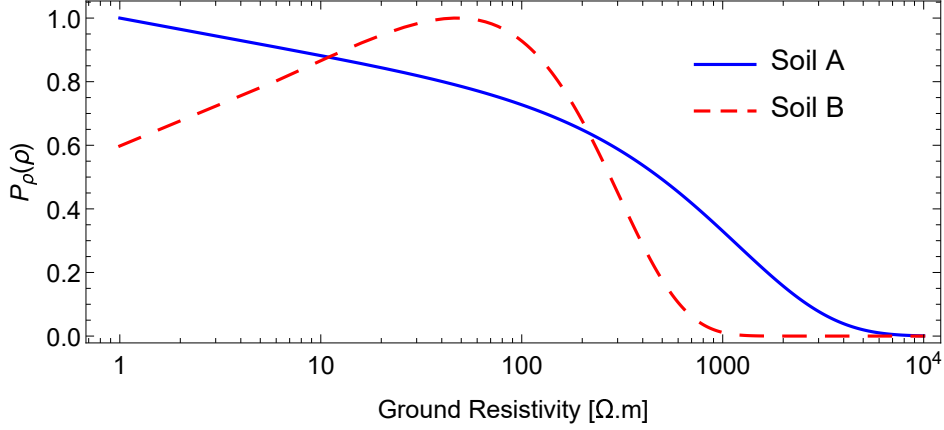


Figure 2.1: Normalized  $P_\rho(\rho)$  obtained from actual measurements in [23].

It is possible to estimate the behavior of the PDFs of ground return impedances  $Z_g$  and admittances  $Y_g$  if some assumptions are made [24]:

- $\rho$  is a continuous random variable;
- $Z_g$  and  $Y_g$  are scalar functions of this continuous random variable;
- $Z_g$ ,  $Y_g$  and  $\rho$  are strictly monotone and differentiable;
- $Z'_g = \frac{\partial Z_g}{\partial \rho}$  and  $Y'_g = \frac{\partial Y_g}{\partial \rho}$  exist in all domain of  $\rho$  considered; and
- $|Z'_g|$  and  $|Y'_g|$  are finite and not null in all domain of  $\rho$ .

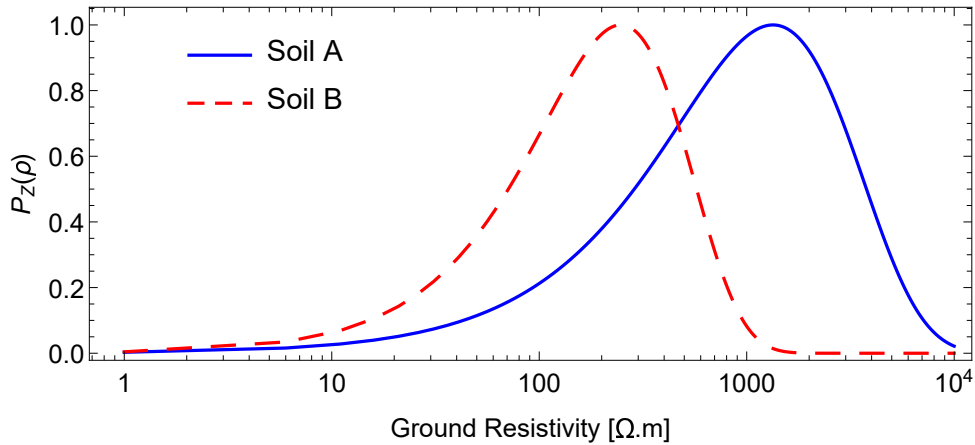
The probability distribution functions of the ground return impedance,  $P_Z(\rho)$ , and admittance,  $P_Y(\rho)$ , with respect to the continuous random variable  $\rho$ , are then postulated related to the probability density function of the resistivity,  $P_\rho(\rho)$  [24, 25]:

$$\begin{aligned} P_Z(\rho) &= \frac{P_\rho(\rho)}{|Z'_g|} \\ P_Y(\rho) &= \frac{P_\rho(\rho)}{|Y'_g|} \end{aligned} \quad (2.4)$$

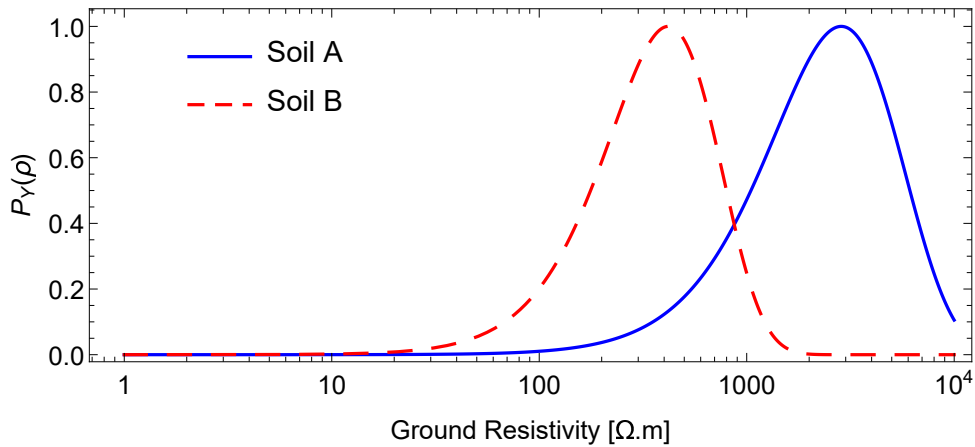
To illustrate the procedure, an example considering the soils of Table 2.2 and the ground return impedance and admittance of a pipe-type cable is presented. At this point, it is only necessary to acknowledge that the ground return impedance and admittance matrices have all the values equal to  $Z_g$  and  $Y_g$ , respectively [26].

Figure 2.2 depicts the normalized probability density functions  $P_Z(\rho)$  and  $P_Y(\rho)$ . The main advantage of using normalized values relies on the fact that the results for a given soil are identical regardless of the frequency considered. Therefore, the normalized  $P_Z(\rho)$  allows to identify a resistivity value in which the ground return impedance should present the highest probability value. Likewise,  $P_Y(\rho)$  provides analogous result considering the ground admittance. Further, the knowledge of these PDF's gives the interval of interest for a given set of resistivity values.

This result indicates that the higher probability of  $Z_g$  occurs around the shape factor  $\beta_W$  for soil A, while for  $Y_g$  it occurs around the average resistivity value. As for soil B, the average value and the shape factor are quite similar and although higher probability of  $Z_g$  is also achieved at a resistivity around the shape factor,  $P_Y(\rho)$  has its maximum value at a higher resistivity. These might be considered as numeric coincidences, but relevant qualitative results are that the interval of confidence for  $P_Y(\rho)$  is narrower than for  $P_Z(\rho)$  and that, when compared with  $P_Z(\rho)$ , the ground return admittance has its highest probability for greater resistivity values.



(a)  $P_Z(\rho)$



(b)  $P_Y(\rho)$

Figure 2.2: Normalized PDFs for pipe-type cable ground return impedance and admittance.

It is worth mentioning that  $P_Y(\rho)$  in (2.4) can only be applied on a pipe-type cable case, once all on the matrix terms are the same and, therefore, configures a scalar value multiplied by a matrix of ones. As it will be seen in Section 3.4, other cable systems configurations demand the inversion of matrix  $\mathbf{Y}_g$  for its inclusion in the modeling and, therefore, shunt impedance is preferred. Further information about the modeling of different cable systems configurations is provided throughout Chapter 3. Although not shown here, the same procedure was applied to different cable configurations and the same behavior was found.

Overall, the probabilistic analysis combined with the knowledge of the measured data enhance the argument that the soil apparent resistivity might present some unknown characteristics, being strongly affected by its surroundings. Also, the same soil can provide a wide range of measured resistivity values and that is the main information that will be carried through the remainder of this document. Although the probabilistic modeling was possible given the assumptions and postulations, to the best knowledge of this author, there are not so many available resistivity probability density functions in the literature as in [23]. Therefore, in the remaining chapters, at least one of these values of apparent resistivity ( $\rho_0 = 1/\sigma_0$ ) is considered: (a) low resistivity, 100  $\Omega\cdot\text{m}$ ; (b) medium to high resistivity, 1  $\text{k}\Omega\cdot\text{m}$ ; (c) very high resistivity, 3  $\text{k}\Omega\cdot\text{m}$ ; and (d) extremely high resistivity, 120  $\text{k}\Omega\cdot\text{m}$  (close to the highest value found in [23]).

Nonetheless, a more detailed representation of soils is needed whenever wide-band electromagnetic transients and fields are studied, once the fixed measured value does not provide soil behavior due to frequency variation. In the next section, soil's frequency dependence is addressed.

## 2.3 Soil Frequency Dependence

To characterize the electromagnetic properties of any material, the most important parameters are the electric resistivity, the electric permittivity and the magnetic permeability [27–29]. Focusing on soils, in most cases the magnetic permeability can be assumed constant and equal to that of free space,  $\mu_0$ . These parameters are involved in the relation between electric and magnetic field, considering the Ampère-Maxwell equation, which reads [29]

$$\vec{\nabla} \times \vec{H} = \kappa \vec{E} = \vec{J}_C + \vec{J}_D \quad (2.5)$$

where  $\vec{E}$  and  $\vec{H}$  are the frequency-domain vectors of the electric and magnetic fields, respectively.  $\kappa$  is the soil immittance and, apart geometric factors, may be associated to the admittance of a infinitesimal volume of soil [30].

Typically,  $\kappa$  has three possible definitions:

- $\boxed{\kappa_1 = \sigma_0 = 1/\rho_0}$ , when only the conduction current density ( $\vec{J}_C = \sigma_0 \vec{E}$ ) is considered, with  $\sigma_0$  and  $\rho_0$ , respectively, the apparent conductivity and resistivity;
- $\boxed{\kappa_2 = \sigma_0 + j\omega\varepsilon_\infty}$ , when both conduction and displacement current densities are considered, i.e., respectively,  $\vec{J}_C = \sigma_0 \vec{E}$  and  $\vec{J}_D = j\omega\varepsilon_\infty \vec{E}$ , with  $\sigma_0$  the same as before and  $\varepsilon_\infty = \varepsilon_r \varepsilon_0$ ; or
- $\boxed{\kappa_3 = \sigma(\omega) + j\omega\varepsilon(\omega)}$ , also when  $\vec{J}_C$  and  $\vec{J}_D$  are considered, but both  $\sigma$  and  $\varepsilon$  are functions of frequency.

Although the soil conductivity is a complex quantity ( $\sigma = \sigma' - j\sigma''$ ) [1], it is commonly assumed as a real number ( $\sigma' = \sigma_0$  and  $\sigma'' = 0$ ) [30–32]. The apparent conductivity,  $\sigma_0 = 1/\rho_0$ , corresponds to the material ability to transport electric charges when an electric field is applied and also of the losses associated with the conducting process. The electric permittivity  $\varepsilon$  is also a complex quantity related with the polarization processes that take place in the medium, when an electric field is applied, and the associated losses, and is given by [29]

$$\varepsilon = \varepsilon' - j\varepsilon'' \quad (2.6)$$

The real parcel ( $\varepsilon'$ ) expresses the material ability to be polarized and to store electric energy, when an electric field is applied. The imaginary parcel ( $\varepsilon''$ ) is associated to the losses occurring during the polarization process. Such losses represent the part of energy of the applied field, which is dissipated as heat because of the friction experienced by the electric dipoles as they continuously move in response to the alternating field. Using the complex permittivity in (2.5) allows to define the so-called equivalent conductivity

$$\sigma(\omega) = \sigma_0 + \omega\varepsilon''(\omega) \quad . \quad (2.7)$$

The total polarization in a medium is the sum of contributions of different mechanisms, such as electronic, ionic, dipolar and interfacial polarization [33]. The quantitative measurement of the time required for a polarization to form or disappear is called relaxation time. If the relaxation time required to form a given polarization mechanism is greater than the period of the applied field, then the polarization is not able to form completely before the direction of the field is reserved. This causes the magnitude of the medium polarization, and of  $\varepsilon'$ , to decrease as the frequency of the applied field increases.

Furthermore, along the frequency interval of decrease of  $\varepsilon'$ , there is an increase of the losses per cycle with a peak of  $\varepsilon''$ , leading to an increase of the equivalent conductivity. Thus, along the frequency interval where  $\varepsilon'$  goes down, the equivalent conductivity goes up, as if one were being transformed into the other, suggesting a causal relationship. This causal relationship between the frequency variation of  $\varepsilon'$  and  $\varepsilon''$  is expressed by the so-called Kramers-Kronig's relations [34]:

$$\varepsilon'(\omega) = \varepsilon_\infty + \frac{2}{\pi} \int_0^\infty \frac{\omega' \varepsilon''(\omega')}{\omega'^2 - \omega^2} d\omega' \quad (2.8)$$

$$\varepsilon''(\omega) = -\frac{2\omega}{\pi} \int_0^\infty \frac{\varepsilon'(\omega') - \varepsilon_\infty}{\omega'^2 - \omega^2} d\omega' \quad (2.9)$$

where the variable of integration  $\omega'$  is real. Considering the complex permittivity and the Kramers-Kronig's relations, the soil immittance can be rewritten as:

$$\kappa = \sigma_0 + j\omega [\varepsilon_\infty + \bar{\kappa}(\omega)] \quad (2.10)$$

and  $\bar{\kappa}$  is responsible for the frequency dependence in  $\varepsilon'(\omega)$  and  $\varepsilon''(\omega)$ . Also, as will be seen in a future section, expression (2.10) is rather suitable to be approximated by a rational model.

Regarding the modeling of  $\kappa$  to perform electromagnetic transients studies, there are several frequency-dependent soil models that can be cited: Scott, Smith-Longmire, Messier, Visacro-Portela, Portela, Visacro-Alipio and Alipio-Visacro. From these, only Smith-Longmire, Messier, Portela and Alipio-Visacro attend the Kramers-Kronig's relations [34], i.e., are causal models. Smith-Longmire and Messier models are both based on Scott's data [31, 35, 36], while Portela was obtained via laboratory measurements [37] and Alipio-Visacro through actual field measurements [32, 33].

As a first analysis, Smith-Longmire, Portela and Alipio-Visacro models are considered because they are all causal models and in some way come from actual measurements. Although Messier model is also a causal model, it is a theoretical model based on Scott's data like Smith-Longmire, so the latter was chosen for its well-known universality [2].

**Smith and Longmire** presented [31] a frequency-dependent soil model based on the consideration of the soil as a RC network. Combined with measurements of the conductivity of concrete,<sup>2</sup> a curve-fit extrapolation for a range from

---

<sup>2</sup>Wilkenfeld, J., *Private communication between Wilkenfeld, Smith and Longmire* [31].

1 Hz up to  $10^{12}$  Hz was obtained. The frequency dependent expressions for conductivity and permittivity are:

$$\sigma(f) = \sigma_0 + 2\pi\epsilon_0 \sum_{n=1}^{13} f_n \alpha_n \frac{(f/f_n)^2}{1 + (f/f_n)^2} \quad (2.11)$$

$$\epsilon'(f) = \epsilon_0 \left[ \epsilon_r + \sum_{n=1}^{13} \frac{\alpha_n}{1 + (f/f_n)^2} \right] \quad (2.12)$$

where  $\sigma_0$  is the low frequency soil conductivity in [S/m] and  $\epsilon_r$  is considered equal to 5 for this model. The coefficients  $\alpha_n$  are in Table A.1 and the parameter  $f_n$ , given in (2.13), is defined as a scaling frequency that includes the information of the water content in the soil sample, which can be adapted to consider the conductivity as an input parameter instead [34]. For more information, see Appendix A.

$$f_n = 10^{n-1} (125 \sigma_0)^{0.8312} \quad (2.13)$$

Since (2.11) and (2.12) are unique expressions in which  $f_n$  scales with water content and all  $f_n$  scale by the same factor, this model is considered a universal model for soils [31].

**Portela** proposed [37] a frequency dependent soil model for a range from 40 Hz up to 2 MHz. The model was based on actual laboratory measurements of field soil samples and considered the whole immittance as

$$\kappa(\omega) = \sigma_0 + \Delta_i \left[ \cot \left( \frac{\pi}{2} \alpha \right) + j \right] \left( \frac{\omega}{2\pi \times 10^6} \right)^\alpha \quad (2.14)$$

where  $\alpha = 0.706$ ,  $\sigma_0$  is the apparent conductivity in [S/m], measured at 100 Hz, and  $\Delta_i = 11.71$  mS/m.

**Alipio and Visacro** proposed [32] a model to consider the frequency dependence of the soil conductivity and permittivity based on a large number of field measurements, the causal Kramers-Kronig relations, and Maxwell equations. The model is also suited for time-domain analysis regarding frequency-dependent soils [38].

$$\sigma(f) = \sigma_0 + K_\sigma f^\gamma \quad (2.15)$$

$$\varepsilon'(f) = \varepsilon_\infty + K_\varepsilon f^{\gamma-1} \quad (2.16)$$

with

$$K_\sigma = \sigma_0 \frac{h(\sigma_0)}{(10^6)^\gamma} \quad (2.17)$$

and

$$K_\varepsilon = \frac{K_\sigma}{2\pi} \tan\left(\frac{\pi}{2}\gamma\right) \quad (2.18)$$

where  $\sigma_0$  and  $\varepsilon_\infty = \varepsilon_r \varepsilon_0$  are the same as before. Parameters  $\gamma$ ,  $\varepsilon_r$  and  $h(\sigma_0)$  are responsible for taking into account the inherent statistical dispersion of the frequency dependent variation of  $\sigma$ . For more information, see Appendix A.

To illustrate the differences between these models, a simple example is presented in Figures 2.3 and 2.4. A soil with apparent resistivity of 3000  $\Omega \cdot \text{m}$  with relative permittivity 20 was considered for the example within a frequency range from 100 Hz up to 10 MHz. These values were arbitrarily chosen so that:

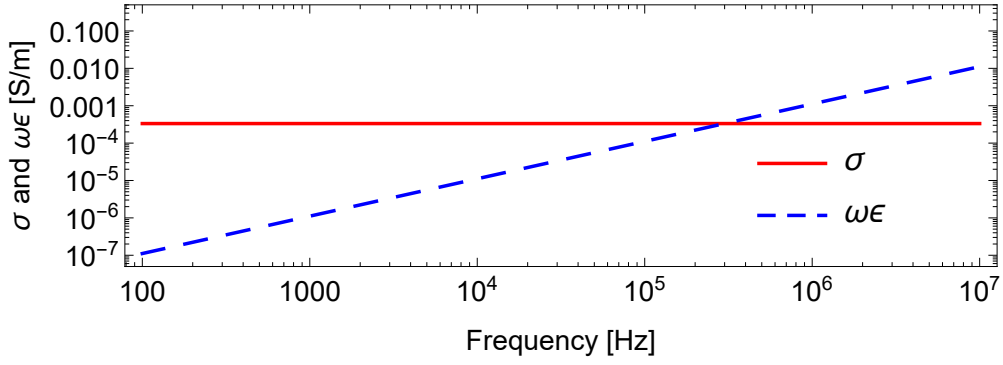
$$\Im\{\kappa\} > \Re\{\kappa\}, \quad \forall \omega > 2\pi n \cdot 10^5 \quad (2.19)$$

where  $n$  is an integer. In other words, the real and imaginary parts of  $\kappa$  achieve the same value at a frequency of a few hundreds of kHz, for all soil models.

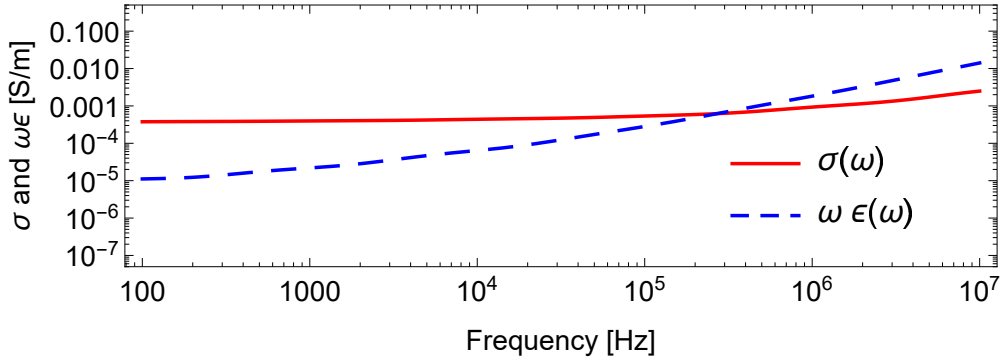
Figure 2.3 depicts the crossing of the real and imaginary parts of  $\kappa$ , while Fig. 2.4 presents the comparison between the absolute value of  $\kappa$  for each model. The case where  $\kappa$  is considered with constant parameters, i.e.,  $\kappa_2$  of the beginning of this Section, is also shown for comparison.

It is possible to observe in Figs. 2.3(a), (b) and (c) that Smith-Longmire and Alipio-Visacro models present quite similar behavior and the crossing of  $\sigma$  and  $\omega\varepsilon$  at a frequency between 200 and 300 kHz, like the  $\kappa_2$  model. From Figs. 2.3(c), Portela model presents this characteristic between 1 and 2 kHz. Furthermore, this analysis together with graphic of the absolute values of  $\kappa$  depicted in Fig. 2.4 make possible to assume that all these soil models have barely the same behavior for frequencies up to 1 kHz.

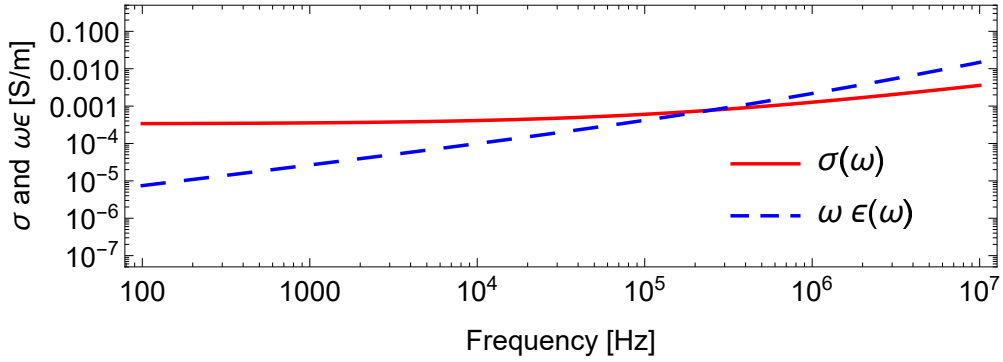
For a higher frequency band, however, there are noticeable differences. One may notice that Portela model presents higher magnitude in frequencies rather lower than the other models and also it escalates quicker. This means that Portela model should present a more damped behavior than the other models when considered in time-domain. Smith-Longmire and Alipio-Visacro models present similar behavior, except within a range between 30 kHz and 4 MHz, the latter frequency being the upper validity limit for Alipio-Visacro model.



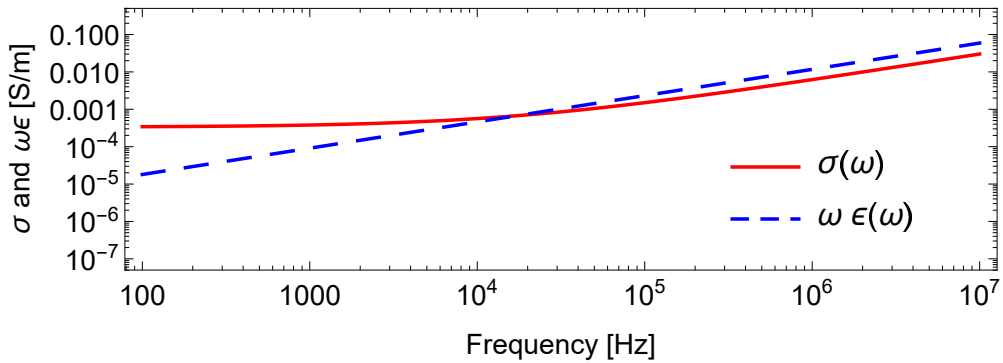
(a) Fixed parameters.  $\rho_0 = 3000 \Omega \cdot \text{m}$  and  $\epsilon_\infty = 20\epsilon_0$



(b) Smith-Longmire.



(c) Alipio-Visacro (parameters for mean results, see Appendix A).



(d) Portela.

Figure 2.3: Variations of  $\sigma$  and  $\omega\epsilon$  with frequency for different soil models.

In the remainder of this document, one theoretical model (Smith-Longmire, SL) and one practical model (Alipio-Visacro, AV) will be addressed whenever the frequency-dependent soil parameter  $\kappa_3$  is needed for comparisons. The choice of AV model instead of Portela model was made because the former is less damped than the latter.

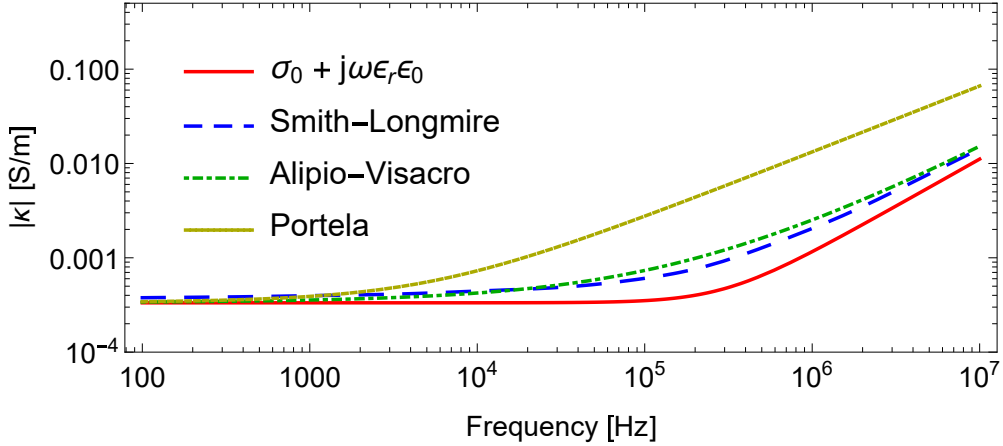


Figure 2.4: Comparison of absolute values of  $\kappa$  regarding different soil models.

## 2.4 Rational Approximation of Soil Models

As already stated in this chapter, the apparent resistivity may assume several different values. Therefore, in order to include the frequency dependence of soil parameters in EMT studies, it is desirable to investigate how the behaviors presented in Fig. 2.4 should be affected by changes of the apparent resistivity. To do so, one can resort to rational approximations in frequency-domain, which parameterize said behaviors in terms of a pole-residue realization, i.e., in terms of relaxation frequencies and a corresponding set of weights each relaxation frequency receives. In this section, the rational approximation of soil models is discussed. The results here obtained were accepted to publication in [2].

The determination of a sum of partial fractions that approximates a function in frequency domain allows for the knowledge of its poles and residues, which leads to time-domain representations in a straightforward way, once the inverse Laplace transform of each partial fraction is an exponential function. Considering the modeling of heavily frequency-dependent components and systems there are several fitting techniques possible [39]. If the time domain behavior is known, or obtained via numerical Laplace transform [40–42], one can fit it via Matrix Pencil Method (MPM) [43–45]. Here the so-called Vector Fitting technique (VF) [46–48] is used.

Considering the soil immittance  $\kappa(s)$  the frequency-domain function to be fit, the process of the rational approximation is done by calculating the pole-residue

representation

$$\kappa(s) \approx d + se + \sum_{i=1}^N \frac{c_i}{s - p_i} \quad (2.20)$$

where  $d$  and  $e$  are real numbers,  $N$  represents the order of approximation,  $c_i$  and  $p_i$  are, respectively, the residues and poles, and can be either real or come in complex conjugate pairs.

This represents an advantage for the analysis of frequency-dependent soil models because the correlation is straightforward with a RLC network [49]. Terms  $d$  and  $e$  represent, respectively, a shunt conductance and a shunt capacitance; real poles should represent series RL branches; and complex conjugate pairs of poles should represent a series built with a series RL branch connected in series to a shunt CG branch.

Due to the asymptotic behavior of frequency-dependent soil models, it is expected that only real poles are to be considered. However, when the residues are negative, calculations may lead to negative resistance and inductance, which is not physically consistent. It is possible to overcome this problem by considering a series RC branch instead of RL, i.e., writing the admittance as (2.21):

$$\frac{1}{R_0} + sC_0 + \sum_{i=1}^N \frac{s/R}{s + 1/RC} \quad , \quad (2.21)$$

which when comparing to (2.20) is slightly different because the numerator inside the sum is not a simple constant. Nonetheless, it is possible to rewrite (2.20) as

$$\kappa(s) = \tilde{d} + s \left[ e + \sum_{i=1}^N \frac{K_i}{s - p_i} \right] \quad , \quad (2.22)$$

if  $\tilde{d} = d - \sum_{i=1}^N c_i/p_i$  and  $K_i = c_i/p_i$  are considered. Further, the comparison of (2.22) with equation (2.10) of Section 2.3 leads to

$$\begin{aligned} \sigma_0 &= \tilde{d} \\ \varepsilon_\infty &= e \\ \bar{\kappa}(s) &= \sum_{i=1}^N \frac{K_i}{s - p_i} \end{aligned} \quad (2.23)$$

where  $K_i$  and  $p_i$  are respectively the residues and the poles of  $\bar{\kappa}(s)$ . In the remainder of this chapter, whenever the terms ‘‘poles’’ and ‘‘residues’’ appear they are referring to  $p_i$  and  $K_i$ , respectively.

Figure 2.5<sup>3</sup> compares the magnitude of  $\kappa$  considering the original formulation by Smith and Longmire and the approximation as (2.22) obtained using the fast-relaxed version of VF, assuming distinct values of  $\rho_0 = 1/\sigma_0$ : 100, 500 and 1000  $\Omega\cdot\text{m}$ . The order of the approximation chosen was  $N = 13$ , following the original proposition by Smith and Longmire. According to the results, there is an excellent agreement between original formulation and the proposed representation. The rms-error of the approximation is of order  $10^{-16}$ , regardless of the choice of the starting poles. Although not presented, similar results were obtained for other values of  $\rho_0$ .

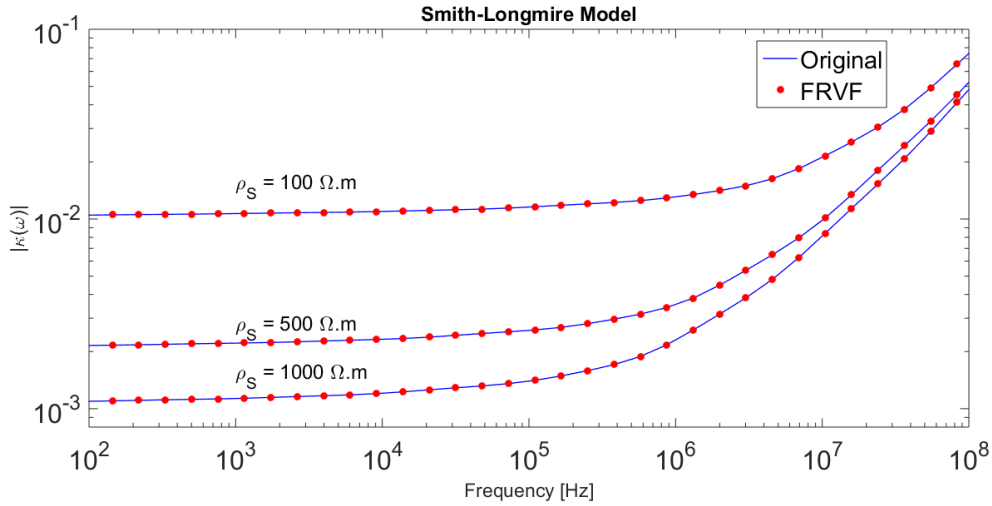


Figure 2.5: Rational Approximation of Smith-Longmire model.

Table 2.3 presents the obtained values of  $K_i$  and  $p_i$  for the three considered soils, as well as the ratio between the values of  $K_i$  and  $K_1$  and between  $p_i$  and  $p_1$ . This table reveals some very interesting aspects considering the Smith-Longmire model. Each soil presents a distinct set of poles, or relaxation frequencies. However, the ratio between the poles follows a power of 10, regardless the value of low-frequency soil resistivity. This means that, for a given soil, if one of the 13 poles is known, the other poles are determined. Also, each soil present a distinct set of constants  $K_i$ . However, once again, the ratio  $K_i/K_1$  presents a universal behavior, regardless the low-frequency soil resistivity.

Therefore, given a soil with known  $K_1$ , the other values of  $K_i$  are determined, i.e., it is possible to express  $p_1$  and  $K_1$  as a function of the low-frequency soil conductivity. Considering the results of Tab. 2.3, the following simple functions can be obtained:

<sup>3</sup>It is worth mentioning that the aim of Fig. 2.5 is to present the quality of the fitting process, even for high frequencies. The same can be said about Fig. 2.6 in the following, where results above 4 MHz represent an extrapolation of AV model.

$$p_1 = \zeta_{p_1} \times \sigma_0^\lambda \quad (2.24)$$

$$K_1 = \zeta_{K_1} \times \sigma_0^\lambda \quad (2.25)$$

where  $\sigma_0$  is the apparent conductivity in mS/m and  $p_1$  is given in rad/ps. The constants  $\zeta_{p_1}$  and  $\zeta_{K_1}$  correspond, respectively, to  $p_1$  and  $K_1$  for the soil of apparent resistivity  $1000 \Omega \cdot \text{m}$ , or  $\sigma_0 = 1 \text{ mS/m}$ , and  $\lambda = 0.8312$ .

Furthermore, (2.24) and (2.25) reveal that  $p_1$  and  $K_1$  have the same type of dependence with the apparent soil conductivity. Finally, considering (2.24) and (2.25), and the universal relations  $K_i/K_1$  and  $p_i/p_1$  shown in Tab. 2.3, a compact representation of the frequency-dependent soil immittance according to (2.22) is obtained.

Regarding Alipio-Visacro model, Fig. 2.6 compares the magnitude of  $\kappa(\omega)$  considering the original formulation and VF approximation. The order of approximation was chosen  $N = 19$  in order to obtain the rms-error as close as possible to the case of Smith-Longmire approximation, i.e., rms-error of order  $10^{-16}$ . According to the results, there is an excellent agreement between original formulation and the proposed representation and similar results were obtained for other values of soil resistivity.

Table 2.4 presents the obtained values of  $K_i$  and  $p_i$  for the three considered soils. It is also presented the ratio between the values of  $K_i$  and  $K_1$  and between  $p_i$  and  $p_1$ . Analogously to what was presented for SL model, this table reveals some very interesting aspects considering the Alipio-Visacro model. It can be seen that all three considered soils can be represented by the same set of poles. Once again, similar results were obtained for other values of soil resistivity.

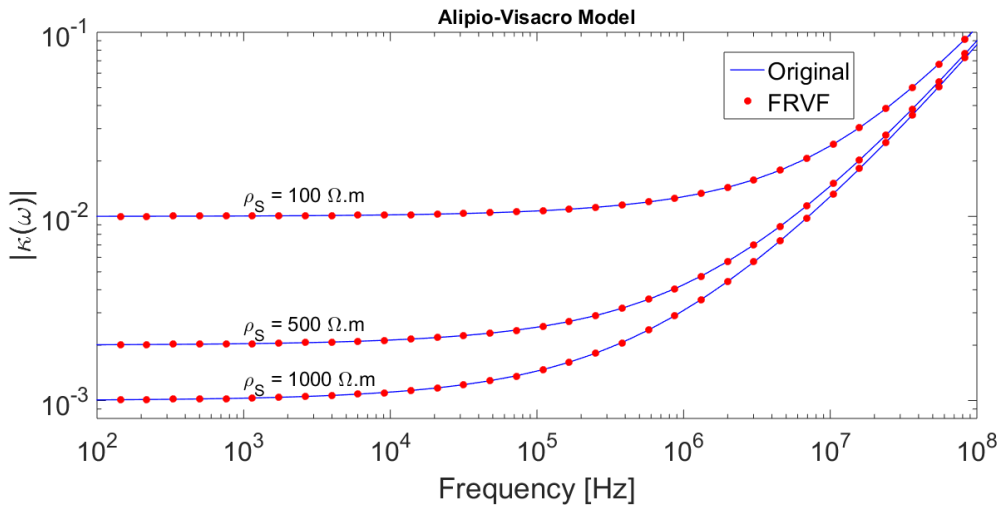


Figure 2.6: Rational Approximation of Alipio-Visacro model.

Table 2.3: Rational model of Smith-Longmire Soil.

| #  | $\rho_0 = 100 \Omega \cdot \text{m}$ |                         | $\rho_0 = 500 \Omega \cdot \text{m}$ |                         | $\rho_0 = 1000 \Omega \cdot \text{m}$ |                         | $K_i/K_1$              | $p_i/p_1$               |
|----|--------------------------------------|-------------------------|--------------------------------------|-------------------------|---------------------------------------|-------------------------|------------------------|-------------------------|
|    | $K_i$                                | $p_i$                   | $K_i$                                | $p_i$                   | $K_i$                                 | $p_i$                   |                        |                         |
| 1  | $1.159 \times 10^1$                  | $-7.564 \times 10^{12}$ | $3.041 \times 10^0$                  | $-1.985 \times 10^{12}$ | $1.709 \times 10^0$                   | $-1.116 \times 10^{12}$ | 1                      | 1                       |
| 2  | $2.625 \times 10^0$                  | $-7.564 \times 10^{11}$ | $6.890 \times 10^{-1}$               | $-1.985 \times 10^{11}$ | $3.873 \times 10^{-1}$                | $-1.116 \times 10^{11}$ | $2.266 \times 10^{-1}$ | $1.000 \times 10^{-1}$  |
| 3  | $6.563 \times 10^{-1}$               | $-7.564 \times 10^{10}$ | $1.722 \times 10^{-1}$               | $-1.985 \times 10^{10}$ | $9.681 \times 10^{-2}$                | $-1.116 \times 10^{10}$ | $5.665 \times 10^{-2}$ | $1.000 \times 10^{-2}$  |
| 4  | $1.453 \times 10^{-1}$               | $-7.564 \times 10^9$    | $3.814 \times 10^{-2}$               | $-1.985 \times 10^9$    | $2.144 \times 10^{-2}$                | $-1.116 \times 10^9$    | $1.254 \times 10^{-2}$ | $1.000 \times 10^{-3}$  |
| 5  | $3.215 \times 10^{-2}$               | $-7.564 \times 10^8$    | $8.436 \times 10^{-3}$               | $-1.985 \times 10^8$    | $4.742 \times 10^{-3}$                | $-1.116 \times 10^8$    | $2.775 \times 10^{-3}$ | $1.000 \times 10^{-4}$  |
| 6  | $8.371 \times 10^{-3}$               | $-7.564 \times 10^7$    | $2.197 \times 10^{-3}$               | $-1.985 \times 10^7$    | $1.235 \times 10^{-3}$                | $-1.116 \times 10^7$    | $7.225 \times 10^{-4}$ | $1.000 \times 10^{-5}$  |
| 7  | $1.822 \times 10^{-3}$               | $-7.564 \times 10^6$    | $4.781 \times 10^{-4}$               | $-1.985 \times 10^6$    | $2.687 \times 10^{-4}$                | $-1.116 \times 10^6$    | $1.572 \times 10^{-4}$ | $1.000 \times 10^{-6}$  |
| 8  | $8.907 \times 10^{-4}$               | $-7.564 \times 10^5$    | $2.338 \times 10^{-4}$               | $-1.985 \times 10^5$    | $1.314 \times 10^{-4}$                | $-1.116 \times 10^5$    | $7.688 \times 10^{-5}$ | $1.000 \times 10^{-7}$  |
| 9  | $3.523 \times 10^{-4}$               | $-7.564 \times 10^4$    | $9.245 \times 10^{-5}$               | $-1.985 \times 10^4$    | $5.196 \times 10^{-5}$                | $-1.116 \times 10^4$    | $3.041 \times 10^{-5}$ | $1.000 \times 10^{-8}$  |
| 10 | $2.264 \times 10^{-4}$               | $-7.564 \times 10^3$    | $5.941 \times 10^{-5}$               | $-1.985 \times 10^3$    | $3.339 \times 10^{-5}$                | $-1.116 \times 10^3$    | $1.954 \times 10^{-5}$ | $1.000 \times 10^{-9}$  |
| 11 | $1.728 \times 10^{-4}$               | $-7.564 \times 10^2$    | $4.535 \times 10^{-5}$               | $-1.985 \times 10^2$    | $2.549 \times 10^{-5}$                | $-1.116 \times 10^2$    | $1.491 \times 10^{-5}$ | $1.000 \times 10^{-10}$ |
| 12 | $1.835 \times 10^{-4}$               | $-7.564 \times 10^1$    | $4.816 \times 10^{-5}$               | $-1.985 \times 10^1$    | $2.707 \times 10^{-5}$                | $-1.116 \times 10^1$    | $1.584 \times 10^{-5}$ | $1.000 \times 10^{-11}$ |
| 13 | $2.277 \times 10^{-4}$               | $-7.564 \times 10^0$    | $5.976 \times 10^{-5}$               | $-1.985 \times 10^0$    | $3.359 \times 10^{-5}$                | $-1.116 \times 10^0$    | $1.965 \times 10^{-5}$ | $1.000 \times 10^{-12}$ |

This leads to the relevant finding that whenever this soil model is considered, regardless of apparent soil conductivity, soils can be approximately represented by a universal set of electric dipoles of well-defined relaxation frequencies. What changes from one soil to other is the role played by each one of the relaxation frequencies, which is defined by the constants  $K_i$ .

On the other hand, according to Table 2.4, even though each soil is modeled by a distinct set of constants  $K_i$ , the ratio  $K_i/K_1$  presents a universal behavior, regardless the apparent soil resistivity. Hence, for a given soil, if  $K_1$  is known, the other values of  $K_i$  can be determined.

Considering the results of Table 2.4, the following function can be obtained for  $K_1$  as a function of the apparent soil conductivity:

$$K_1 = \xi_{K_1} \times \sigma_0^\phi \quad (2.26)$$

where  $\sigma_0$  is the apparent conductivity in mS/m. The constant  $\xi_{K_1}$  corresponds to  $K_1$  for the soil of apparent resistivity 1000  $\Omega$ .m, or  $\sigma_0 = 1$  mS/m, and  $\phi = 0.2699$ . Ultimately, considering the universal set of poles and the constants  $K_i$ , a compact representation of the frequency-dependent soil immittance according to (2.22) is also obtained.

One straightforward application of these obtained soil models is the implementation of Ampère-Maxwell equation in time-domain. Although it is not in the scope of this Thesis, by applying (2.22) in (2.5), the Laplace Inverse Transform leads to [2, 38]:

$$\vec{\nabla} \times \vec{\mathcal{H}} = \sigma_0 \vec{\mathcal{E}} + \varepsilon_\infty \frac{\partial \vec{\mathcal{E}}}{\partial t} + \left[ \sum_{i=1}^N K_i e^{-p_i t} \right] * \frac{\partial \vec{\mathcal{E}}}{\partial t} \quad (2.27)$$

where  $\varepsilon_\infty = \varepsilon_r \varepsilon_0$  and  $*$  represents the convolution.

## 2.5 Discussion

This chapter presented some relevant aspects regarding soil characteristics and modeling. From a geological perspective alone, a large number of variables strongly influence the determination of soil resistivity, including the surrounding temperature.

One way to approach the uncertainties caused by the composition variables is to assess statistical behavior of measured apparent resistivity, by means of probabilistic models. PDFs for ground return impedance and admittance of a pipe-type cable were obtained and it was seen that the probabilistic analysis enhances the argument that the soil apparent resistivity might present some unknown characteristics, being strongly affected by its surroundings.

Table 2.4: Rational model of Alipio-Visacro Soil.

| #  | $\rho_0 = 100 \Omega \cdot \text{m}$ |                         | $\rho_0 = 500 \Omega \cdot \text{m}$ |                         | $\rho_0 = 1000 \Omega \cdot \text{m}$ |                         | $K_i/K_1$              | $p_i/p_1$               |
|----|--------------------------------------|-------------------------|--------------------------------------|-------------------------|---------------------------------------|-------------------------|------------------------|-------------------------|
|    | $K_i$                                | $p_i$                   | $K_i$                                | $p_i$                   | $K_i$                                 | $p_i$                   |                        |                         |
| 1  | $7.451 \times 10^0$                  | $-2.239 \times 10^{13}$ | $4.825 \times 10^0$                  | $-2.239 \times 10^{13}$ | $4.002 \times 10^0$                   | $-2.239 \times 10^{13}$ | 1                      | 1                       |
| 2  | $1.907 \times 10^0$                  | $-5.860 \times 10^{12}$ | $1.235 \times 10^0$                  | $-5.860 \times 10^{12}$ | $1.024 \times 10^0$                   | $-5.860 \times 10^{12}$ | $2.559 \times 10^{-1}$ | $2.617 \times 10^{-1}$  |
| 3  | $9.861 \times 10^{-1}$               | $-2.342 \times 10^{12}$ | $6.386 \times 10^{-1}$               | $-2.342 \times 10^{12}$ | $5.296 \times 10^{-1}$                | $-2.342 \times 10^{12}$ | $1.323 \times 10^{-1}$ | $1.046 \times 10^{-1}$  |
| 4  | $6.157 \times 10^{-1}$               | $-9.971 \times 10^{11}$ | $3.987 \times 10^{-1}$               | $-9.971 \times 10^{11}$ | $3.307 \times 10^{-1}$                | $-9.971 \times 10^{11}$ | $8.263 \times 10^{-2}$ | $4.453 \times 10^{-2}$  |
| 5  | $3.973 \times 10^{-1}$               | $-4.194 \times 10^{11}$ | $2.573 \times 10^{-1}$               | $-4.195 \times 10^{11}$ | $2.134 \times 10^{-1}$                | $-4.195 \times 10^{11}$ | $5.332 \times 10^{-2}$ | $1.873 \times 10^{-2}$  |
| 6  | $2.547 \times 10^{-1}$               | $-1.710 \times 10^{11}$ | $1.649 \times 10^{-1}$               | $-1.710 \times 10^{11}$ | $1.368 \times 10^{-1}$                | $-1.710 \times 10^{11}$ | $3.418 \times 10^{-2}$ | $7.634 \times 10^{-3}$  |
| 7  | $1.606 \times 10^{-1}$               | $-6.703 \times 10^{10}$ | $1.040 \times 10^{-1}$               | $-6.703 \times 10^{10}$ | $8.622 \times 10^{-2}$                | $-6.703 \times 10^{10}$ | $2.155 \times 10^{-2}$ | $2.993 \times 10^{-3}$  |
| 8  | $9.914 \times 10^{-2}$               | $-2.516 \times 10^{10}$ | $6.420 \times 10^{-2}$               | $-2.516 \times 10^{10}$ | $5.324 \times 10^{-2}$                | $-2.516 \times 10^{10}$ | $1.331 \times 10^{-2}$ | $1.124 \times 10^{-3}$  |
| 9  | $5.981 \times 10^{-2}$               | $-8.992 \times 10^9$    | $3.873 \times 10^{-2}$               | $-8.993 \times 10^9$    | $3.212 \times 10^{-2}$                | $-8.993 \times 10^9$    | $8.026 \times 10^{-3}$ | $4.016 \times 10^{-4}$  |
| 10 | $3.515 \times 10^{-2}$               | $-3.043 \times 10^9$    | $2.276 \times 10^{-2}$               | $-3.043 \times 10^9$    | $1.888 \times 10^{-2}$                | $-3.043 \times 10^9$    | $4.717 \times 10^{-3}$ | $1.359 \times 10^{-4}$  |
| 11 | $2.006 \times 10^{-2}$               | $-9.680 \times 10^8$    | $1.299 \times 10^{-2}$               | $-9.681 \times 10^8$    | $1.077 \times 10^{-2}$                | $-9.681 \times 10^8$    | $2.692 \times 10^{-3}$ | $4.323 \times 10^{-5}$  |
| 12 | $1.107 \times 10^{-2}$               | $-2.869 \times 10^8$    | $7.170 \times 10^{-3}$               | $-2.869 \times 10^8$    | $5.946 \times 10^{-3}$                | $-2.869 \times 10^8$    | $1.486 \times 10^{-3}$ | $1.281 \times 10^{-5}$  |
| 13 | $5.882 \times 10^{-3}$               | $-7.832 \times 10^7$    | $3.809 \times 10^{-3}$               | $-7.833 \times 10^7$    | $3.159 \times 10^{-3}$                | $-7.833 \times 10^7$    | $7.893 \times 10^{-4}$ | $3.497 \times 10^{-6}$  |
| 14 | $2.989 \times 10^{-3}$               | $-1.939 \times 10^7$    | $1.935 \times 10^{-3}$               | $-1.940 \times 10^7$    | $1.605 \times 10^{-3}$                | $-1.939 \times 10^7$    | $4.011 \times 10^{-4}$ | $8.659 \times 10^{-7}$  |
| 15 | $1.440 \times 10^{-3}$               | $-4.260 \times 10^6$    | $9.325 \times 10^{-4}$               | $-4.261 \times 10^6$    | $7.734 \times 10^{-4}$                | $-4.261 \times 10^6$    | $1.932 \times 10^{-4}$ | $1.902 \times 10^{-7}$  |
| 16 | $6.498 \times 10^{-4}$               | $-8.026 \times 10^5$    | $4.209 \times 10^{-4}$               | $-8.028 \times 10^5$    | $3.490 \times 10^{-4}$                | $-8.028 \times 10^5$    | $8.721 \times 10^{-5}$ | $3.584 \times 10^{-8}$  |
| 17 | $2.694 \times 10^{-4}$               | $-1.225 \times 10^5$    | $1.745 \times 10^{-4}$               | $-1.225 \times 10^5$    | $1.447 \times 10^{-4}$                | $-1.225 \times 10^5$    | $3.615 \times 10^{-5}$ | $5.469 \times 10^{-9}$  |
| 18 | $9.907 \times 10^{-5}$               | $-1.349 \times 10^4$    | $6.417 \times 10^{-5}$               | $-1.350 \times 10^4$    | $5.321 \times 10^{-5}$                | $-1.349 \times 10^4$    | $1.330 \times 10^{-5}$ | $6.024 \times 10^{-10}$ |
| 19 | $3.014 \times 10^{-5}$               | $-7.899 \times 10^2$    | $1.952 \times 10^{-5}$               | $-7.902 \times 10^2$    | $1.619 \times 10^{-5}$                | $-7.901 \times 10^2$    | $4.045 \times 10^{-6}$ | $3.527 \times 10^{-11}$ |

Further, a study on how the soil immittance  $\kappa$  should be considered was presented. This immittance relates electromagnetic fields and corresponds to the earth return path of transmission systems. It can usually assume three different values: a constant conductivity; a complex combination between conductivity and permittivity and; the complete model, i.e., a frequency-dependent parameter. For the latter, causal soil models were reviewed and compared.

In the following, rational approximations of two of the models were presented and very interesting results were obtained. Both Smith-Longmire and Alipio-Visacro models present universal relations between its poles and residues, when the rational approximation is considered as a RC network. This allowed for the fitting of exponential functions relating poles and residues to the apparent conductivity value enabling to obtain a rational approximation for any desired conductivity value without having to resort to new fitting calculations. Furthermore, Alipio-Visacro model presents the interesting feature of not changing the poles, i.e., it maintains the relaxation frequencies regardless of conductivity value only varying the residues.

The rational approximation is essential to this research because it improves the representation of frequency-dependent soils, allows for its inclusion on ground return expressions, aids the sensitivity analysis and it represents the soil models as functions of the Laplace variable  $s$ , which is of paramount importance to the implementation of time-domain responses either using recursive convolutions or the Numerical Laplace Transform.

# Chapter 3

## Cable System Modeling

As power systems grow in size and complexity there is an increasing demand on enlarging the transmission links in order to attend consumers and strengthen networks. The usage of cable systems has gained interest in densely populated cities and in the so-called submarine electric power systems, the latter mostly due to offshore oil exploitation and the harnessing of renewable energy sources. The fact of cables systems are buried into something, i.e., land or sea, makes the velocity of the ground return mode smaller than the one of overhead lines.

Single-core coaxial cables (SC-cables) are usually composed by two metallic parts<sup>1</sup>, a core and a sheath. Pipe-type three-phase cables (PT-cables) can be interpreted as the combination of three SC-cables inside a metallic armor, i.e., seven metallic parts in total. The modeling and analysis of a transmission system based on cables is thus far more complicated than the one of overhead lines, due to the quantity of electromagnetic interactions between conductive parts.

This chapter aims to review the inclusion of cable systems on EMT simulation. The voltage and current relations of a cable system is often treated in terms of a modified nodal analysis, that is here recapitulated. However, the assembly of the nodal admittance matrix depends on the characteristic admittance and propagation function, which in turn depend on each cable's impedance and admittance matrices and on the information of how the cable systems are settled.

As the research main interest is the ground influence, special attention is given to ground return quantities, namely, ground return impedance and ground return admittance. For the latter, a novel closed-form expression is presented.

---

<sup>1</sup>It is also possible to consider a metallic armor around each SC-cable, i.e., a third metallic part, separated from the sheath by an insulation layer, but it is not in the scope of this work.

### 3.1 Assembly of Matrices $\mathbf{Z}$ and $\mathbf{Y}$

Pollaczek [50] and Carson [51] presented the pioneer works towards line modeling and ground return characteristics. Later, the coaxial cables electromagnetic theory, strongly dependent on Bessel functions, was developed by Schelkunoff [52]. Wedepohl and Wilcox [53] presented approximations to substitute the Bessel functions and Ametani [26] presented a general formulation for cable's impedance and admittance.

The mathematical representation of cable systems is based on the analysis of the so-called Telegrapher's equations, which in frequency domain can be written as:

$$\begin{aligned} \frac{\partial V}{\partial x} &= -\mathbf{Z} I \\ \frac{\partial I}{\partial x} &= -\mathbf{Y} V \end{aligned} \quad (3.1)$$

where  $\mathbf{Z}$  and  $\mathbf{Y}$  are the  $n \times n$  impedance and admittance matrices, respectively, for a  $n$ -conductor system;  $V$  is the vector of voltages;  $I$  is the vector of currents; and  $x$  is the longitudinal axis in which the cable is analyzed.

In the scope of this research the single core coaxial cable (SC-cable) consisting of core and sheath conductors is considered. Different arrangements considering the three-phase cable system can be utilized and are addressed in a future section. Here the objective is to briefly present the involved impedances and admittances that assemble the respective matrices. Figure 3.1 depicts the SC-cable and the radii of its layers.

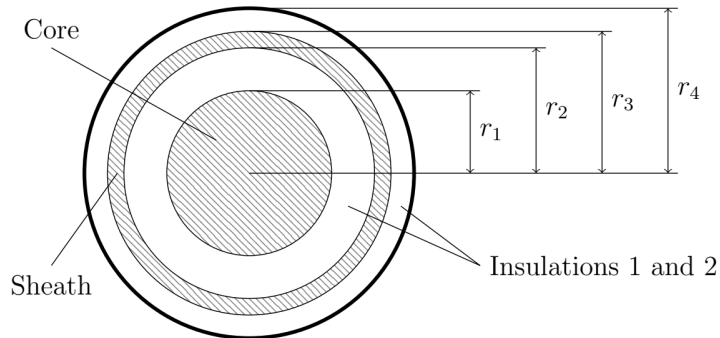


Figure 3.1: Radii of SC-cable layers.

As this type of cable has two conductive parts, the three-phase SC-cable system matrices  $\mathbf{Z}$  and  $\mathbf{Y}$  are actually  $6 \times 6$ . Both self and mutual quantities are determined by  $2 \times 2$  blocks in order to contemplate the interactions between core and sheath. Three basic assumptions are made [54]: homogeneous system; ideal isotropic materials, with constant resistivity, permittivity and permeability; and longitudinal currents in insulation negligible compared to the ones in conductors.

Considering the radii of cable layer depicted in Fig. 3.1, seven different per-unit-length impedances are represented [52, 53] and are listed below. For more details, see Appendix B.

$z_1$ : the inner impedance of the core.

$z_2$ : the impedance due to time-varying magnetic field in insulation 1, i.e., between core and sheath.

$z_3$ : the inner sheath internal impedance.

$z_4$ : the sheath mutual impedance.

$z_5$ : the outer sheath internal impedance.

$z_6$ : the impedance due to time-varying flux in insulation 2, i.e., between sheath and the earth.

$z_0$ : the self impedance of earth return path, so-called ground return impedance. The expression regarding this impedance will be addressed in a future section. At this point is suffice to acknowledge that this self impedance is a function of the external radius  $r_4$ , the depth the cable is buried in and the soil propagation constant, which, likewise core and sheath, depends on its resistivity.

The  $2 \times 2$  self impedance matrix is then assembled, without the ground return impedance:

$$\mathbf{Z}_{self} = \begin{bmatrix} z_1 + z_2 + z_3 - 2z_4 + z_5 + z_6 & -z_4 + z_5 + z_6 \\ -z_4 + z_5 + z_6 & z_5 + z_6 \end{bmatrix} \quad (3.2)$$

and the three-phase  $6 \times 6$  impedance matrix  $\mathbf{Z}_{in}$  is thus:

$$\mathbf{Z}_{in} = \begin{bmatrix} \mathbf{Z}_{self} & \mathbf{0}_{2 \times 2} & \mathbf{0}_{2 \times 2} \\ \mathbf{0}_{2 \times 2} & \mathbf{Z}_{self} & \mathbf{0}_{2 \times 2} \\ \mathbf{0}_{2 \times 2} & \mathbf{0}_{2 \times 2} & \mathbf{Z}_{self} \end{bmatrix} \quad (3.3)$$

where  $\mathbf{0}_{2 \times 2}$  are  $2 \times 2$  matrices with all elements equal to zero.

The ground return impedance matrix  $\mathbf{Z}_g$  is also  $6 \times 6$  and built with  $2 \times 2$  blocks. For each cable, self blocks  $\mathbf{Z}_{s_i}$  are  $2 \times 2$  matrices with all elements equal to  $z_0$  calculated considering the respective depths. The mutual blocks  $\mathbf{Z}_{m_{ij}}$  are  $2 \times 2$  matrices with all elements equal to the mutual version of  $z_0$ , i.e., the ground return mutual impedance  $z_{ij}$  between the  $i$ -th and the  $j$ -th cables:

$$\mathbf{Z}_{s_i} = \begin{bmatrix} z_0 & z_0 \\ z_0 & z_0 \end{bmatrix} \text{ and } \mathbf{Z}_{m_{ij}} = \begin{bmatrix} z_{ij} & z_{ij} \\ z_{ij} & z_{ij} \end{bmatrix} \quad (3.4)$$

and  $\mathbf{Z}_g$  is assembled as:

$$\mathbf{Z}_g = \begin{bmatrix} \mathbf{Z}_{s_1} & \mathbf{Z}_{m_{12}} & \mathbf{Z}_{m_{13}} \\ \mathbf{Z}_{m_{21}} & \mathbf{Z}_{s_2} & \mathbf{Z}_{m_{23}} \\ \mathbf{Z}_{m_{31}} & \mathbf{Z}_{m_{32}} & \mathbf{Z}_{s_3} \end{bmatrix} \quad (3.5)$$

where  $\mathbf{Z}_{m_{ij}} = \mathbf{Z}_{m_{ji}}$ . Hence, the three-phase cable system impedance matrix is obtained as:

$$\mathbf{Z} = \mathbf{Z}_{in} + \mathbf{Z}_g \quad (3.6)$$

The procedure to assemble the shunt admittance matrix is rather similar but simpler, since only two per-unit-length admittances are considered inside the cable, i.e.,  $y_1$  and  $y_2$ , regarding the leakage conductance and the capacitance of both insulation parts indicated in Fig. 3.1. The earth return admittance  $y_0$ , aside Sunde's development in [55], was typically neglected [26, 50, 53]. More recently, anew interest was given to the ground return admittance [56–60]. As the main interest at this point is to review the assembly of the admittance matrix, details about the formulation will be given in a future section.

The structure is also based on  $2 \times 2$  blocks to be joined in a  $6 \times 6$  matrix that represents the three-phase system. The  $2 \times 2$  self admittance matrix is assembled, without the ground return admittance as:

$$\mathbf{Y}_{self} = \begin{bmatrix} y_1 & -y_1 \\ -y_1 & y_1 + y_2 \end{bmatrix} \quad (3.7)$$

where  $y_1$  and  $y_2$  consider the conductances and the capacitances of, respectively, insulations 1 and 2 (see Appendix B). The three-phase  $6 \times 6$  admittance matrix  $\mathbf{Y}_{in}$  is then:

$$\mathbf{Y}_{in} = \begin{bmatrix} \mathbf{Y}_{self} & \mathbf{0}_{2 \times 2} & \mathbf{0}_{2 \times 2} \\ \mathbf{0}_{2 \times 2} & \mathbf{Y}_{self} & \mathbf{0}_{2 \times 2} \\ \mathbf{0}_{2 \times 2} & \mathbf{0}_{2 \times 2} & \mathbf{Y}_{self} \end{bmatrix} \quad (3.8)$$

where  $\mathbf{0}_{2 \times 2}$  are  $2 \times 2$  matrices with all elements equal to zero.

The ground return admittance matrix  $\mathbf{Y}_g$  is also  $6 \times 6$  and assembled with  $2 \times 2$  blocks. Like  $\mathbf{Z}_g$ , self blocks  $\mathbf{Y}_{s_i}$  are  $2 \times 2$  matrices with all elements equal to the self ground return admittance  $y_0$  calculated considering each cable depth. The mutual blocks  $\mathbf{Y}_{m_{ij}}$  are  $2 \times 2$  matrices with all elements equal to the ground return mutual admittance  $y_{ij}$  between the  $i$ -th and the  $j$ -th cables:

$$\mathbf{Y}_{s_i} = \begin{bmatrix} y_0 & y_0 \\ y_0 & y_0 \end{bmatrix} \text{ and } \mathbf{Y}_{m_{ij}} = \begin{bmatrix} y_{ij} & y_{ij} \\ y_{ij} & y_{ij} \end{bmatrix} \quad (3.9)$$

and  $\mathbf{Y}_g$  is assembled as:

$$\mathbf{Y}_g = \begin{bmatrix} \mathbf{Y}_{s_1} & \mathbf{Y}_{m_{12}} & \mathbf{Y}_{m_{13}} \\ \mathbf{Y}_{m_{21}} & \mathbf{Y}_{s_2} & \mathbf{Y}_{m_{23}} \\ \mathbf{Y}_{m_{31}} & \mathbf{Y}_{m_{32}} & \mathbf{Y}_{s_3} \end{bmatrix} \quad (3.10)$$

where  $\mathbf{Y}_{m_{ij}} = \mathbf{Y}_{m_{ji}}$ . Hence, the three-phase cable system admittance matrix is obtained as:

$$\mathbf{Y} = [\mathbf{Y}_{in}^{-1} + \mathbf{Y}_g^{-1}]^{-1} \quad (3.11)$$

where  $\mathbf{Y}_g^{-1}$  is considered by assembling a shunt impedance matrix  $\mathbf{Z}_{shunt}$ , as it will be addressed in Section 3.4.

Regarding the PT-cable, it is interpreted as one cable with an external metallic armor that wraps three SC-cables. Therefore, one main difference in the modeling is that an extra row and an extra column are added in all matrices involved in equations (3.6) and (3.11), so that the interactions between the three SC-cables and the armor are taken into account. Also, as the ground return quantities represent the interaction of the outermost layer with soil, only the armor of the pipe interacts and, thus, the matrix  $\mathbf{Z}_g$  is written as:

$$\mathbf{Z}_g = \begin{bmatrix} Z_g & \cdots & Z_g \\ \vdots & \ddots & \vdots \\ Z_g & \cdots & Z_g \end{bmatrix}_{7 \times 7} = Z_g \begin{bmatrix} 1 & \cdots & 1 \\ \vdots & \ddots & \vdots \\ 1 & \cdots & 1 \end{bmatrix}_{7 \times 7}, \quad (3.12)$$

and matrix  $\mathbf{Z}_{shunt}$  obeys the same rules.

## 3.2 Typical Cable Systems Configurations

As the ground return quantities are the ones affected by soil resistivity, the characteristics of typical cable system configurations and their ground return impedance matrices are here presented. For the sake of clarity, their ground return

admittance matrices obey the same formation logic. Fig. 3.2 presents different arrangements of single-core coaxial cables (SC-cables), considering the core and the metallic sheath as the conductor parts. Medium 1 is considered to be the soil and Medium 2 the air. The ground return impedance matrix is given by (3.5).

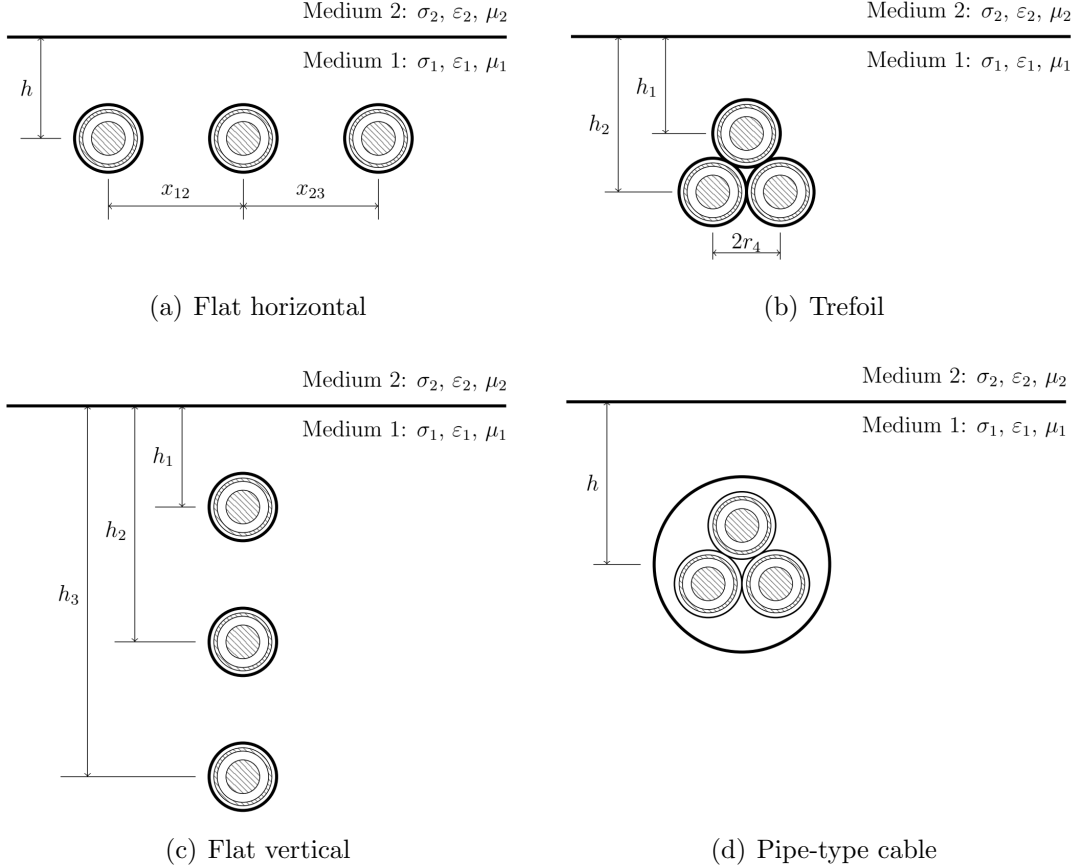


Figure 3.2: Configurations of cables systems.

Figure 3.2 (a) depicts the cable system with a horizontal flat configuration. In this case, it is possible to affirm that all self ground return impedances are the same, i.e.,  $\mathbf{Z}_{s1} = \mathbf{Z}_{s2} = \mathbf{Z}_{s3} = \mathbf{Z}_s$ , for its depths are the same. However, two different mutual ground return impedances,  $\mathbf{Z}_{m1}$  (between center and the extremity cables, individually) and  $\mathbf{Z}_{m2}$  (between extremity cables) exist, because the distance between the center cable to the others is equal in both situations. Therefore, in (3.5),  $\mathbf{Z}_{m12} = \mathbf{Z}_{m23} = \mathbf{Z}_{m1}$  and  $\mathbf{Z}_{m13} = \mathbf{Z}_{m2}$ .

Figure 3.2 (b) shows the cable system with a trefoil configuration. In this case, one of the cables is less buried than the others, therefore, there exists two different self ground return impedance values, i.e.,  $\mathbf{Z}_{s1}$  and  $\mathbf{Z}_{s2} = \mathbf{Z}_{s3}$ . Also, the distance between the three cables are the same, so the mutual ground return impedance is the same, i.e.,  $\mathbf{Z}_{m12} = \mathbf{Z}_{m13} = \mathbf{Z}_{m23} = \mathbf{Z}_m$ .

Figure 3.2 (c) presents the cable system with a vertical flat configuration. In this case all the cables are in the same horizontal position. As they all are buried in different depths, different self ground return impedances are obtained, i.e.,  $\mathbf{Z}_{s1} \neq \mathbf{Z}_{s2} \neq \mathbf{Z}_{s3}$ . Also, different mutual ground return impedances,  $Z_{m1}$  (between center and extremity) and  $Z_{m2}$  (between upper and lower cables), are found, i.e.,  $\mathbf{Z}_{m12} = \mathbf{Z}_{m23} = \mathbf{Z}_{m1}$  and  $\mathbf{Z}_{m13} = \mathbf{Z}_{m2}$ .

Figure 3.2 (d) presents the pipe-type three-phase cable. As already stated in the previous Section, all terms of matrices  $\mathbf{Z}_g$  and  $\mathbf{Y}_g$  have the same values  $Z_g$  and  $Y_g$ , respectively, regardless of the inside cables positions.

### 3.3 Voltage and Current Relations

Even though it is possible to apply (3.6) and (3.11) in (3.1), a more practical approach is to use  $\mathbf{Z}$  and  $\mathbf{Y}$  to determine the frequency domain voltages and currents at cable system ends, or nodes, by means of the modified nodal analysis [61], considering the three-phase system nodes as depicted in Fig 3.3. Once obtained, time-domain voltages and currents can be found by using the Numerical Laplace Transform [40–42].

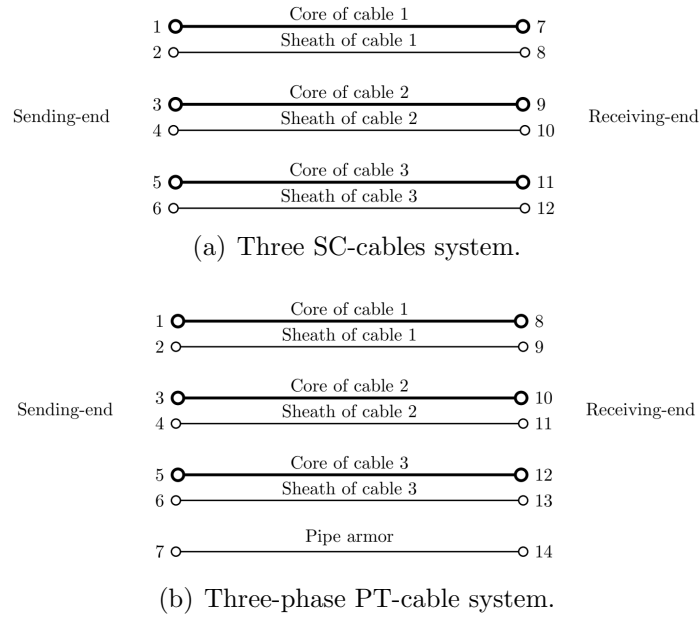


Figure 3.3: Nodes considered for typical cable systems.

The modified nodal analysis approach is represented by the frequency domain matrix equation:

$$\begin{bmatrix} \mathbf{I}_{in} \\ \mathbf{V}_{in} \end{bmatrix} = \begin{bmatrix} \mathbf{Y}_n & \mathbf{D} \\ \mathbf{D}^T & \mathbf{0} \end{bmatrix} \begin{bmatrix} \mathbf{V}_{out} \\ \mathbf{I}_{out} \end{bmatrix} \quad (3.13)$$

where  $\mathbf{I}_{in}$  are current sources,  $\mathbf{V}_{in}$  are voltage sources,  $\mathbf{I}_{out}$  and  $\mathbf{V}_{out}$  are the variables to be calculated,  $\mathbf{Y}_n$  is the cable system nodal admittance matrix,  $\mathbf{D}$  is a matrix that each column represents the from-to node connections that each voltage source  $\mathbf{V}_{in}$  is placed in the circuit and  $T$  indicates the transposed matrix. The whole system of (3.13) is of order  $(2n + ns) \times (2n + ns)$ , where  $n$  is the number of conductors and  $ns$  represents the number of voltage sources considered for evaluation.

Regarding the nodal admittance matrix of the cable system itself, it depends on the two transfer matrices presented below, namely, the characteristic admittance  $\mathbf{Y}_c$  and the propagation function, also called voltage deformation matrix,  $\mathbf{H}_c$ :

$$\mathbf{Y}_c = \mathbf{Z}^{-1} \sqrt{\mathbf{Z}\mathbf{Y}} \quad (3.14)$$

$$\mathbf{H}_c = \exp\left(-\ell \sqrt{\mathbf{Z}\mathbf{Y}}\right) \quad (3.15)$$

where  $\ell$  is the cable system length.  $\mathbf{Y}_n$  is then given by:

$$\mathbf{Y}_n = \begin{bmatrix} \mathbf{Y}_c (\mathbf{U} + \mathbf{H}_c^2) (\mathbf{U} - \mathbf{H}_c^2)^{-1} & -2\mathbf{Y}_c (\mathbf{U} - \mathbf{H}_c^2)^{-1} \\ -2\mathbf{Y}_c (\mathbf{U} - \mathbf{H}_c^2)^{-1} & \mathbf{Y}_c (\mathbf{U} + \mathbf{H}_c^2) (\mathbf{U} - \mathbf{H}_c^2)^{-1} \end{bmatrix} \quad (3.16)$$

and  $\mathbf{U}$ , for a three-phase cable system considering core and sheath, is a  $6 \times 6$  identity matrix.

### 3.4 Novel Expression for Ground Admittance

Assuming quasi-TEM propagation and considering the wire voltage to ground definition [3, 58]:

$$V = - \int_0^{h-r} E_z dz = \phi(0, h-r) - \phi(0, 0) + j\omega \int_0^{h-r} A_z(0, \xi) d\xi \quad (3.17)$$

where  $z$  is the vertical axis pointing to the cable's depth,  $E_z$  is the  $z$ -component of the electric field,  $r$  is the radius,  $h$  is the depth,  $\phi$  is the electric scalar potential and  $A_z$  is the  $z$ -component of the magnetic vector potential, the ground return impedance and admittance matrices can be written as [3, 58]:

$$\mathbf{Z}_g = \frac{j\omega\mu_1}{2\pi} [\mathbf{\Lambda} + \mathbf{S}] \quad (3.18)$$

$$\mathbf{Y}_g = 2\pi(\sigma_1 + j\omega\varepsilon_1) [\mathbf{\Lambda} - \mathbf{T}]^{-1} \quad (3.19)$$

where  $\mu_1$ ,  $\sigma_1$  and  $\varepsilon_1$  are the soil parameters and, typically,  $\mu_1 = \mu_0$ . The elements in  $\mathbf{\Lambda}$ ,  $\mathbf{S}$  and  $\mathbf{T}$  are, respectively,

$$\Lambda_{ij} = K_0(d_{ij}\gamma_1) - K_0(D_{ij}\gamma_1) \quad (3.20)$$

$$S_{ij} = \int_{-\infty}^{\infty} \frac{e^{-(h_i+h_j)u_1}}{u_1 + u_2} e^{-x_{ij}\lambda} d\lambda \quad (3.21)$$

$$T_{ij} = \int_{-\infty}^{\infty} \frac{u_1}{u_2} \frac{e^{-(h_i+h_j)u_1/2} - e^{-(h_i+h_j)u_1}}{n^2u_1 + u_2} e^{-x_{ij}\lambda} d\lambda \quad (3.22)$$

being  $K_0$  the modified Bessel function of second kind and order zero,  $n = \gamma_2/\gamma_1$ ,  $u_1 = \sqrt{\lambda^2 + \gamma_1^2}$ ,  $u_2 = \sqrt{\lambda^2 + \gamma_2^2}$ ,  $d_{ij} = \sqrt{(h_i - h_j)^2 + x_{ij}^2}$ , and  $D_{ij} = \sqrt{(h_i + h_j)^2 + x_{ij}^2}$ .

Eq. (3.18) is essentially the same expression as proposed by Pollaczek [50] and Carson [51] almost one hundred years ago, while (3.19) was proposed more recently [58, 59] based on a quasi-TEM approximation of a full-wave formulation between the conductor voltage with respect to ground and the injected current.

The main drawback in using (3.18) and (3.19) lies in the numerical evaluation of the so-called Sommerfeld integrals in (3.21) and (3.22) as they present a highly oscillatory kernel and time-consuming Gauss quadrature rules must be used, see [56, 57, 62]. One way to overcome such difficulty is to use approximate formulae for the integrals. Regarding overhead lines, different formulations with approximations were proposed in [63]. As for the underground cable systems, closed-form approximations were largely considered for evaluating the ground return impedance [4, 53, 64]. As for the ground return admittance, given that EMTP-type programs typically use Pollaczek formulation [50] for the calculation of the per-unit-length parameters, the common hypothesis is to consider long cables and good conductor soil, so earth return admittance is neglected. However, recent works have studied the earth return admittance contribution in underground system modeling [57, 59, 60].

The closed-form expression of the ground return impedance considered in the development of this work was proposed in [4] and is given by

$$Z_{ij} = \frac{j\omega\mu}{2\pi} \left[ K_0(\gamma_1 d) + \frac{\ell^2 - x^2}{D^2} K_2(\gamma_1 D) - 2 \frac{\ell^2 - x^2}{\gamma_1^2 D^4} (1 + \ell\gamma_1) \exp(-\ell\gamma_1) \right] \quad (3.23)$$

where  $d$ ,  $D$ ,  $\gamma_1$  and  $K(\cdot)$  are the same as before,  $\ell = h_1 + h_2$  each  $Z_{ij}$  represents the mutual terms of (3.5). The self terms are calculated by considering  $\ell = 2h$  and  $x = r$ , being  $h$  the cable's depth and  $r$  its outermost radius. For more details, see

## Appendix B.

Since the earth return admittance plays an important role on underground cable systems, even more as shorter cables in highly resistive soils are considered [59], a closed-form expression for ground admittance is also desirable. This section derives an expression for the ground return admittance matrix suited for frequency and time domain simulations, regarding underground cable systems, and without having to resort to time consuming computation [5].

Considering  $\mathbf{T}$  in (3.19), it is possible to use a series expansion as the integral decays rapidly with  $\lambda$  [65, 66]. Thus a closed-form approximation can be obtained if it is assumed that

$$\frac{u_1}{n^2 u_1 + u_2} \approx \frac{\gamma_1^2}{u_1 (\gamma_1^2 + \gamma_2^2)} \quad (3.24)$$

which is a suitable approximation as long as  $|\gamma_2| \ll |\gamma_1|$ , typically the case for underground cables.

By applying (3.24) in (3.22), it is possible to obtain a closed-form expression by considering the leading term of the series expansion of the approximated integral [65, 66] as presented in (3.25). Thus the elements in  $\mathbf{T} \approx \overline{\mathbf{T}}$  where

$$\overline{T}_{ij} = \frac{2\gamma_1^2}{\gamma_1^2 + \gamma_2^2} \ln \left[ \frac{2\gamma_2^2 + \gamma_1^2 \left( 2 + \gamma_2 \sqrt{(h_i + h_j)^2 + x_{ij}^2} \right)}{\gamma_2^2 + \gamma_1^2 \left( 1 + \gamma_2 \sqrt{(h_i + h_j)^2 + x_{ij}^2} \right)} \right] \quad (3.25)$$

As the calculation of  $\mathbf{Y}_g$  depends on the inverse of the term  $[\mathbf{\Lambda} - \mathbf{T}]$ , one can write the closed-form expression for the terms of a shunt impedance matrix  $\mathbf{Z}_{shunt}$ :

$$Z_{shunt_{ij}} = \frac{K_0(\gamma_1 d) + K_0(\gamma_1 D) - \frac{2\gamma_1^2}{\gamma_1^2 + \gamma_2^2} \ln \left[ \frac{2\gamma_2^2 + \gamma_1^2 \left( 2 + \gamma_2 \sqrt{(h_i + h_j)^2 + x_{ij}^2} \right)}{\gamma_2^2 + \gamma_1^2 \left( 1 + \gamma_2 \sqrt{(h_i + h_j)^2 + x_{ij}^2} \right)} \right]}{2\pi(\sigma_1 + j\omega\varepsilon_1)} \quad (3.26)$$

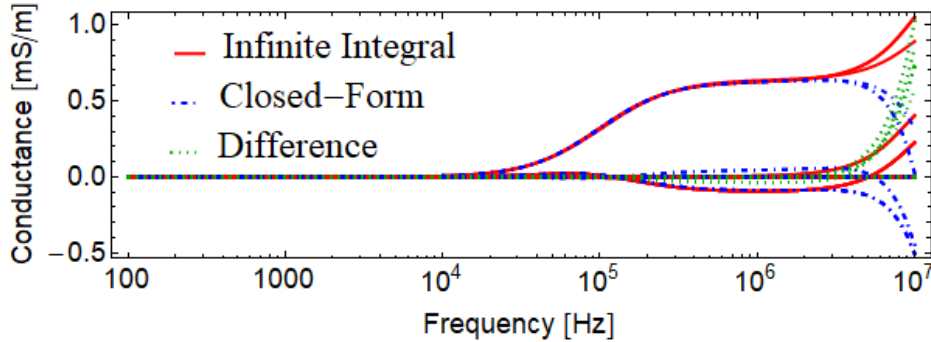
and then include it on (3.11) as  $\mathbf{Y} = [\mathbf{Y}_{in}^{-1} + \mathbf{Z}_{shunt}]^{-1}$ .

To validate the proposed expression, some results are presented regarding the cable system of Fig. 3.2 (a), with ground resistivity  $1000 \Omega \cdot \text{m}$  and relative permittivity 10, i.e., considering  $\kappa_2 = (1/1000) + j10\omega\varepsilon_0$ . The complete admittance in frequency-domain, i.e., conductance and capacitance, is presented, as well as the respective modal characteristic admittance and modal propagation function. The whole system was simulated using the Wolfram Language considering Modified Nodal Analysis and time responses are obtained via the Numerical Laplace Transform.

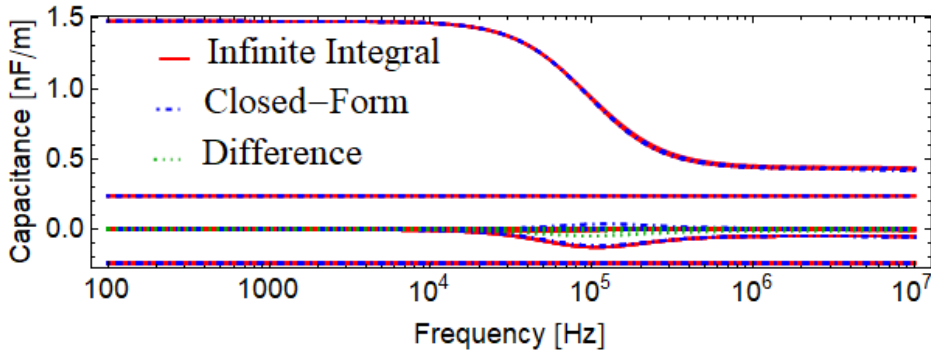
Figure 3.4 shows the elements of the per unit length conductance and capacitance for the cable system and Fig. 3.5 depicts the comparisons for modal characteristic admittance and modal propagation functions. The results using closed-form expressions are very close to those obtained by the infinite integrals. The mismatches are more pronounced for mutual elements in the conductance matrix for frequencies above 3 MHz. It is worth mentioning that when considering higher values for  $\rho_0$ , the mismatches for the conductance should happen at lower frequencies, but regarding the capacitance there is negligible differences.

Regarding time-domain validation, several circuits were studied and, although not presented, similar results were obtained for all performed tests. Results are shown here for inter-sheath and ground modes excitation schemes as depicted in Fig. 3.6 and the inter-sheath mode excitation scheme of a simple 1.5 km cross-bonded system divided in three 500 m sections, depicted in Fig. 3.7.

For all cases, voltages at the receiving-end of the core of cable 1 are presented in Figures 3.8, 3.9 and 3.10, considering ground resistivity of  $1000 \Omega \cdot \text{m}$  and  $3000 \Omega \cdot \text{m}$ . Both the agreement between the closed-form formulation with the infinite integral (less than 2% mismatches between formulations) and the fact that earth return admittance affects the results can be observed.

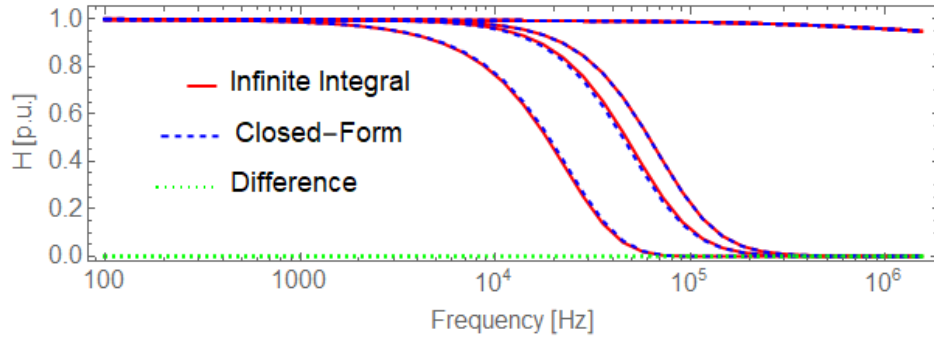


(a) Conductance.

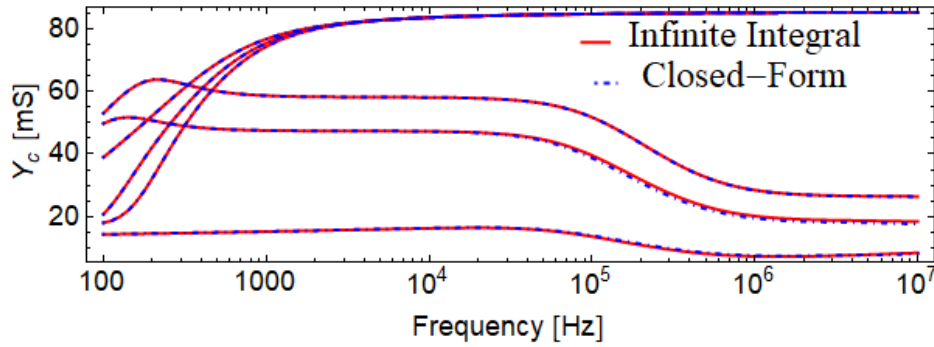


(b) Capacitance.

Figure 3.4: Conductance and capacitance of cable system.

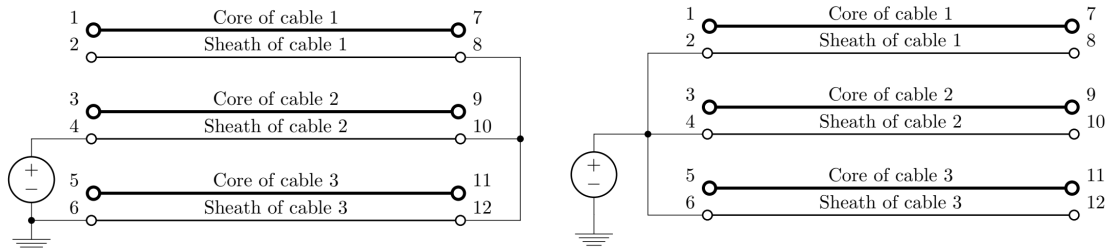


(a)  $\mathbf{H}_{modal}$



(b)  $\mathbf{Y}_{cmodal}$

Figure 3.5: Modal propagation function and characteristic admittance.



(a) Inter-sheath mode.

(b) Ground mode.

Figure 3.6: Excitation schemes.

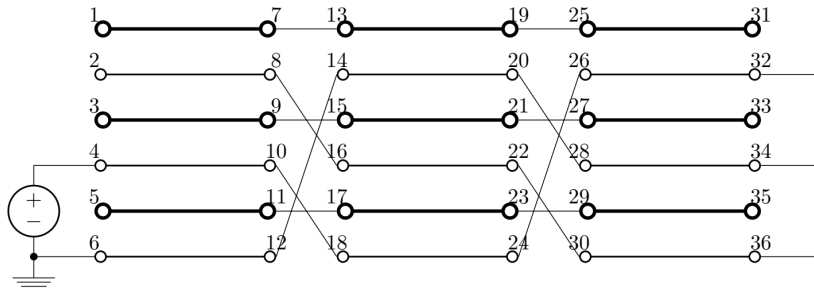
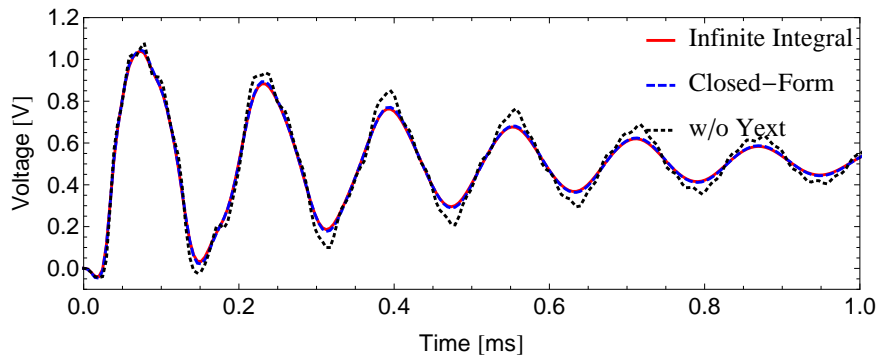
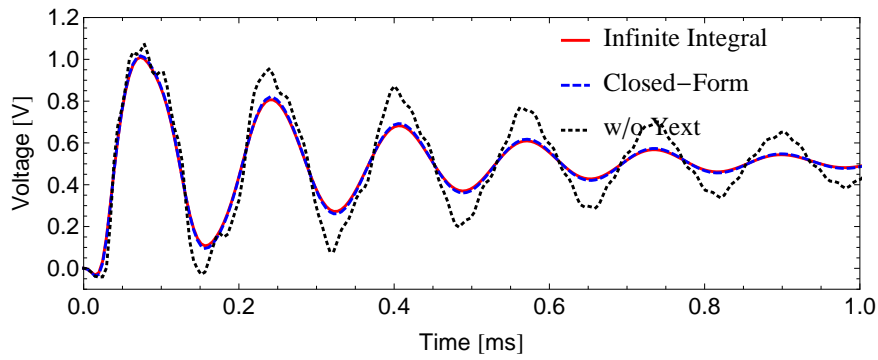


Figure 3.7: Cross-bonding inter-sheath excitation scheme.

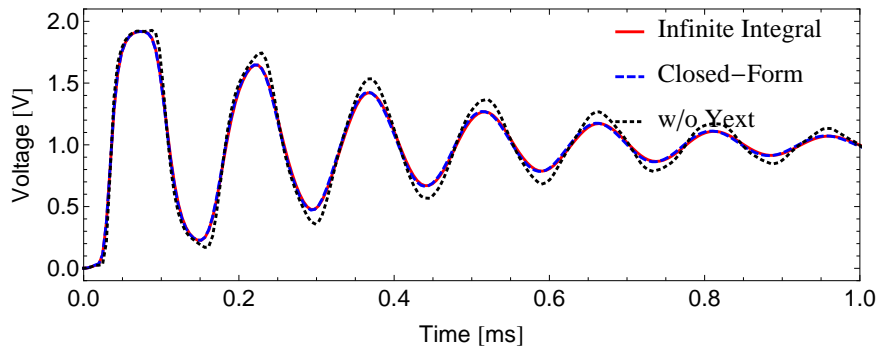


(a)  $\rho_g = 1000 \Omega \cdot \text{m}$ .

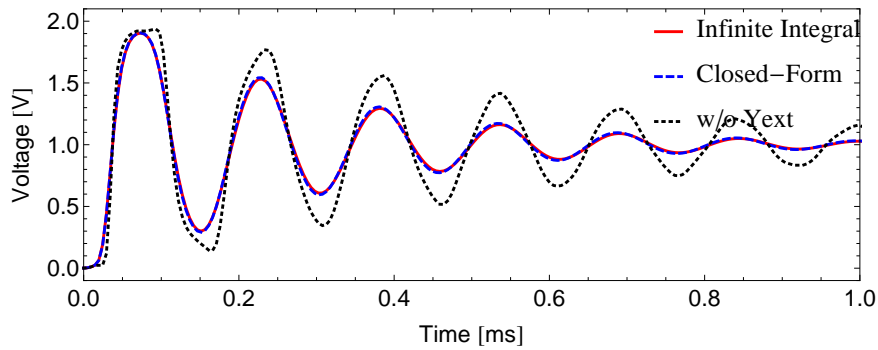


(b)  $\rho_g = 3000 \Omega \cdot \text{m}$ .

Figure 3.8: Voltage at terminal 7 – excitation of intersheath mode.

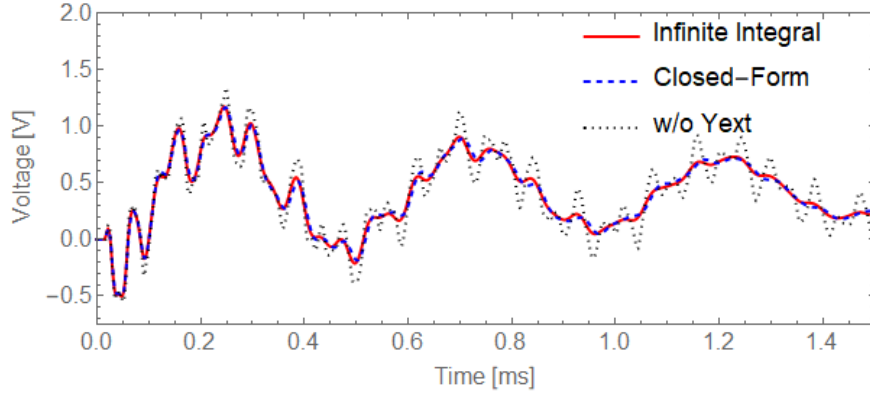


(a)  $\rho_g = 1000 \Omega \cdot \text{m}$ .

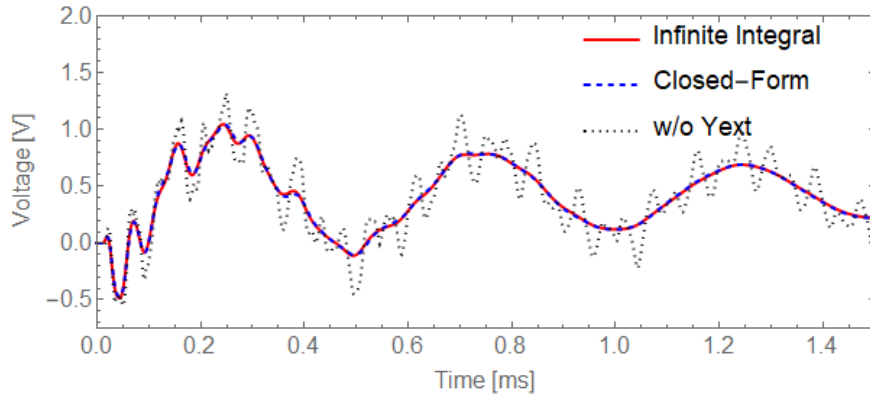


(b)  $\rho_g = 3000 \Omega \cdot \text{m}$ .

Figure 3.9: Voltage at terminal 7 – excitation of ground mode.



(a)  $\rho_g = 1000 \Omega \cdot \text{m}$ .



(b)  $\rho_g = 3000 \Omega \cdot \text{m}$ .

Figure 3.10: Voltage at terminal 31 – cross-bonded cable system.

The simulations were evaluated in Wolfram Mathematica platform using the Gauss-Kronrod integration scheme. All the simulations were run on an Intel Core i7-4790 CPU @ 3.60GHz machine with 4.0GB RAM; for simulations, the total computation time using infinite integrals took roughly 390 s while using closed-form expression it took less than 1.8 s, considering the same number of samples.

### 3.5 Natural Modes of Propagation

A straightforward manipulation of (3.1) should lead to the writing of those wave equations in terms of only the voltage or the current:

$$\begin{aligned} \frac{\partial^2 V}{\partial x^2} &= \mathbf{ZY} V \\ \frac{\partial^2 I}{\partial x^2} &= \mathbf{YZ} I \end{aligned} \quad (3.27)$$

where  $\mathbf{ZY} = (\mathbf{YZ})^T$ .

Since the matrix multiplication  $\mathbf{ZY}$  results in a dense matrix, a rather interesting approach is to carry a decoupled analysis. This is done by decomposing the matrix in

eigenvalues and eigenvectors, i.e., by carrying a modal analysis. The modal voltages and currents,  $V_m$  and  $I_m$  respectively, are obtained by:

$$\begin{aligned} V &= \mathbf{T}_V V_m \\ I &= \mathbf{T}_I I_m \end{aligned} \quad (3.28)$$

where  $\mathbf{T}_V$  and  $\mathbf{T}_I$  are the transformation matrices. Further, they are dense matrices with rank  $n$  that do not depend on the circuit length and, except for very simple cases,  $\mathbf{T}_V \neq \mathbf{T}_I$ . Also,  $\mathbf{T}_V$  contains the voltage eigenvectors and  $\mathbf{T}_I$  contains the current eigenvectors.

By applying (3.28) in (3.27), one gets:

$$\begin{aligned} \frac{\partial^2 \mathbf{T}_V V_m}{\partial x^2} &= \mathbf{Z} \mathbf{Y} \mathbf{T}_V V_m \\ \frac{\partial^2 \mathbf{T}_I I_m}{\partial x^2} &= \mathbf{Y} \mathbf{Z} \mathbf{T}_I I_m \end{aligned} \quad (3.29)$$

and, therefore,

$$\begin{aligned} \frac{\partial^2 V_m}{\partial x^2} &= \mathbf{T}_V^{-1} \mathbf{Z} \mathbf{Y} \mathbf{T}_V V_m \\ \frac{\partial^2 I_m}{\partial x^2} &= \mathbf{T}_I^{-1} \mathbf{Y} \mathbf{Z} \mathbf{T}_I I_m \end{aligned} \quad (3.30)$$

The decoupled system is obtained when  $\mathbf{T}_V^{-1} \mathbf{Z} \mathbf{Y} \mathbf{T}_V = \mathbf{T}_I^{-1} \mathbf{Y} \mathbf{Z} \mathbf{T}_I = \mathbf{\Lambda}$ , with  $\mathbf{\Lambda}$  a diagonal matrix composed by the system eigenvalues  $\lambda_i$ . This means that the whole  $6 \times 6$  three-phase cable system can now be represented by 6 single-phase systems. If a comparison between this formulation and the single-phase line is made, one should note that the propagation constants  $\gamma_i$  are related to the eigenvalues as  $\gamma_i = \sqrt{\lambda_i}$ .

These  $\gamma_i$  represent the 6 natural modes of propagation for the the  $6 \times 6$  three-phase cable system and are described as: 1 ground mode, 2 inter-sheath modes and 3 coaxial modes. Similar approach can be used to evaluate the propagation modes on a pipe-type cable system. In this case, there are 7 modes of propagation: 1 ground mode, 3 inter-sheath modes and 3 coaxial modes. Either way, these modes might be assessed by investigating the real part of the transformation matrix  $\mathbf{T}_I$ , by rotating the eigenvectors in order to minimize its imaginary parts [3, 54, 67]. Additional information and analysis of the pipe-type cable modes can be found in [68].

Furthermore, each propagation constant is a frequency-dependent complex quantity given by:

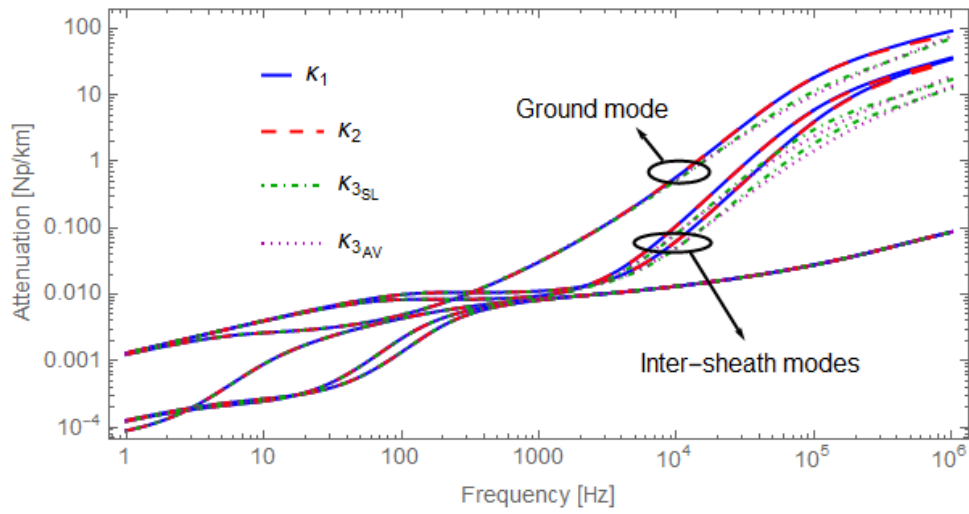
$$\gamma_i = \alpha_i + j\beta_i \quad (3.31)$$

where  $\alpha_i$  and  $\beta_i$  represent, respectively, each mode attenuation in [Np/km] and phase shift in [rad/km]. With  $\beta_i$  it is also possible to obtain each mode propagation velocity:

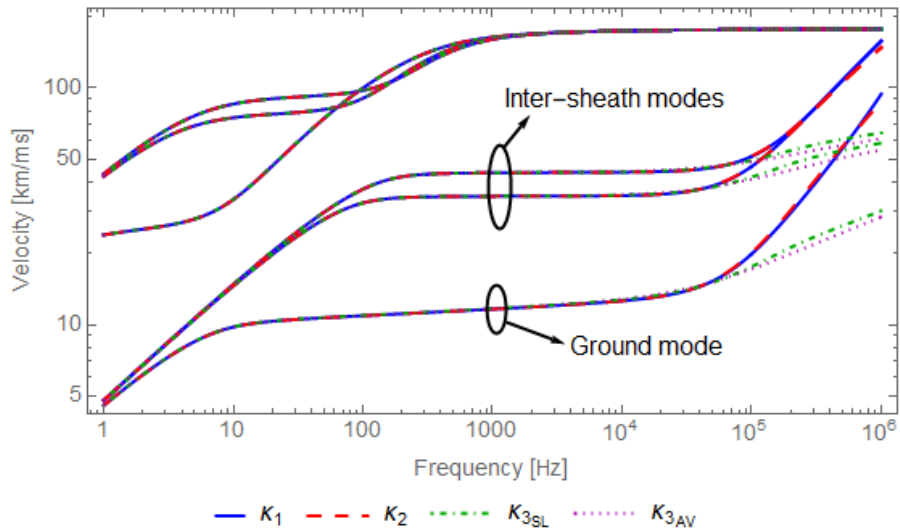
$$\nu_i = \frac{\omega}{\beta_i} \quad (3.32)$$

where  $\nu_i$  is the mode velocity in [km/ms] and  $\omega = 2\pi f$  is the angular frequency in [rad/s].

An illustration of the impact of frequency dependence of the soil model on the modes of propagation is presented in Fig. 3.11.



(a) Modes attenuation



(b) Modes velocity

Figure 3.11: Comparison of modes attenuation and velocity regarding frequency dependence.  $\kappa_1 = \sigma_0 = 1/\rho_0$ ,  $\kappa_2 = \sigma_0 + j\omega\varepsilon_\infty$ ,  $\kappa_{3_{SL}}$  considers Smith-Longmire model, and  $\kappa_{3_{AV}}$  considers Alipio-Visacro model.

This is a first application of the rational models obtained in Section 2.4 and the ground return admittance closed-form expression presented in Section 3.4. The soil is considered with  $\rho_0 = 3000 \Omega \cdot \text{m}$  and  $\varepsilon_\infty = 20 \varepsilon_0$ . Other values of soil resistivity and permittivity were considered and are not presented here because the qualitative analysis is essentially the same. It is possible to note that inter-sheath and ground modes are the ones affected by soil's frequency dependence, while coaxial modes remain unaltered. When comparing modes obtained with  $\kappa_1$  and  $\kappa_2$ , little differences are observed, and only at higher frequencies where the  $\omega\varepsilon$  term in the same order of the conductivity, as seen in Chapter 2.

The major differences are found when the frequency dependence of the resistivity and the permittivity are taken into account. Regarding modes attenuation, differences are not observed at frequencies as low as 3 kHz and for higher frequencies the differences are not very large. As the considered cables are insulated, the modes are less attenuated when considering frequency dependence [58]. Nevertheless, with the inclusion of frequency-dependent soils there is a possibility of resonances that could lead to greater overvoltages. As for the modes velocities, ground and inter-sheath modes become slower at frequencies above 50 kHz.

It is worth mentioning that for frequencies above approximately 1.6 MHz there are numerical issues related to the implementation of the Bessel functions  $K_0$  and  $K_1$  on version 11.3 of Wolfram Mathematica<sup>®</sup>, as depicted in Fig. 3.12. By considering numerical implementation of said functions regarding series expansion [69], it was possible to obtain results depicted in Fig. 3.13. They show that frequency-dependent models (SL and AV) present higher attenuation in the ground mode near 2 MHz and above and also a growing difference between modes velocities.

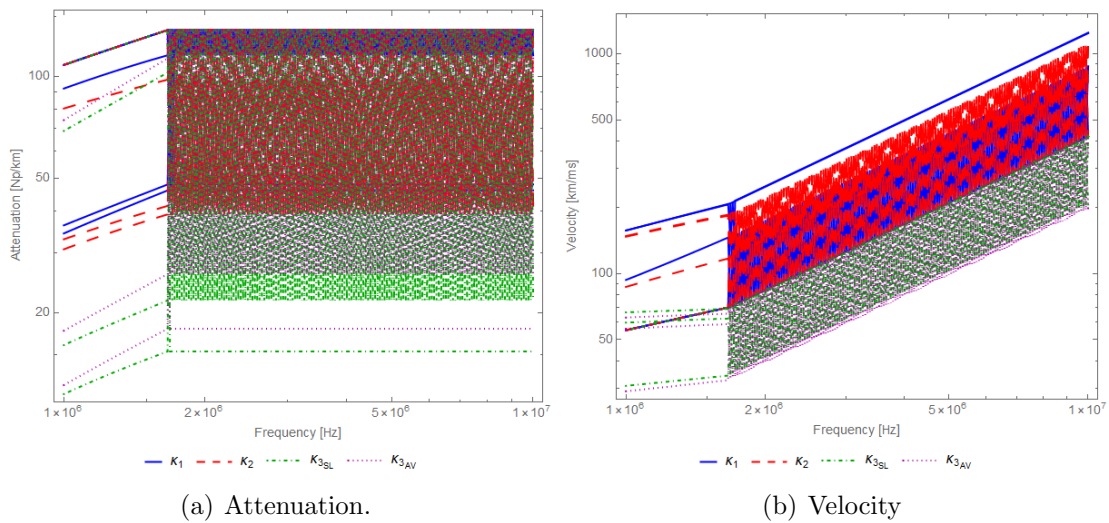


Figure 3.12: Numerical issues related to modes propagation calculation above 1.6 MHz.  $\kappa_1 = \sigma_0 = 1/\rho_0$ ,  $\kappa_2 = \sigma_0 + j\omega\varepsilon_\infty$ ,  $\kappa_{3_{SL}}$  considers Smith-Longmire model, and  $\kappa_{3_{AV}}$  considers Alipio-Visacro model.

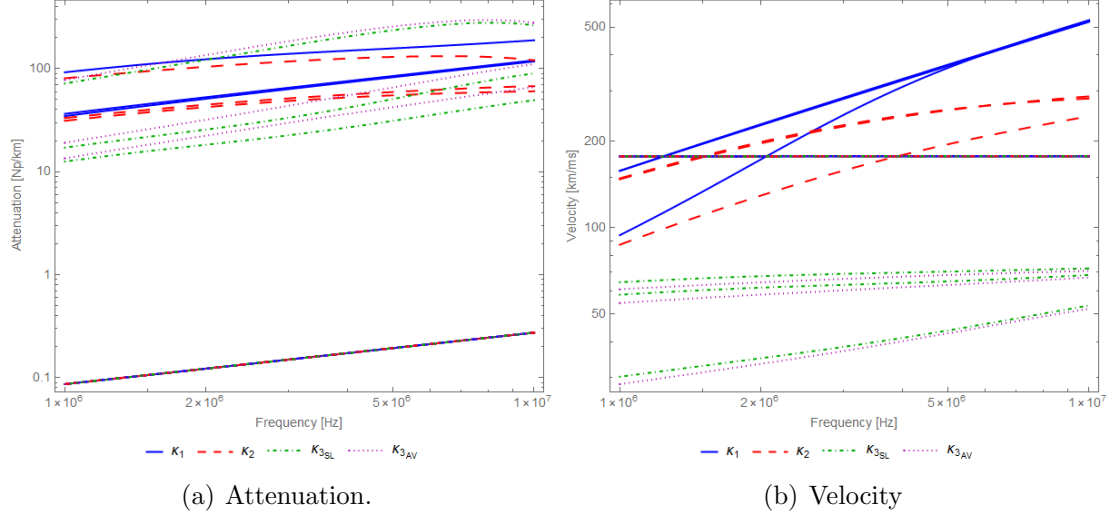


Figure 3.13: Modes propagation between 1 MHz and 10 MHz. Series expansion approach of Bessel functions [69].  $\kappa_1 = \sigma_0 = 1/\rho_0$ ,  $\kappa_2 = \sigma_0 + j\omega\varepsilon_\infty$ ,  $\kappa_{3SL}$  considers Smith-Longmire model, and  $\kappa_{3AV}$  considers Alipio-Visacro model.

### 3.6 Discussion

This chapter covered important aspects of cable system representation for EMT studies. The assembly of impedance and admittance matrices as well as typical cable systems configurations were reviewed. Formulations of ground return impedances and admittances based on quasi-TEM approximations were presented and a novel closed-form expression was derived for the ground return admittance, suited for underground cable systems transient simulations. It was obtained considering an approximated integrand that allows a closed-form solution for the infinite integral. It is worth mentioning that the goal was not to derive a new model for the earth return quantities, but to obtain an approximate expression that avoids the calculation of infinite integrals associated with the ground return admittance matrix. The proposed expression provided useful results for frequencies up to a few MHz. Time responses indicated a suitable accuracy with higher computational efficiency.

The ground return admittance closed-form expression is of paramount importance on the whole of this study and have been used in Chapter 2 in order to calculate the admittance probability density function. Furthermore, it contributes on simulations by improving computation speed when comparing it to the respective infinite integral being more than 200 times faster. This represents a strong advantage, even more when a large set of simulation is needed.

An application of the rational model of frequency-dependent soils altogether with the ground return admittance closed-form expression developed here was also presented. The investigation of the effects of soil frequency-dependence on the natural

modes of propagation of the three-phase SC-cable system showed that only ground and inter-sheath modes of propagation are affected by the soil modeling and different behavior due to frequency-dependence was obtained when  $\kappa_2$  or  $\kappa_3$  (SL or AV) were considered, with  $\kappa_2$  not affecting the results up to frequencies near 1 MHz. When  $\kappa_3$  is considered, the affected modes present the same attenuation behavior up to about 3 kHz. Between 3 kHz and 2 MHz they are less damped than  $\kappa_1$  and  $\kappa_2$ , and above 2 MHz  $\kappa_3$  provides higher attenuation. Regarding modes velocities, when  $\kappa_3$  is considered modes are slower above 50 kHz, and  $\kappa_2$  only affects the velocities at frequencies near 1 MHz and above.

Numerical issues were verified on the implementation of Bessel functions above a few megahertz. To avoid further complications and to maintain the frequency range of observation within the valid limits of the models considered, the frequency-domain results of the next Chapter will be presented up to 1 MHz.

# Chapter 4

## Uncertainties Assessment

Despite the frequency-dependent characteristic, simulations regarding EMT behavior of an underground cable system often consider fixed soil parameters. Nevertheless, some investigation should be made in order to evaluate whether it is possible or not to make this consideration, for it could bring inaccuracy to results. Different analyses regarding the influence of soil on the behavior of cable systems responses are included in this Chapter, namely, the sensitivity to a soil fixed resistivity value ( $\rho_0 = 1/\sigma_0$ ) and time-domain energization test cases. The values of  $\kappa_1$  and  $\kappa_2$  of Section 2.3, the rational models of Section 2.4, and the closed-form expressions of Section 3.4 are considered in all results here presented.

### 4.1 Sensitivity Analysis

Regarding overhead lines, a discussion on how inaccuracies related to poor knowledge of soil resistivity value affect the calculation of transients was presented in [70], by calculating the sensitivities of the line mode impedances to the ratio resistivity over frequency, i.e.,  $\rho/f$ . Also, the necessity of a sensitivity analysis due to parameter inaccuracy is addressed in [71].

As seen in the previous chapter, ground return impedances and admittances are the two parameters that interface the ground resistivity with the underground cable system modeling. For both quantities it is possible to resort to closed-form expressions in order to avoid calculating infinite integrals. Since they are closed-form expressions, the assessment of their behavior due to the apparent resistivity  $\rho_0$  variation should be straightforward.

Consider the SC-cable systems described in Chapter 3 and let  $Z_{g_{ij}}$  and  $Y_{g_{ij}}$  be the  $ij$  elements of the  $2 \times 2$  block matrices that assemble three-phase  $6 \times 6$  matrices  $\mathbf{Z}_g$  and  $\mathbf{Y}_g$ , respectively. Since both are functions of soil propagation factor,  $\gamma = \sqrt{j\omega\mu\kappa}$ , and, as seen in Section 2.3,  $\kappa$  can assume different values but always as a function of soil resistivity, it is possible to state that  $Z_{g_{ij}}$  and  $Y_{g_{ij}}$  are functions of  $\rho_0 = 1/\sigma_0$ .

To illustrate the statement, consider  $Z_{g_{ij}}$ . If  $\rho_0$  varies by  $\Delta\rho_0$ ,  $Z_{g_{ij}}$  will also vary by  $\Delta Z_{g_{ij}}$  and if this variation  $\Delta\rho_0$  is small enough,  $\Delta Z_{g_{ij}}$  can be estimated from [70]:

$$\Delta Z_{g_{ij}} = \frac{\partial Z_{g_{ij}}}{\partial \rho_0} \Delta \rho_0 \quad (4.1)$$

and the relative change, or per-unit, given by

$$\frac{\Delta Z_{g_{ij}}}{Z_{g_{ij}}} = \left( \frac{\rho_0}{Z_{g_{ij}}} \frac{\partial Z_{g_{ij}}}{\partial \rho_0} \right) \frac{\Delta \rho_0}{\rho_0} \quad (4.2)$$

From (4.2) the expression for calculating the sensitivity of the ground return impedance to soil resistivity is given by:

$$S_Z = \frac{\rho_0}{Z_{g_{ij}}} \frac{\partial Z_{g_{ij}}}{\partial \rho_0} \quad (4.3)$$

or

$$S_Z = \frac{\rho_0 \frac{\partial}{\partial \rho_0} \left\{ \frac{j\omega\mu}{2\pi} \left[ K_0(\gamma_1 d) + \frac{\ell^2 - x^2}{D^2} K_2(\gamma_1 D) - 2 \frac{\ell^2 - x^2}{\gamma_1^2 D^4} (1 + \ell\gamma_1) \exp(-\ell\gamma_1) \right] \right\}}{\frac{j\omega\mu}{2\pi} \left[ K_0(\gamma_1 d) + \frac{\ell^2 - x^2}{D^2} K_2(\gamma_1 D) - 2 \frac{\ell^2 - x^2}{\gamma_1^2 D^4} (1 + \ell\gamma_1) \exp(-\ell\gamma_1) \right]} \quad (4.4)$$

where  $\gamma_1 = \sqrt{j\omega\mu\kappa}$ .

Analogously, the sensitivity of the ground return admittance to  $\rho_0$  should be given by:

$$S_Y = \frac{\rho_0}{Y_{g_{ij}}} \frac{\partial Y_{g_{ij}}}{\partial \rho_0} \quad (4.5)$$

However, equation (3.19) of Chapter 3 states that the ground return admittance matrix is obtained through inversion of the matrix  $[\mathbf{\Lambda} - \mathbf{T}]$ , where  $\Lambda_{ij}$  are calculated by Bessel functions and a closed-form expression was obtained for  $T_{ij}$ . Furthermore, equation (3.26) shows the closed-form expression for each matrix element before the inversion operation. Therefore, it is reasonable to assume that (4.3) may be applied to investigate the sensitivity of  $Y_{g_{ij}}$  to  $\rho_0$  by means of the respective shunt impedance:

$$S_{Z_{shunt}} = \frac{\rho_0}{Z_{shunt_{ij}}} \frac{\partial Z_{shunt_{ij}}}{\partial \rho_0} \quad (4.6)$$

or

$$S_{Z_{shunt}} = \frac{\rho_0 \frac{\partial}{\partial \rho_0} \left\{ \frac{K_0(\gamma_1 d) + K_0(\gamma_1 D) - \frac{2\gamma_1^2}{\gamma_1^2 + \gamma_2^2} \ln \left[ \frac{2\gamma_2^2 + \gamma_1^2 \left( 2 + \gamma_2 \sqrt{(h_i + h_j)^2 + x_{ij}^2} \right)}{\gamma_2^2 + \gamma_1^2 \left( 1 + \gamma_2 \sqrt{(h_i + h_j)^2 + x_{ij}^2} \right)} \right]}{2\pi\kappa} \right\}}{K_0(\gamma_1 d) + K_0(\gamma_1 D) - \frac{2\gamma_1^2}{\gamma_1^2 + \gamma_2^2} \ln \left[ \frac{2\gamma_2^2 + \gamma_1^2 \left( 2 + \gamma_2 \sqrt{(h_i + h_j)^2 + x_{ij}^2} \right)}{\gamma_2^2 + \gamma_1^2 \left( 1 + \gamma_2 \sqrt{(h_i + h_j)^2 + x_{ij}^2} \right)} \right]}{2\pi\kappa} \quad (4.7)$$

where  $\gamma_1$  is the same as before and  $\gamma_2$  corresponds to the other medium propagation constant, e.g., the air.

This section addresses a discussion on the application of (4.4) and (4.7) to the typical cable systems configurations of Section 3.2. As the only interest is in the ground return quantities, the necessary data for the calculations are: each SC-cable outermost radius  $r_4 = 4.25$  cm; each cable depth  $h_i$ ; and the horizontal distance between them  $x_{ij}$ . Results here are presented regarding different soil models  $\kappa_1$ ,  $\kappa_2$ ,  $\kappa_{3SL}$  (Smith-Longmire model), and  $\kappa_{3SL}$  (Alipio-Visacro model), and considering four fixed values of  $\rho_0$  (100  $\Omega\cdot\text{m}$ , 500  $\Omega\cdot\text{m}$ , 1000  $\Omega\cdot\text{m}$  and 3000  $\Omega\cdot\text{m}$ ), within a frequency range from 1 Hz up to 1 MHz.

According to Chapter 3 review, the terms of the ground return longitudinal impedance matrix are slightly changed due to the geometric configuration considered, as different depths or distances between each phase affect the self and mutual impedances. However, when dealing with pipe-type configuration, both ground return impedance and admittance are scalar and multiplied by a matrix of ones with the rank equal to the number of conductive parts, and, therefore, results regarding the pipe are presented first in Fig. 4.1.

One advantage of presenting these results first is to compare how the modeling of soil affects the wide-band behavior of the sensitivity curves. All figures point to a growing tendency of the sensitivity due to frequency increase, for frequencies up to a few kilohertz. By comparing Figs. 4.1(a) and (b) it is possible to affirm that the permittivity as an isolated parameter begins to affect the sensitivity at frequencies above a few hundreds of kilohertz for a resistivity of 1000  $\Omega\cdot\text{m}$ , but this limit frequency lowers to around 100 kHz when the resistivity reaches 3000  $\Omega\cdot\text{m}$ . When there is an interdependence between the resistivity and the permittivity, as is the case of Smith-Longmire and Alipio-Visacro models, the higher the ground resistivity is, the sensitivity is more affected at frequencies around tens of kilohertz.

The same behavior can be noticed for other cable systems configurations, as it might be seen Figures 4.2 to 4.5. Nevertheless, these cases present differences regarding the self and mutual impedance sensitivity behaviors.

Fig. 4.2 depicts the results for the horizontal flat configuration for the same four  $\kappa$  models as before, for the self impedance, which is equal for the three phases, and the two different values of mutual impedances, i.e., between center and extremity phases and between extremity phases. From the columns of the graphics it is possible to note that the mutual impedances present higher sensitivity peak value than the self impedance, but respecting the initial assessment that low resistive soils are more sensitive with respect to a fixed frequency.

Same type of analysis is depicted for the trefoil configuration in Fig. 4.3. In this configuration, mutual impedances are equal, but there is two different values of series impedances. As the phases are very close to each other, all sensitivities present very similar behavior and it is not possible to point out which of the matrix terms are more sensitive.

When the flat vertical configuration is considered, there are three different self impedances, for the cables are buried at three different depths, and two different mutual impedances, for the same reason of the flat horizontal case. Sensitivities curves of self and mutual impedances are depicted in Figs. 4.4 and 4.5, respectively. Similar results to the flat horizontal configuration were obtained, with small changes due to depth differences.

Additional results considering fixed values of frequency and a ground resistivity range are placed in Appendix C. These results confirm the tendency of the longitudinal impedance sensitivity be more impacted to lower resistivity at higher frequencies.

Figure 4.6 presents the results comparing the soil modeling effects on the sensitivity calculation, regarding the ground return shunt impedance of pipe-type cable. In cases with fixed value of soil resistivity, i.e., Figs. 4.6(a) and (b), regardless of the apparent resistivity taken into account, the shunt impedance presents a constant sensitivity for frequencies up to approximately 100 kHz. That means that for a given change on the soil resistivity values considered, the frequency does not have a role on the variation of the shunt impedance. As for the frequency-dependent models in Figs. 4.6(c) and (d), the limit frequency for the constant behavior is far lower, even if less resistive soils are considered. Also, when compared to Smith-Longmire model, sensitivity behavior considering Alipio-Visacro model is smoother.

Similar observations can be made from the results considering other cable system configurations on Figures 4.7 to 4.10, once again with noticeable differences only at frequencies above 100 kHz. The comparison of self shunt impedance results in Figs. 4.7, 4.8 and 4.9 shows negligible differences concerning the cables depths. Also,

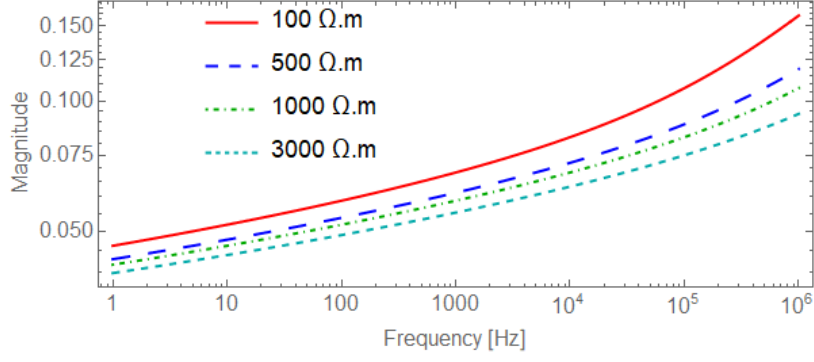
one may note that the larger are the distances between cables, the more affected the mutual shunt impedance sensitivities are. This can be seen when comparing the results of flat configurations – horizontal in Fig. 4.7 and vertical in Fig. 4.10 – with the results for the trefoil configuration in Fig. 4.8. Furthermore, one can not infer what is the more or less sensitive case due to soil resistivity.

Additional results considering fixed values of frequency over a ground resistivity range are placed in Appendix D. They confirm that the ground return shunt impedance sensitivity presents a variant behavior at higher frequencies. Also, it is possible to observe that for a typical consideration of soil resistivity between  $100 \Omega\cdot\text{m}$  and  $1000 \Omega\cdot\text{m}$ , the sensitivity is fairly close to the constant value here found for the frequency-independent models and very close to the same value, when SL and AV models are considered.

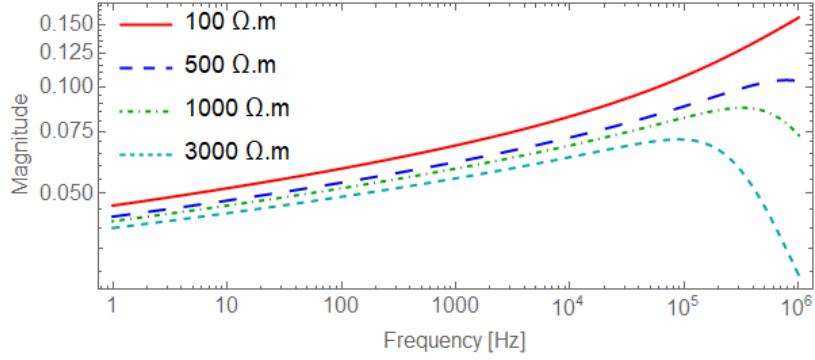
### Discussion about the Sensitivity Analysis

Regarding the longitudinal impedance, it is possible to observe that flat configurations present some differences between self and mutual terms and, therefore, the sensitivity curves are more affected by soil resistivity. This is explained by considering that the three cables are separated by a piece of soil and thus are most susceptible to soil interaction. Results also indicated that the deeper the cable is buried, the more the sensitivity curve is affected. In general, when  $\kappa_1$  is considered impedances presented higher values for sensitivity at higher frequencies and for lower resistivity values. When frequency is considered, however, the sensitivity curve may reach values lower at higher frequencies than at lower frequencies. All of these results can be assessed from a different point of view, by considering resistivity value variation at fixed frequencies, in Appendix C.

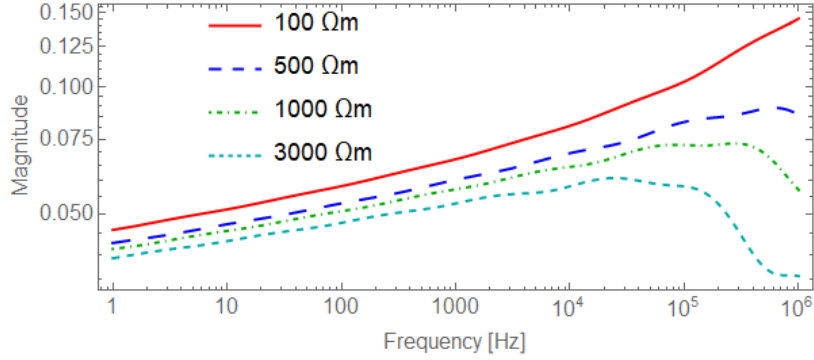
When shunt impedance sensitivity is considered, regardless of the geometric profile of the cable system or the soil model, there is little difference in the sensitivity curves for frequencies up to 1 kHz. Between 1 kHz and 100 kHz, models  $\kappa_1$  and  $\kappa_2$  remain barely unaltered whereas  $\kappa_{SL}$  and  $\kappa_{AV}$  make the sensitivity values smaller when greater resistivity values are considered. Above 100 kHz, regardless of  $\kappa$  considered, the sensitivity curves are strongly affected but not in a consistent way, i.e., it is not possible to infer a well-behaved pattern. This is confirmed by the graphics of Appendix D where sensitivity curves are plotted over resistivity variation at fixed frequencies.



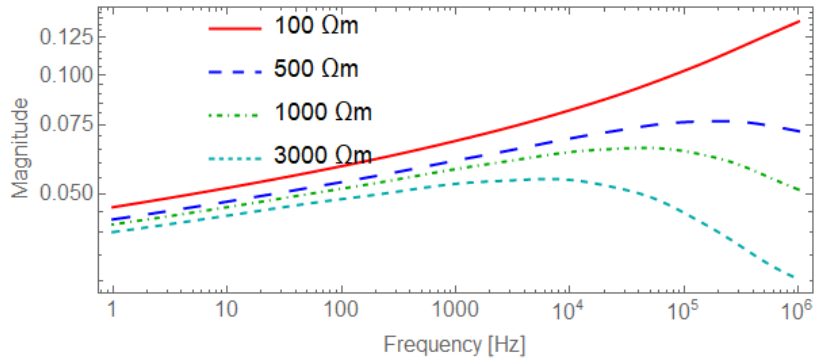
(a)  $\kappa = \sigma_0 = 1/\rho_0$



(b)  $\kappa = \sigma_0 + j\omega\epsilon_r\epsilon_0$



(c) Smith-Longmire



(d) Alipio-Visacro

Figure 4.1: Sensitivities of series impedance for pipe-type cable configuration. Figures (a):  $\kappa = \sigma_0 = 1/\rho_0$ ; (b):  $\kappa = \sigma_0 + j\omega\epsilon_r\epsilon_0$ ; (c): Smith-Longmire; and (d): Alipio-Visacro.

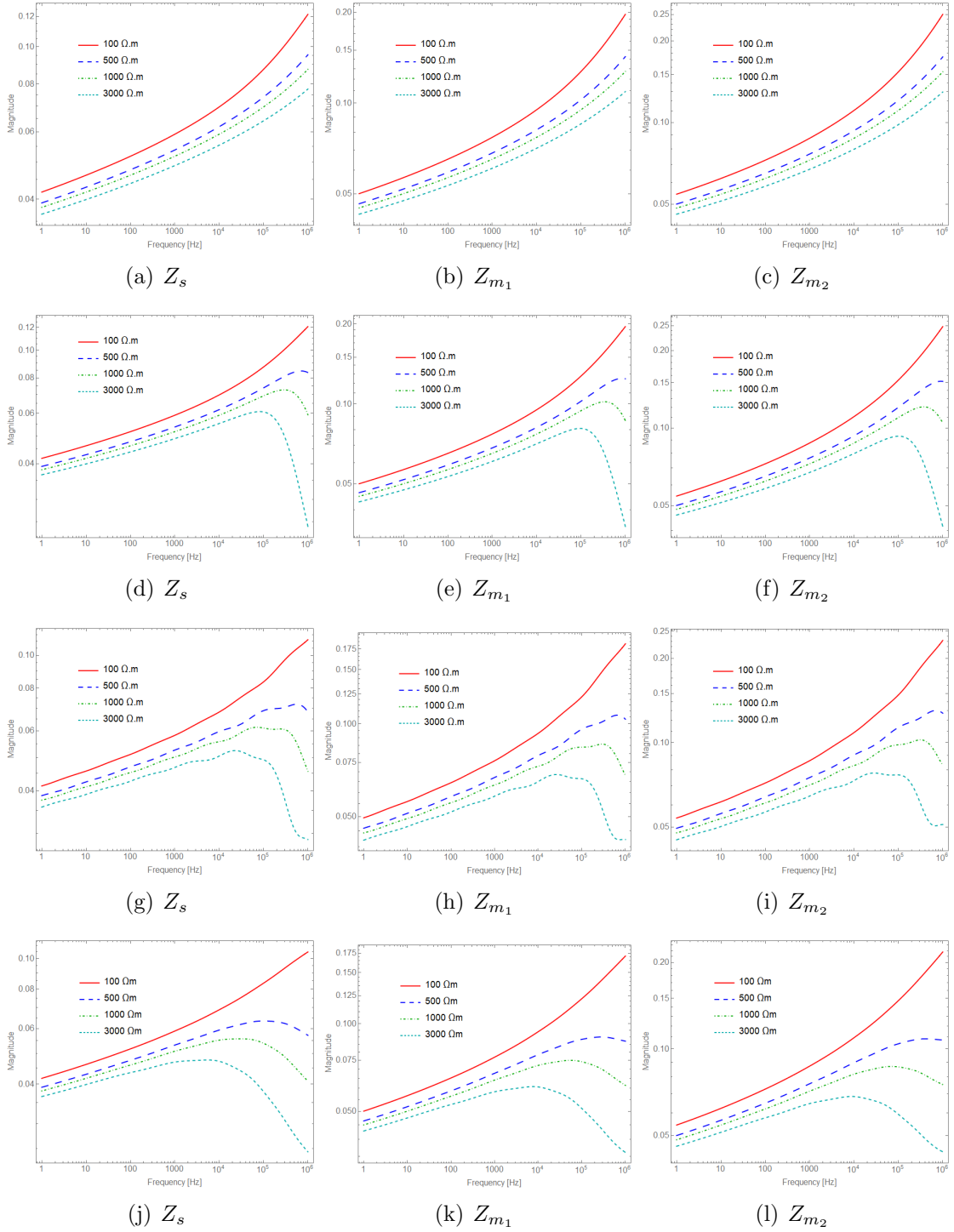


Figure 4.2: Sensitivities of series impedance for flat horizontal configuration. Figures (a)–(c):  $\kappa = \sigma_0 = 1/\rho_0$ ; (d)–(f):  $\kappa = \sigma_0 + j\omega\epsilon_r\epsilon_0$ ; (g)–(i): Smith-Longmire; and (j)–(l): Alipio-Visacro.

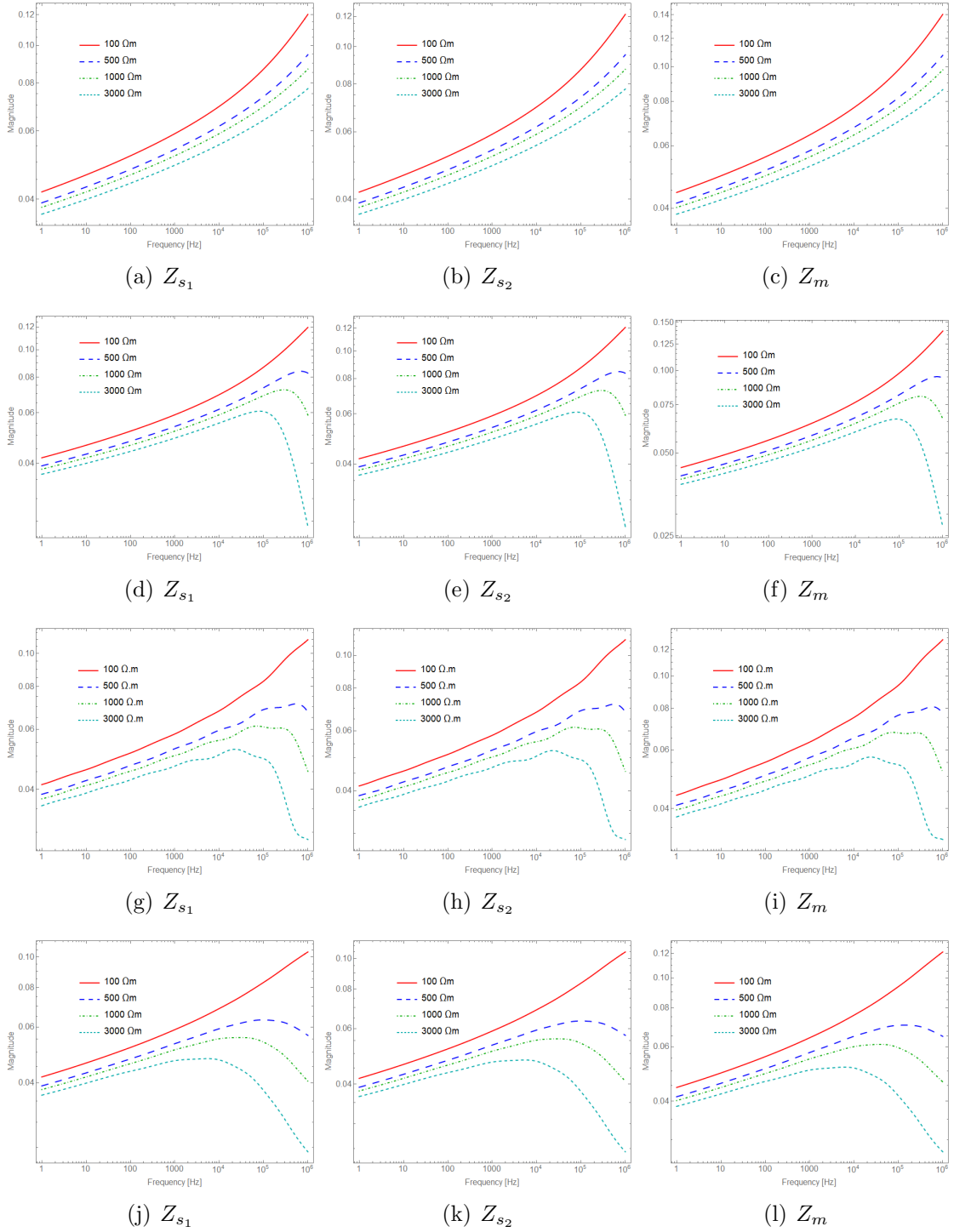


Figure 4.3: Sensitivities of series impedance for trefoil configuration. Figures (a)–(c):  $\kappa = \sigma_0 = 1/\rho_0$ ; (d)–(f):  $\kappa = \sigma_0 + j\omega\epsilon_r\epsilon_0$ ; (g)–(i): Smith-Longmire; and (j)–(l): Alipio-Visacro.

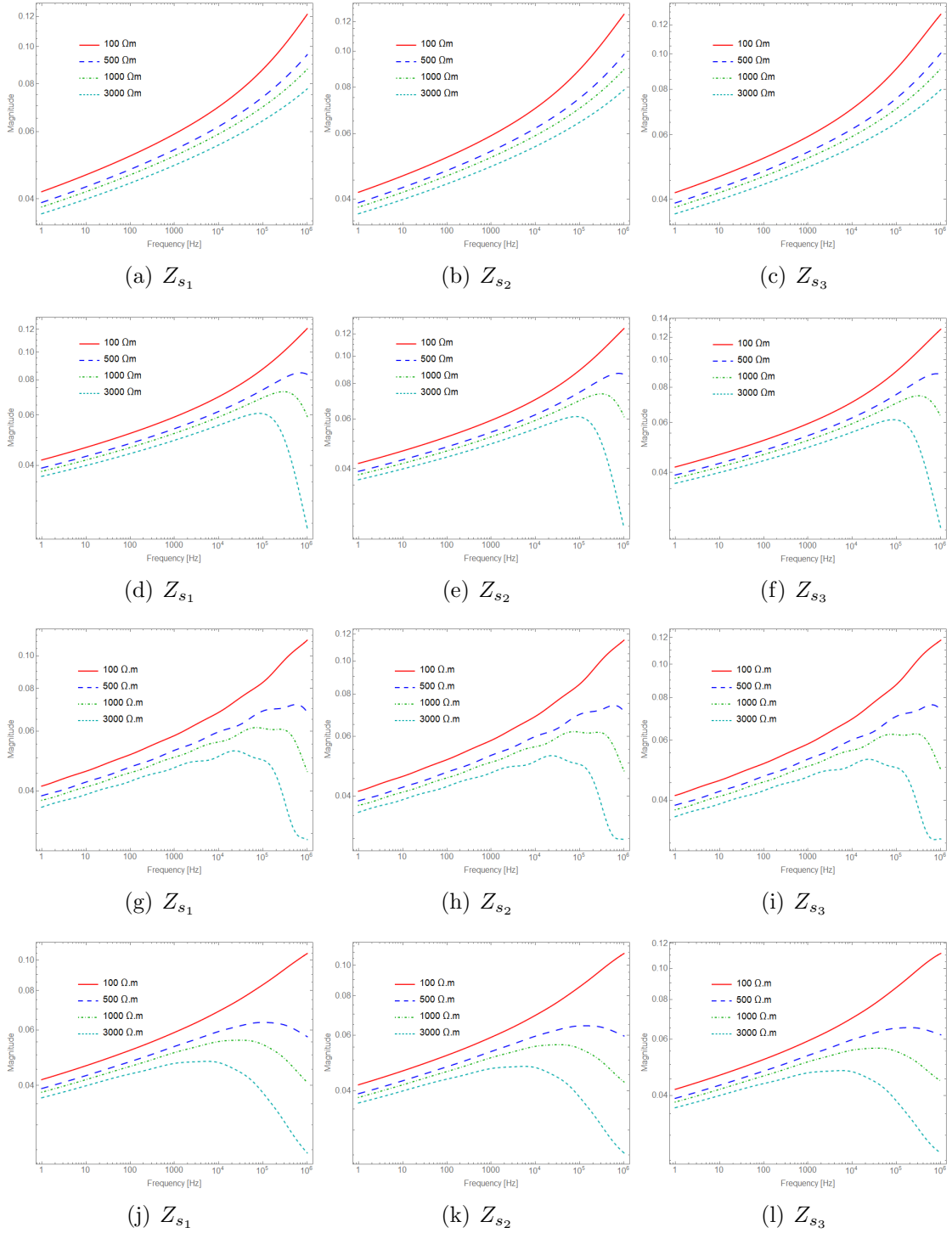


Figure 4.4: Sensitivities of series self impedance for flat vertical configuration. Figures (a)–(c):  $\kappa = \sigma_0 = 1/\rho_0$ ; (d)–(f):  $\kappa = \sigma_0 + j\omega\varepsilon_r\varepsilon_0$ ; (g)–(i): Smith-Longmire; and (j)–(l): Alipio-Visacro.

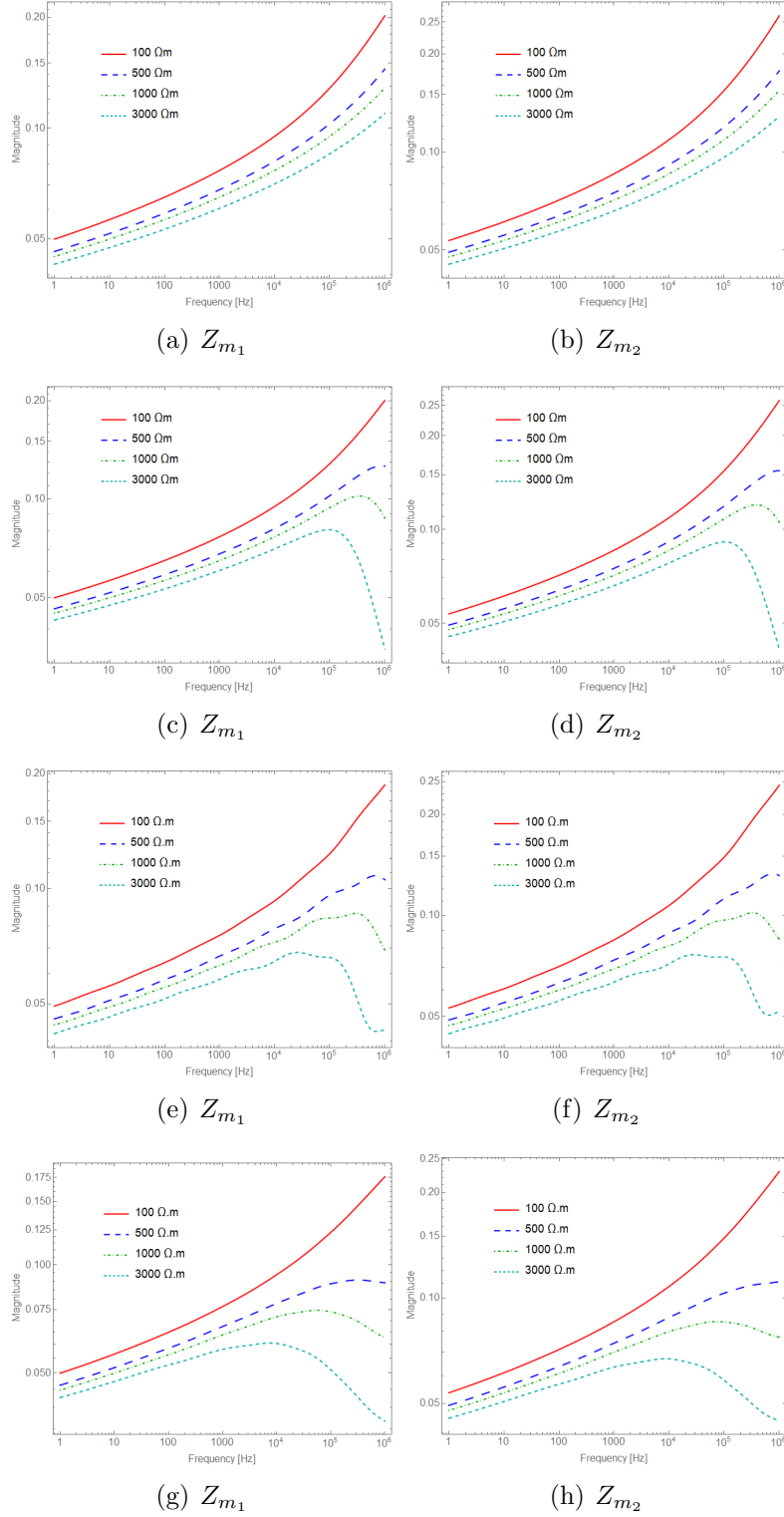
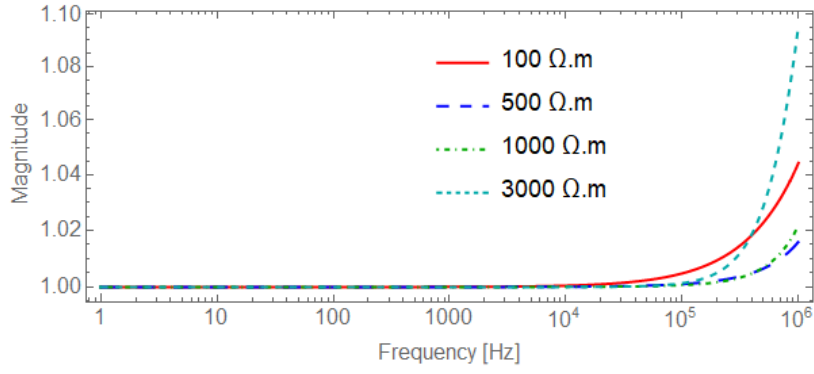
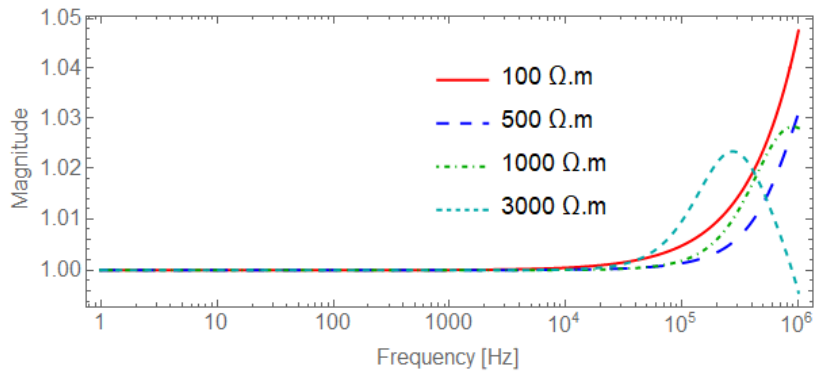


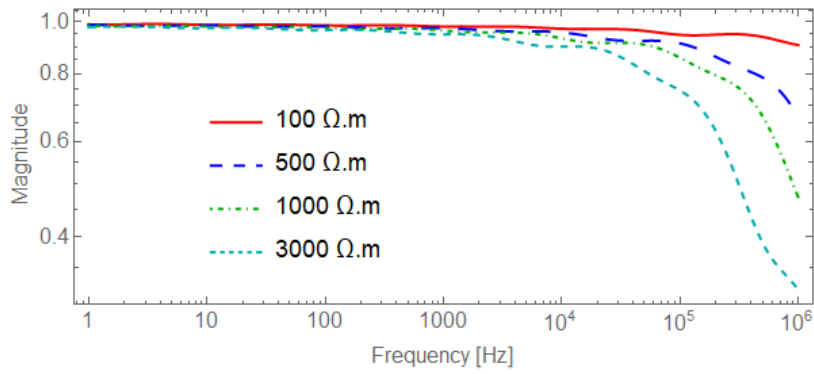
Figure 4.5: Sensitivities of series mutual impedance for flat vertical configuration. Figures (a) and (b):  $\kappa = \sigma_0 = 1/\rho_0$ ; (c) and (d):  $\kappa = \sigma_0 + j\omega\epsilon_r\epsilon_0$ ; (e) and (f): Smith-Longmire; and (g) and (h): Alipio-Visacro.



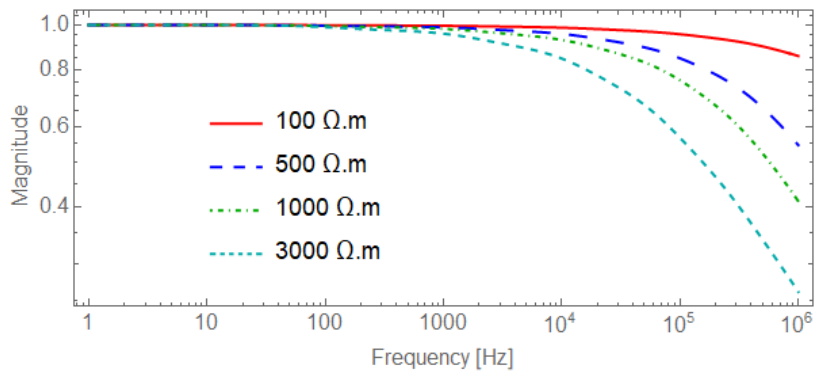
(a)  $\kappa = \sigma_0 = 1/\rho_0$



(b)  $\kappa = \sigma_0 + j\omega\epsilon_r\epsilon_0$



(c) Smith-Longmire



(d) Alipio-Visacro

Figure 4.6: Sensitivities of shunt impedance for pipe-type cable configuration. Figures (a):  $\kappa = \sigma_0 = 1/\rho_0$ ; (b):  $\kappa = \sigma_0 + j\omega\epsilon_r\epsilon_0$ ; (c): Smith-Longmire; and (d): Alipio-Visacro.

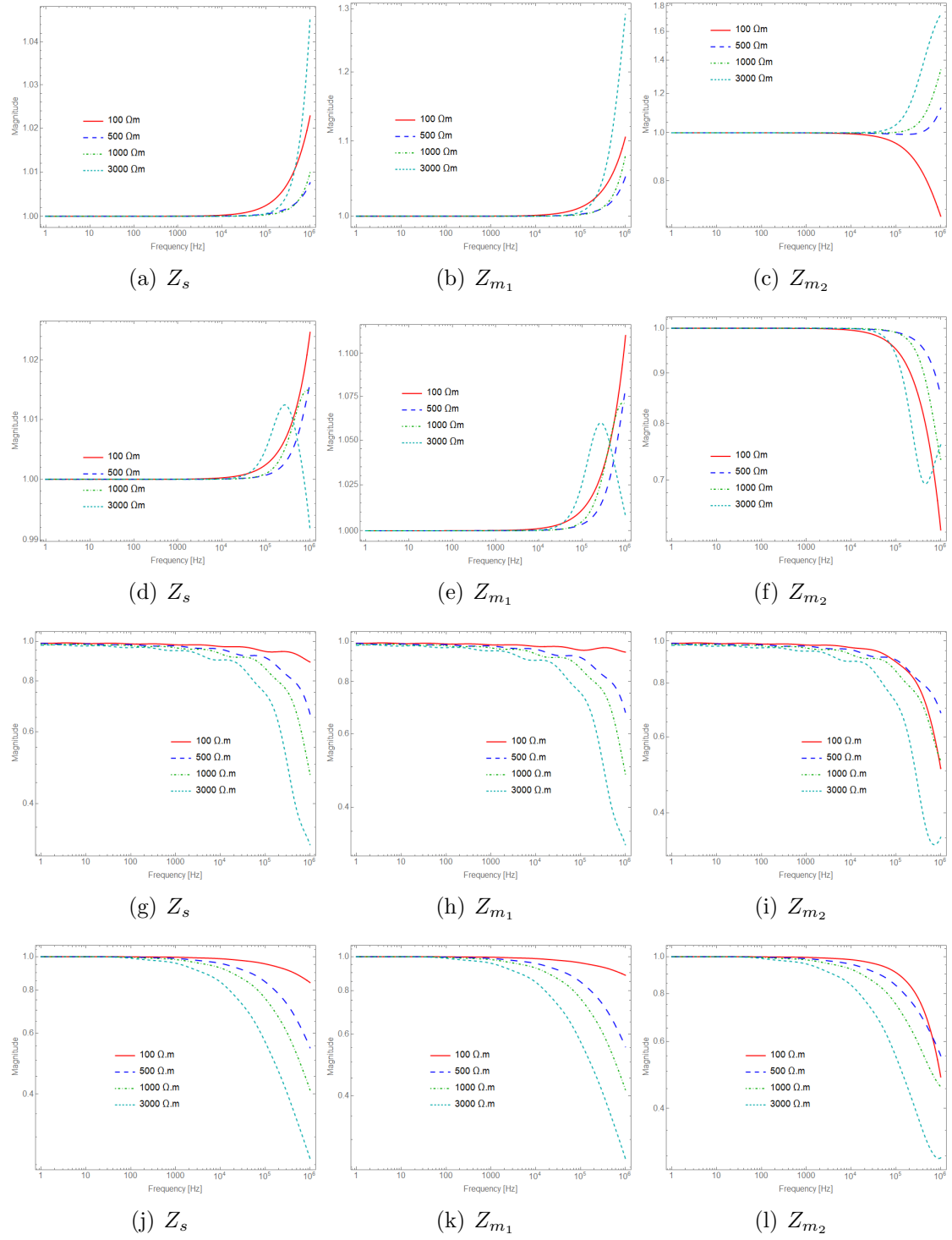


Figure 4.7: Sensitivities of shunt impedance for flat horizontal configuration. Figures (a)–(c):  $\kappa = \sigma_0 = 1/\rho_0$ ; (d)–(f):  $\kappa = \sigma_0 + j\omega\varepsilon_r\varepsilon_0$ ; (g)–(i): Smith-Longmire; and (j)–(l): Alipio-Visacro.

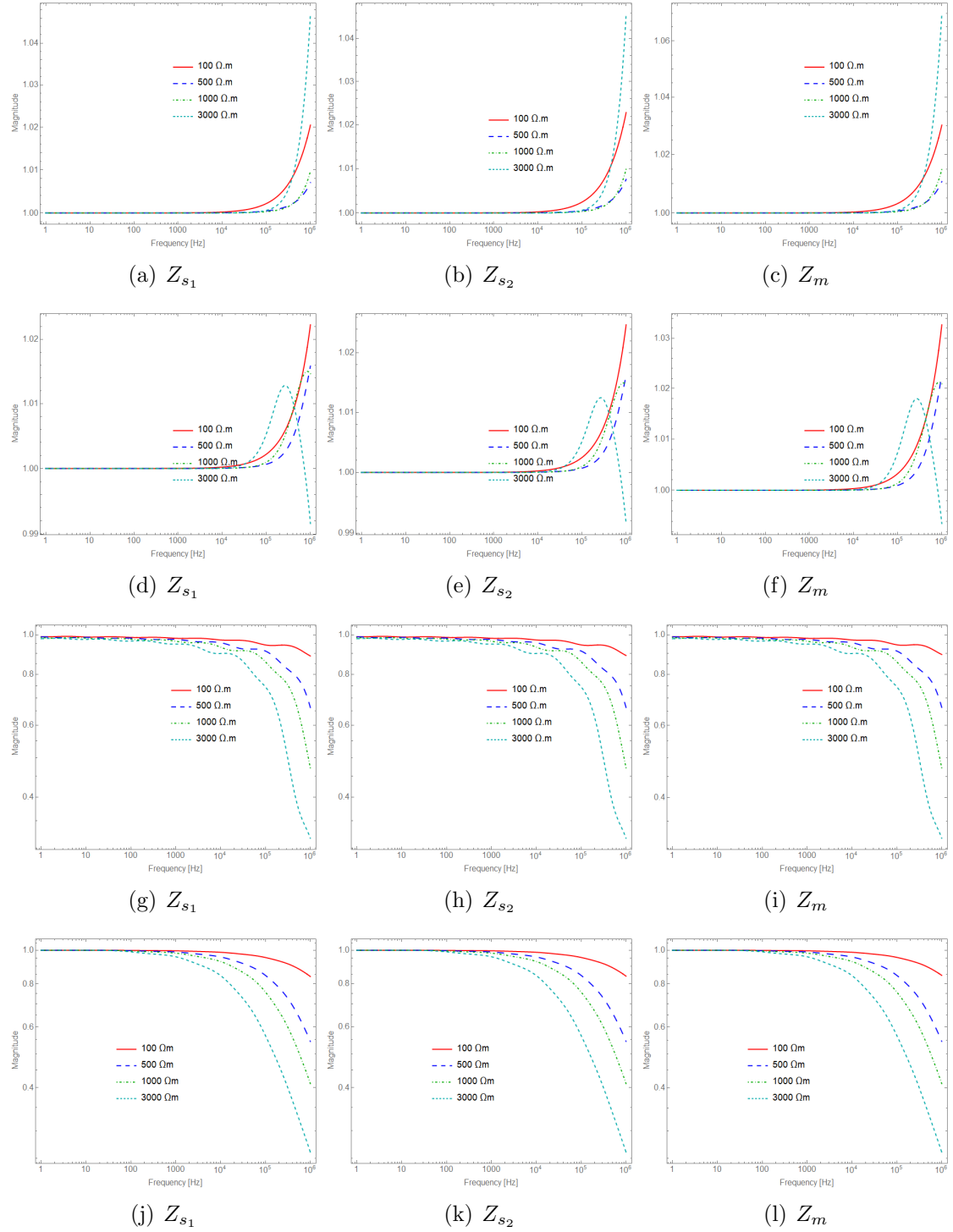


Figure 4.8: Sensitivities of shunt impedance for trefoil configuration. Figures (a)–(c):  $\kappa = \sigma_0 = 1/\rho_0$ ; (d)–(f):  $\kappa = \sigma_0 + j\omega\epsilon_r\epsilon_0$ ; (g)–(i): Smith-Longmire; and (j)–(l): Alipio-Visacro.

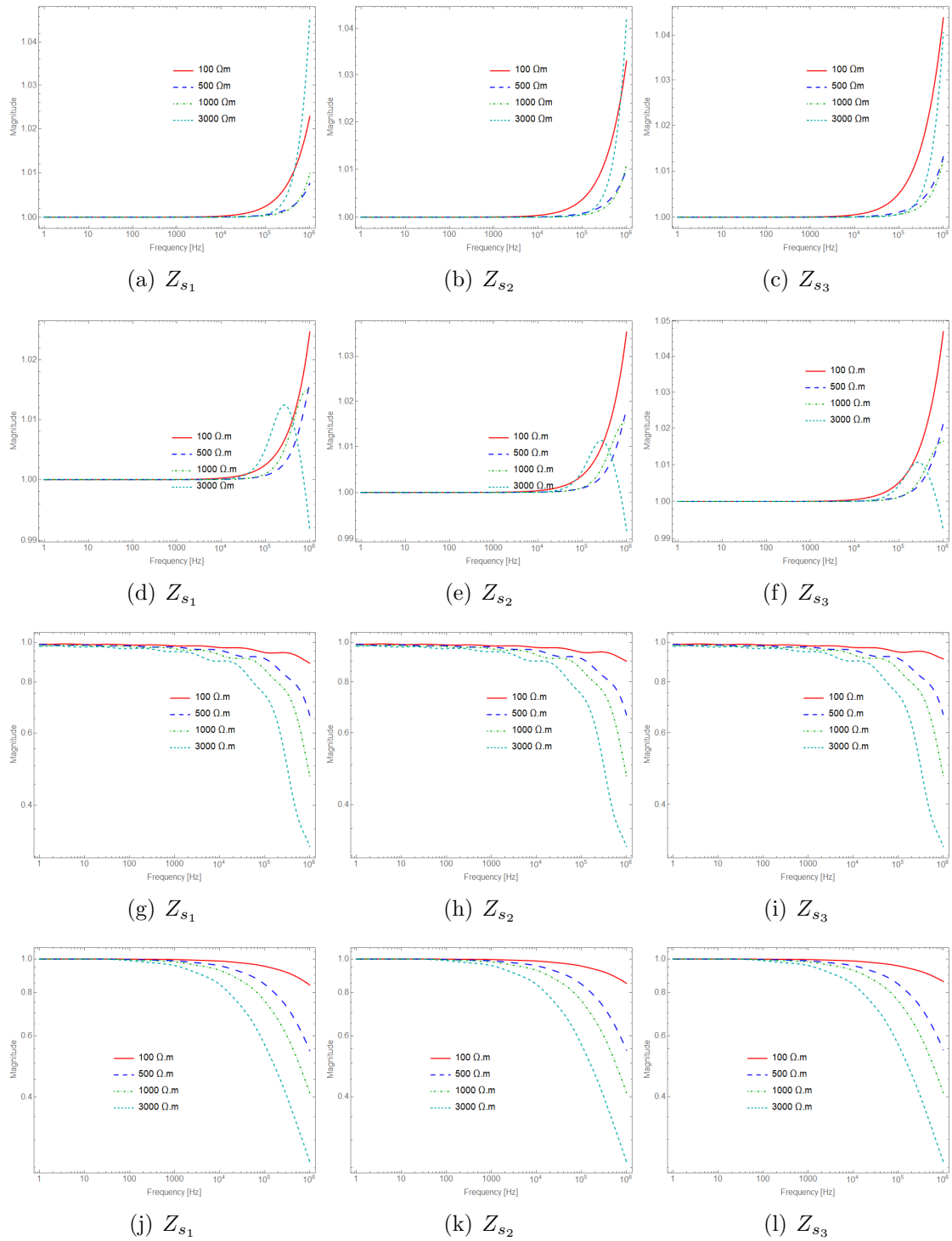


Figure 4.9: Sensitivities of shunt self impedance for flat vertical configuration. Figures (a)–(c):  $\kappa = \sigma_0 = 1/\rho_0$ ; (d)–(f):  $\kappa = \sigma_0 + j\omega\epsilon_r\epsilon_0$ ; (g)–(i): Smith-Longmire; and (j)–(l): Alipio-Visacro.

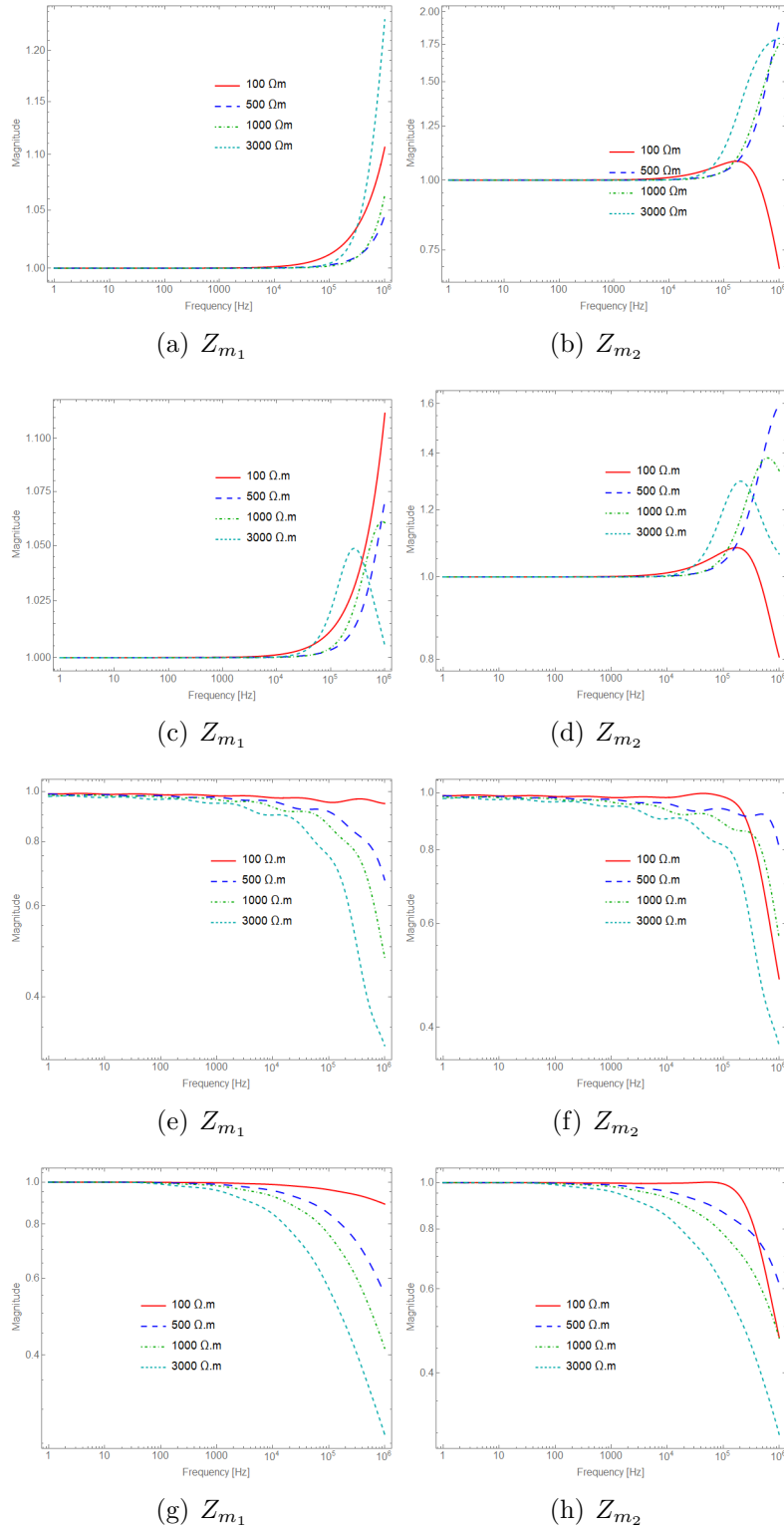


Figure 4.10: Sensitivities of shunt mutual impedance for flat vertical configuration. Figures (a) and (b):  $\kappa = \sigma_0 = 1/\rho_0$ ; (c) and (d):  $\kappa = \sigma_0 + j\omega\epsilon_r\epsilon_0$ ; (e) and (f): Smith-Longmire; and (g) and (h): Alipio-Visacro.

## 4.2 Test Cases

In this section, results of energization of three-phase SC-cable systems are presented with the energization source represented by a 1 pu ac voltage source. As greater lengths should require cross-bonding schemes, a 500 m section of the cable system is considered. The objective is to present the overvoltage results for sinusoidal sources with respect to different frequencies. The ground return matrix terms for vertical configuration present greater differences regarding the sensitivity to  $\rho_0$ , so it is the one considered here. The configuration is as depicted in Fig. 3.2(c), with the three SC-cables buried at depths  $h_1 = 1.0$  m,  $h_2 = 1.3$  m and  $h_3 = 1.6$  m, respectively.

In order to compare the influence of the soil model, i.e.,  $\kappa$ , two cases are studied following the description below:

**Case 1** *the energization of the sheath of one of the cables with all other terminals opened; and*

**Case 2** *the energization of the core of one of the cables with all the sheaths grounded at sending-end and all terminals opened in the receiving-end.*

Furthermore, three different values of soil apparent resistivity (100  $\Omega\cdot\text{m}$ , 3000  $\Omega\cdot\text{m}$  and 120000  $\Omega\cdot\text{m}$ ) and three different values of frequency for the source are considered (3 kHz, 50 kHz and 200 kHz). The choice of these values was based on the discussions and results presented in Sections 2.2 and 3.5.

### 4.2.1 Case 1

For this Case, the goal is to investigate the voltage at terminal 11, when terminal 2 is energized, as depicted in Fig. 4.11. This means that the sheath closest to the air-soil interface is energized and the voltage at the core of the deepest buried cable is evaluated.

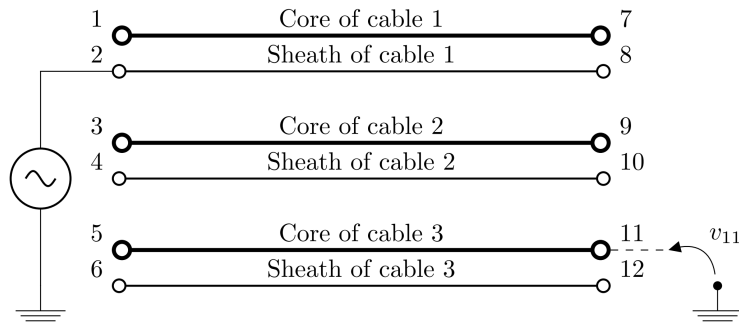


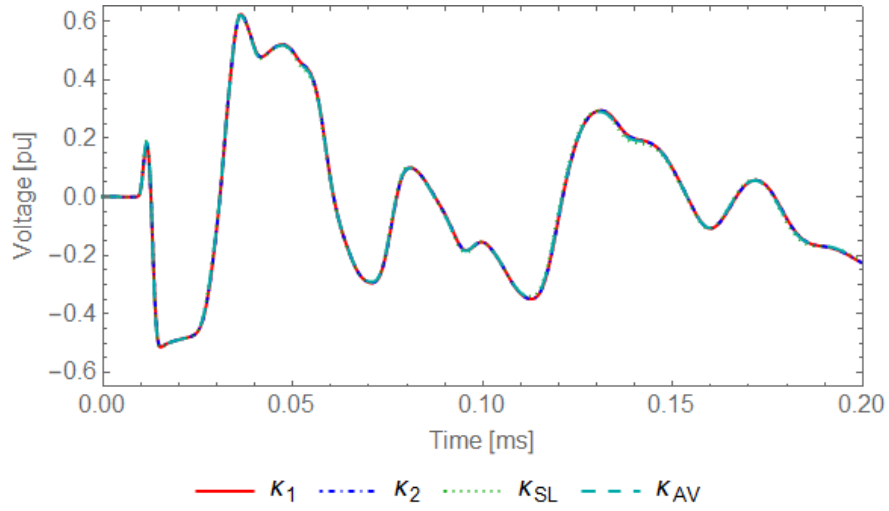
Figure 4.11: Energization scheme of Case 1.

Figures 4.12(a), (b) and (c) present the results when soil resistivity is considered  $100 \Omega\cdot\text{m}$ , when node 2 is energized with a 1.0 pu voltage source and frequencies 3 kHz, 50 kHz and 200 kHz, respectively. As it was seen in the sensitivity analysis, this value of resistivity leads to a more sensitive behavior of both ground impedance and admittance when higher frequencies are to be considered. For this case, only in Fig. 4.12(c) with a frequency of 200 kHz some differences may be observed between the models that do not account for frequency-dependence and the others, i.e., Smith-Longmire and Alipio-Visacro models. It can be seen that these frequency-dependent models lead to a slight increase on the transient overvoltage, for this value of soil resistivity.

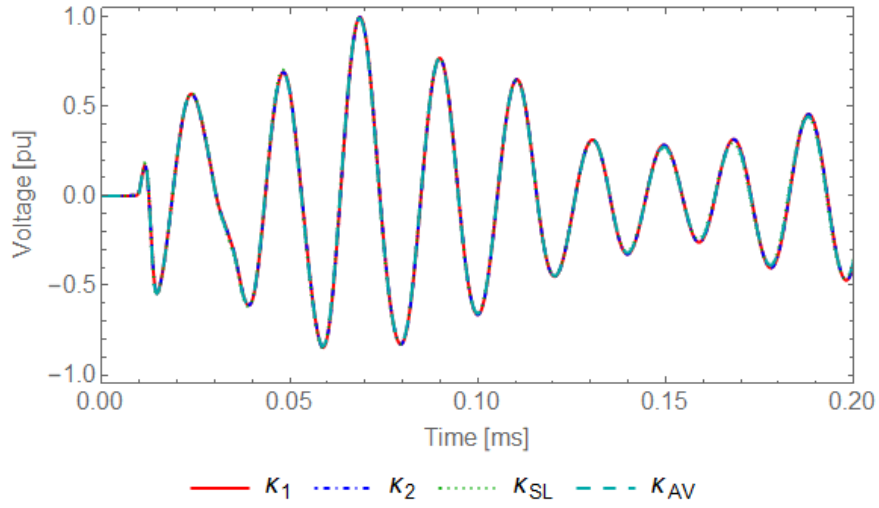
Figures 4.13(a), (b) and (c) present the results when soil resistivity is considered  $3000 \Omega\cdot\text{m}$ , in the same energization conditions. In this case, all results already show differences between formulations of soil. In Fig. 4.13(a), the consideration of frequency-dependence provides different overvoltages, with waveform of similar frequency but with slightly different amplitude. Also, it can be said that both Smith-Longmire and Alipio-Visacro models have the same behavior, which is not the same case when the frequency rises, as in Figs. 4.13(b) and (c). When the 50 kHz source is applied an even more damped behavior is assessed if  $\kappa_1$  or  $\kappa_2$  are used in relation to the other models. Further, Alipio-Visacro model gives higher peaks than Smith-Longmire, although they result in waveforms of the same phase. However, regarding the 200 kHz source, the peaks are even higher for Alipio-Visacro and there is a phase shift with respect to Smith-Longmire.

Still in the analysis of Case 1, Figures 4.14(a), (b) and (c) present the results when soil resistivity is considered  $120 \text{ k}\Omega\cdot\text{m}$ . This is an extreme case and it is only discussed here as a theoretical extrapolation, considering that the one resistivity value presented in [23], and mentioned in Section 2.2, surrounds all 500 m of the cable system length. This high resistive soil provokes noticeable differences between all models considered, even  $\kappa_1$  and  $\kappa_2$ . The characteristics seen in the two previous analyses are only observed in Fig. 4.14(a) for a frequency of 3 kHz. In Fig. 4.14(b), results show that  $\kappa_2$  presents higher peaks than  $\kappa_1$ , and Smith-Longmire have greater overvoltages than all other models. Once again, when the frequency rises as much as 200 kHz greater differences are seen, for the higher overvoltage is obtained with  $\kappa_2$ .

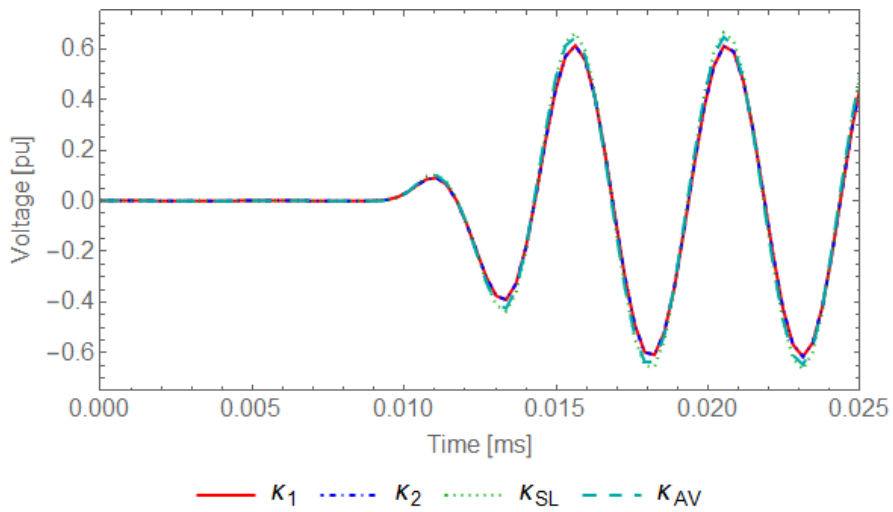
Nevertheless, the overall result indicates good agreement with the sensitivity analysis. When all Figures 4.12, 4.13 and 4.14 are analyzed together, one can observe that the higher the frequency, the more affected is the cable system that is buried in a more resistive soil. This can be assessed in Table 4.1, which presents the per-unit values of the maximum overvoltage obtained. From the transient performance point of view, it is interesting to know the voltages that the cable system is submitted.



(a) 3 kHz.

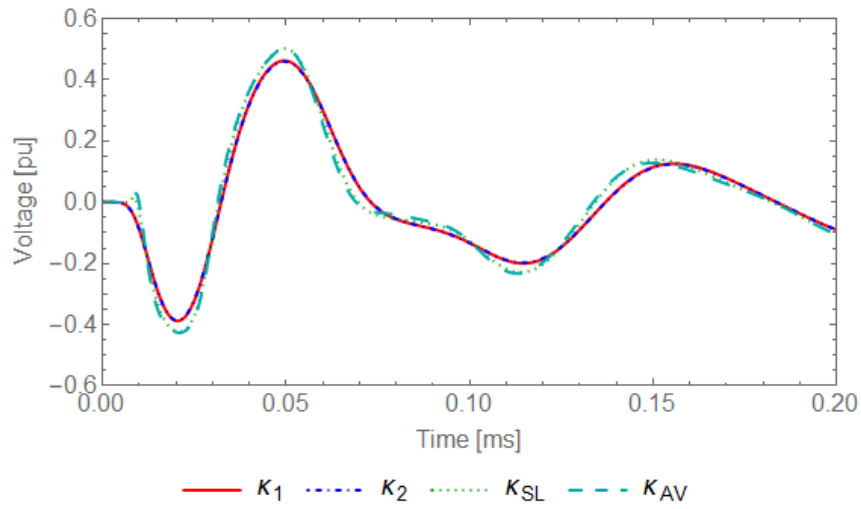


(b) 50 kHz.

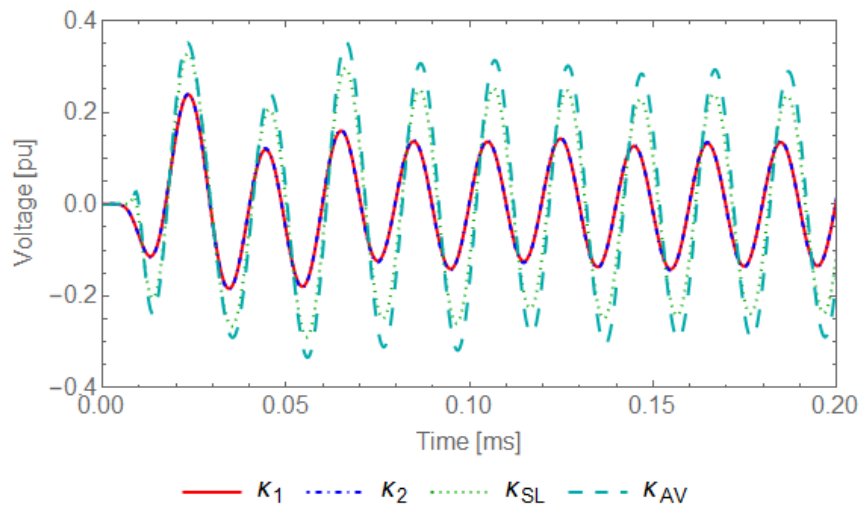


(c) 200 kHz.

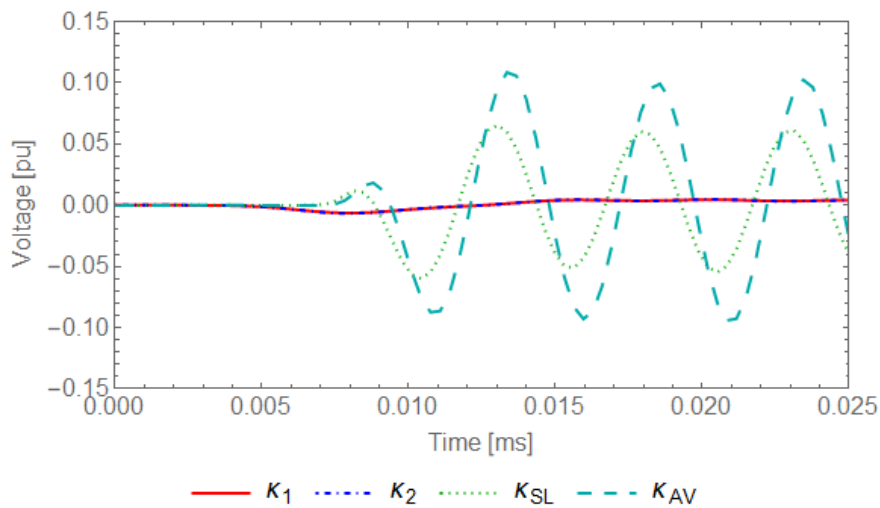
Figure 4.12: Case 1 – soil resistivity  $100 \Omega \cdot \text{m}$ .  $\kappa_1 = \sigma_0 = 1/\rho_0$ ,  $\kappa_2 = \sigma_0 + j\omega\epsilon_\infty$ ,  $\kappa_{SL}$  considers Smith-Longmire model, and  $\kappa_{AV}$  considers Alipio-Visacro model.



(a) 3 kHz.

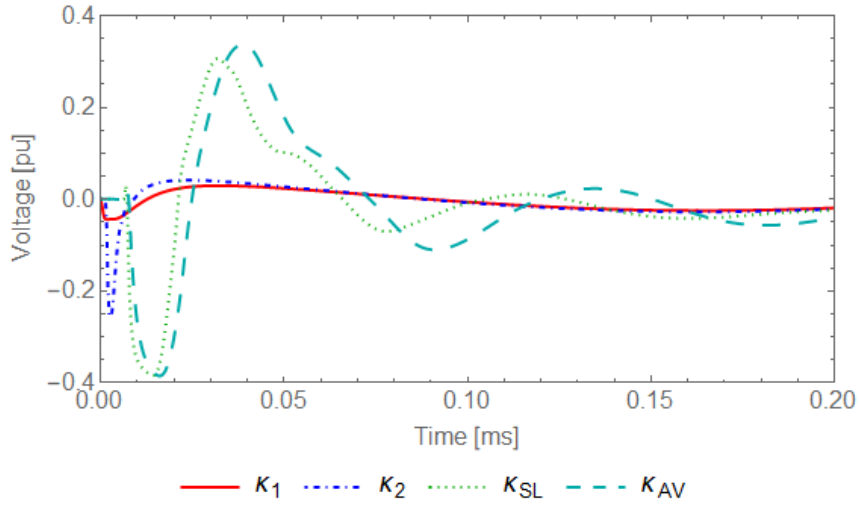


(b) 50 kHz.

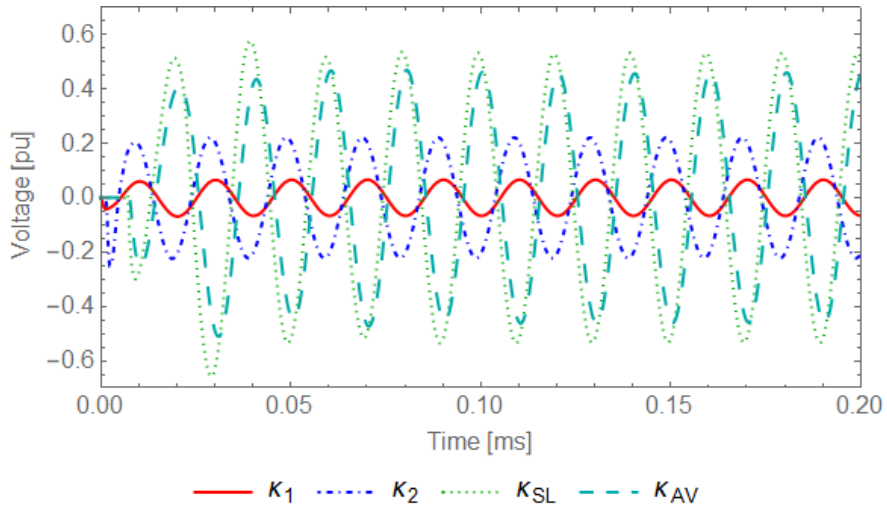


(c) 200 kHz.

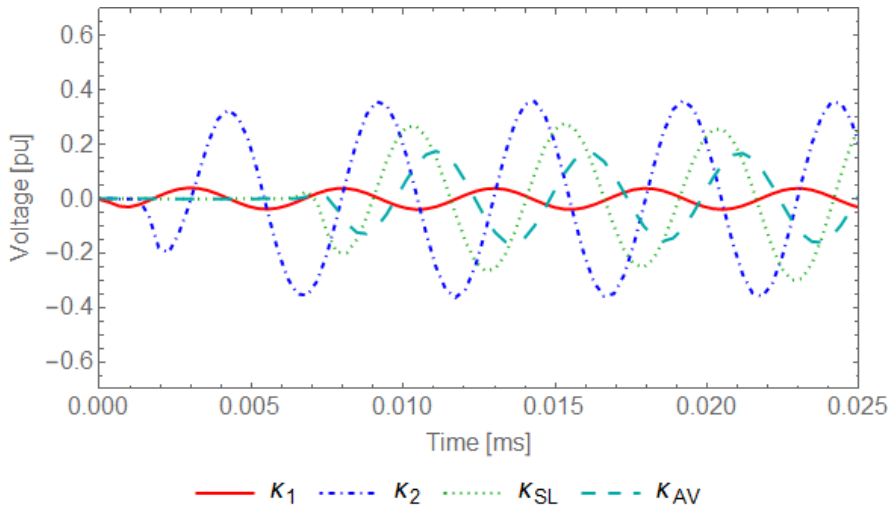
Figure 4.13: Case 1 – soil resistivity  $3000 \Omega \cdot \text{m}$ .  $\kappa_1 = \sigma_0 = 1/\rho_0$ ,  $\kappa_2 = \sigma_0 + j\omega\epsilon_\infty$ ,  $\kappa_{SL}$  considers Smith-Longmire model, and  $\kappa_{AV}$  considers Alipio-Visacro model.



(a) 3 kHz.



(b) 50 kHz.



(c) 200 kHz.

Figure 4.14: Case 1 – soil resistivity  $120 \text{ k}\Omega\cdot\text{m}$ .  $\kappa_1 = \sigma_0 = 1/\rho_0$ ,  $\kappa_2 = \sigma_0 + j\omega\epsilon_\infty$ ,  $\kappa_{SL}$  considers Smith-Longmire model, and  $\kappa_{AV}$  considers Alipio-Visacro model.

Table 4.1: Maximum voltage at terminal 11 for Case 1, in [pu].

| Frequency | Soil          | $\rho_0$                  |                            |                                   |
|-----------|---------------|---------------------------|----------------------------|-----------------------------------|
|           |               | 100 $\Omega\cdot\text{m}$ | 3000 $\Omega\cdot\text{m}$ | 120 $\text{k}\Omega\cdot\text{m}$ |
| 3 kHz     | $\kappa_1$    | 0.6236                    | 0.4624                     | 0.0369                            |
|           | $\kappa_2$    | 0.6233                    | 0.4597                     | 0.0421                            |
|           | $\kappa_{SL}$ | 0.6266                    | 0.5020                     | 0.3066                            |
|           | $\kappa_{AV}$ | 0.6207                    | 0.5023                     | 0.3372                            |
| 50 kHz    | $\kappa_1$    | 0.9966                    | 0.2386                     | 0.0684                            |
|           | $\kappa_2$    | 0.9952                    | 0.2398                     | 0.2245                            |
|           | $\kappa_{SL}$ | 0.9955                    | 0.3275                     | 0.5774                            |
|           | $\kappa_{AV}$ | 0.9884                    | 0.3536                     | 0.4704                            |
| 200 kHz   | $\kappa_1$    | 0.6208                    | 0.0045                     | 0.0476                            |
|           | $\kappa_2$    | 0.6210                    | 0.0047                     | 0.3704                            |
|           | $\kappa_{SL}$ | 0.6703                    | 0.0654                     | 0.3212                            |
|           | $\kappa_{AV}$ | 0.6495                    | 0.1085                     | 0.1757                            |

#### 4.2.2 Case 2

For this Case, the aim result is to investigate the voltage at terminal 11, when terminal 1 is energized, as depicted in Fig. 4.15. This means that the core closest to the air-soil interface is energized and the voltage at the core of the deepest buried cable is evaluated.

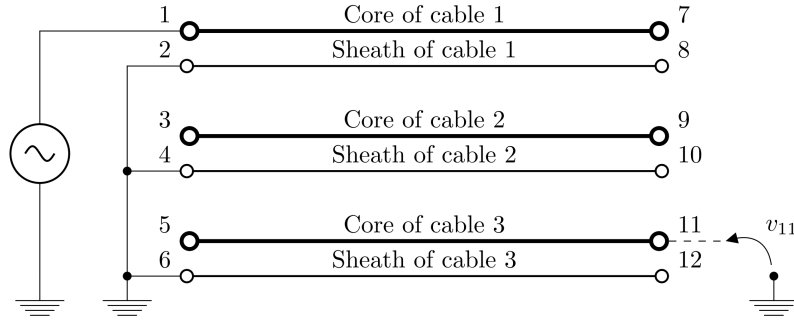


Figure 4.15: Energization scheme of Case 2.

Figures 4.16(a), (b) and (c) depict the results considering soil resistivity 100  $\Omega\cdot\text{m}$ , when node 1 is energized with a 1.0 pu voltage source and frequencies 3 kHz, 50 kHz and 200 kHz, respectively. As before, only when high frequency is considered soil modeling affects the evaluated voltage. Also, both Smith-Longmire and Alipio-Visacro have the same behavior.

For the same energization scheme, Figures 4.17(a), (b) and (c) present the results regarding a soil resistivity of 3000  $\Omega\cdot\text{m}$ . It is possible to observe that with the 3 kHz source the voltages obtained are slightly higher when both  $\kappa_3$  are considered and this

is also seen for the 50 kHz source, except for the first two peaks, which have rather the same amplitude. However, when the 200 kHz source is applied, Alipio-Visacro model becomes the most damped model and  $\kappa_1$  and  $\kappa_2$  present the higher peaks.

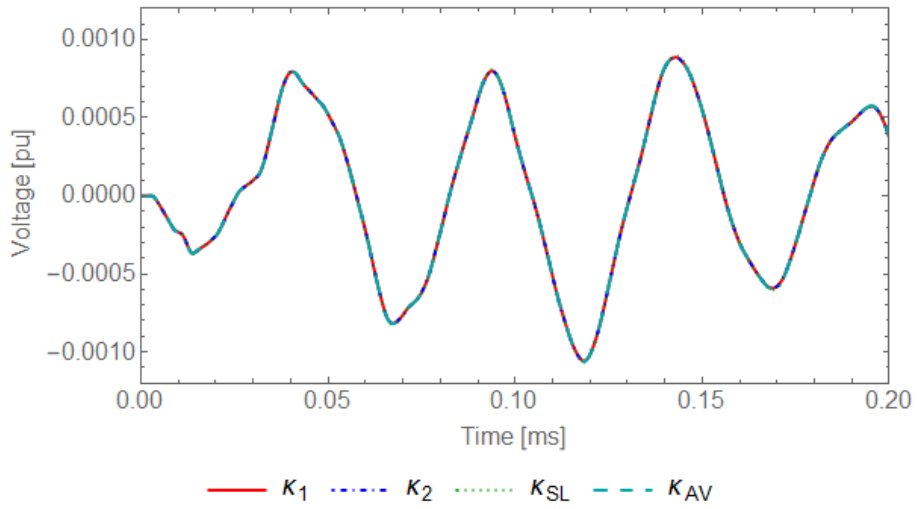
Considering the results for the extremely-resistive-soil in Figs. 4.18(a), (b) and (c), one may note for all the frequencies evaluated that  $\kappa_3$  models present most damped behavior,  $\kappa_2$  gives the higher peaks and both  $\kappa_1$  and  $\kappa_2$  respond in a higher frequency oscillatory behavior.

These results also provide agreement with the sensitivity analysis and other previously analyzed issues in the sense that the behavior of the system when soil is modeled as  $\kappa_1$  and  $\kappa_2$  is barely the same even for the soil of  $3000 \Omega \cdot \text{m}$ . Further, at frequencies higher than the ones that cause differences on the natural modes of propagation, the soil models affect strongly the cable system responses.

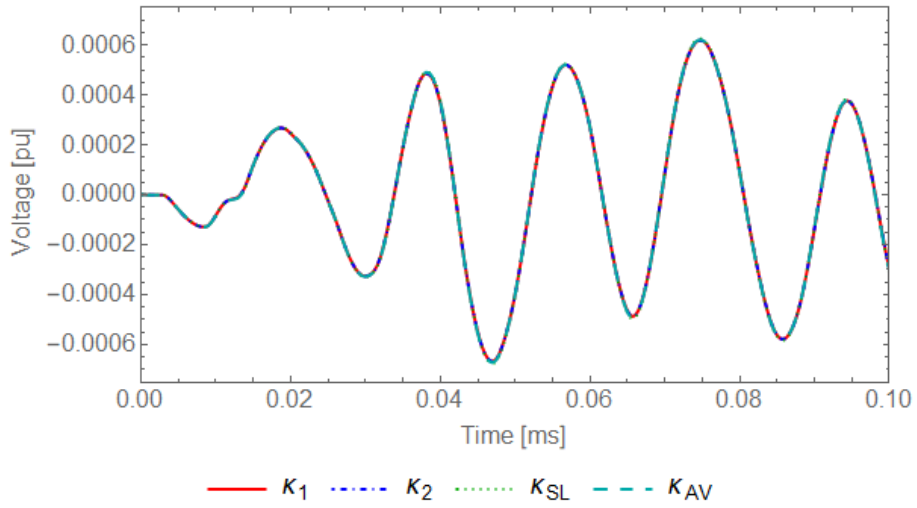
Analogously as previously presented for the other case, Table 4.2 presents the per-unit values of the maximum overvoltage caused by the energization of Fig. 4.15, regarding all graphics of Figures 4.16, 4.17 and 4.18. Unlike the results of Table 4.1, the overvoltages here verified are significantly low and it is possible to state that in the case that sheaths are grounded, more accurate modeling of the soil is not required.

Table 4.2: Maximum overvoltage for Case 2, in [pu].

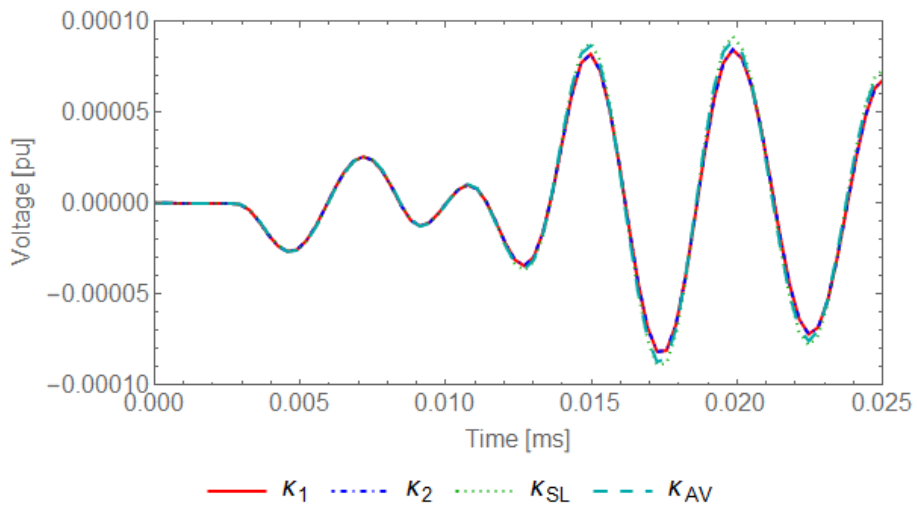
| Frequency | Soil          | $\rho_0$                    |                              |                               |
|-----------|---------------|-----------------------------|------------------------------|-------------------------------|
|           |               | 100 $\Omega \cdot \text{m}$ | 3000 $\Omega \cdot \text{m}$ | 120 k $\Omega \cdot \text{m}$ |
| 3 kHz     | $\kappa_1$    | $8.872 \times 10^{-4}$      | $5.331 \times 10^{-4}$       | $1.254 \times 10^{-3}$        |
|           | $\kappa_2$    | $8.873 \times 10^{-4}$      | $5.349 \times 10^{-4}$       | $2.057 \times 10^{-3}$        |
|           | $\kappa_{SL}$ | $8.974 \times 10^{-4}$      | $6.012 \times 10^{-4}$       | $7.888 \times 10^{-4}$        |
|           | $\kappa_{AV}$ | $8.913 \times 10^{-4}$      | $6.210 \times 10^{-4}$       | $5.557 \times 10^{-4}$        |
| 50 kHz    | $\kappa_1$    | $6.188 \times 10^{-4}$      | $3.341 \times 10^{-4}$       | $2.359 \times 10^{-3}$        |
|           | $\kappa_2$    | $6.189 \times 10^{-4}$      | $3.363 \times 10^{-4}$       | $3.617 \times 10^{-3}$        |
|           | $\kappa_{SL}$ | $6.240 \times 10^{-4}$      | $4.117 \times 10^{-4}$       | $1.149 \times 10^{-3}$        |
|           | $\kappa_{AV}$ | $6.206 \times 10^{-4}$      | $4.264 \times 10^{-4}$       | $8.159 \times 10^{-4}$        |
| 200 kHz   | $\kappa_1$    | $9.531 \times 10^{-5}$      | $8.897 \times 10^{-5}$       | $7.741 \times 10^{-4}$        |
|           | $\kappa_2$    | $9.536 \times 10^{-5}$      | $8.977 \times 10^{-5}$       | $1.339 \times 10^{-3}$        |
|           | $\kappa_{SL}$ | $1.032 \times 10^{-4}$      | $6.653 \times 10^{-5}$       | $1.338 \times 10^{-4}$        |
|           | $\kappa_{AV}$ | $9.861 \times 10^{-5}$      | $5.880 \times 10^{-5}$       | $1.280 \times 10^{-4}$        |



(a) 3 kHz.

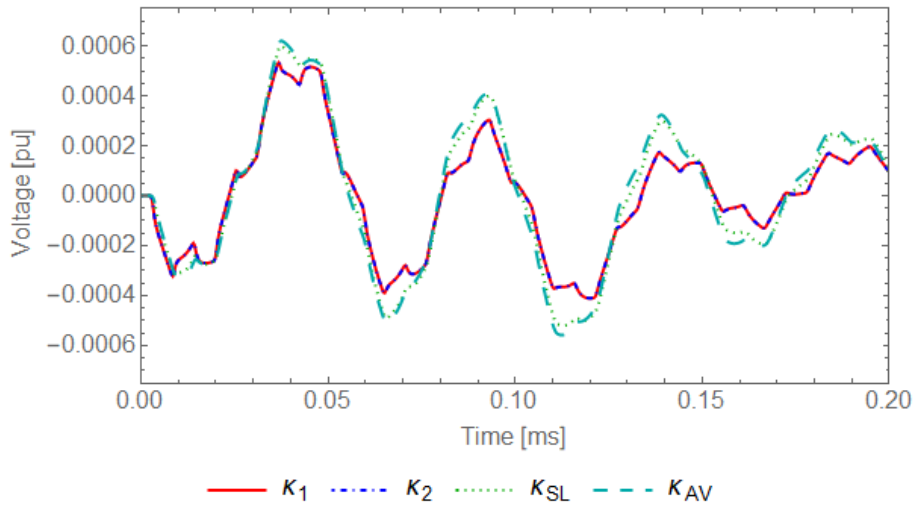


(b) 50 kHz.

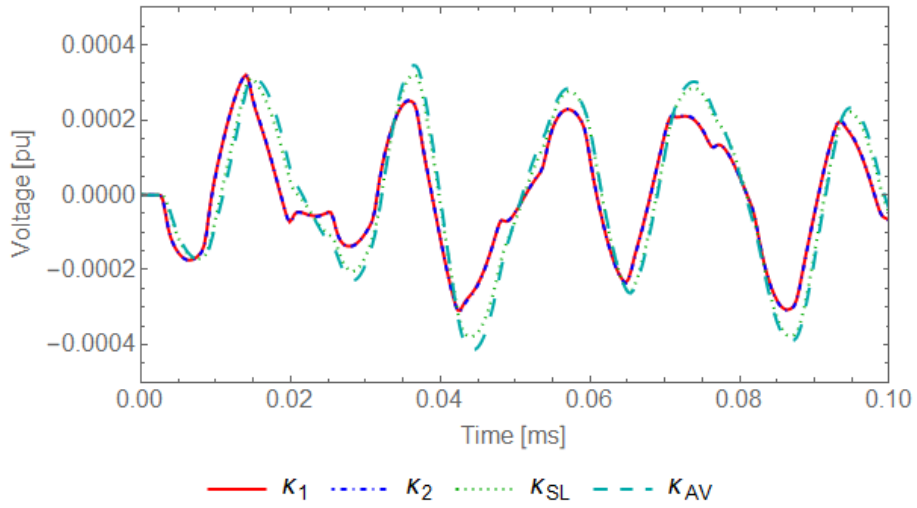


(c) 200 kHz.

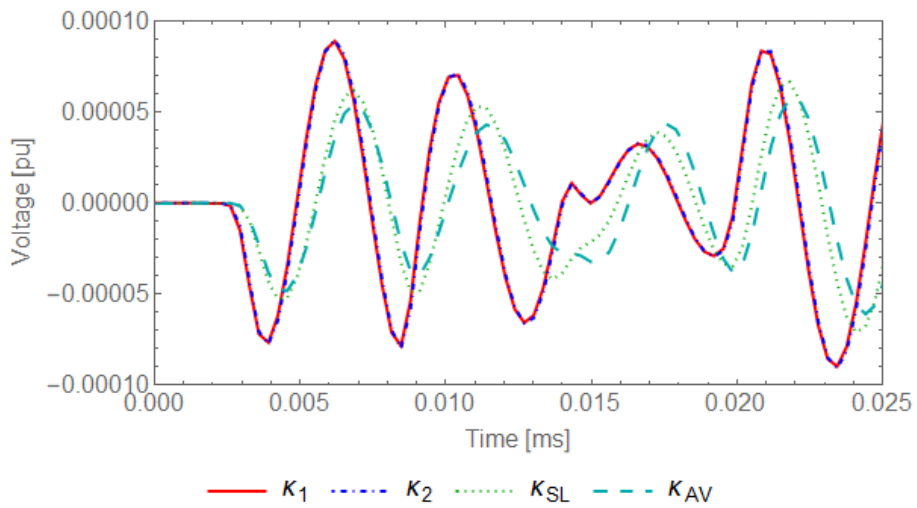
Figure 4.16: Case 2 – soil resistivity  $100 \Omega \cdot \text{m}$ .  $\kappa_1 = \sigma_0 = 1/\rho_0$ ,  $\kappa_2 = \sigma_0 + j\omega\epsilon_\infty$ ,  $\kappa_{SL}$  considers Smith-Longmire model, and  $\kappa_{AV}$  considers Alipio-Visacro model.



(a) 3 kHz.

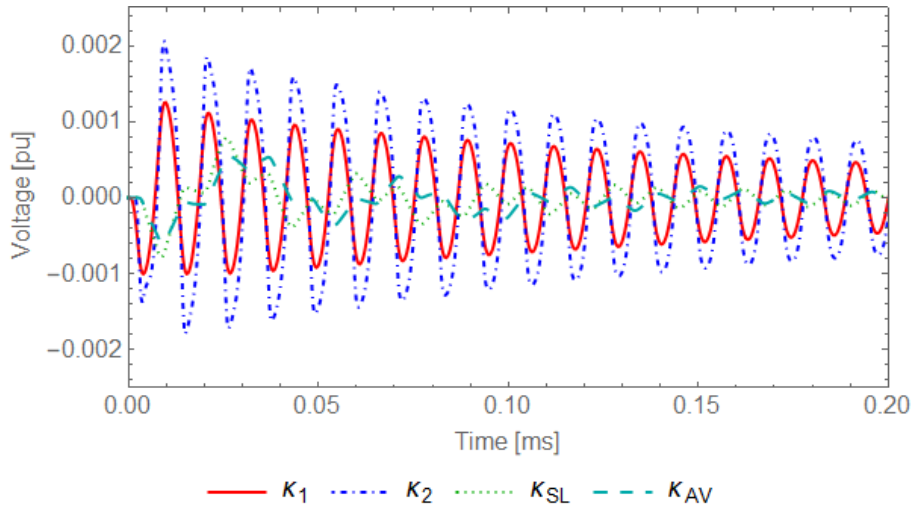


(b) 50 kHz.

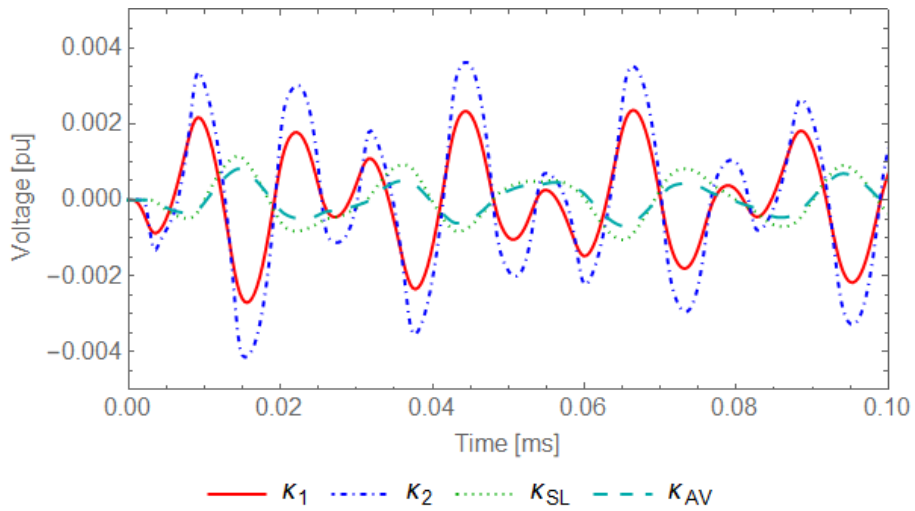


(c) 200 kHz.

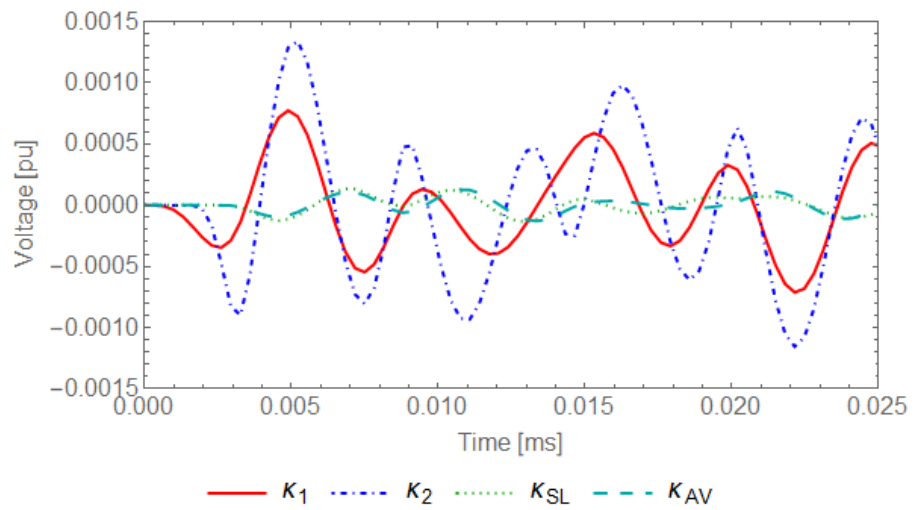
Figure 4.17: Case 2 – soil resistivity  $3000 \Omega \cdot \text{m}$ .  $\kappa_1 = \sigma_0 = 1/\rho_0$ ,  $\kappa_2 = \sigma_0 + j\omega\epsilon_\infty$ ,  $\kappa_{SL}$  considers Smith-Longmire model, and  $\kappa_{AV}$  considers Alipio-Visacro model.



(a) 3 kHz.



(b) 50 kHz.



(c) 200 kHz.

Figure 4.18: Case 2 – soil resistivity  $120 \text{ k}\Omega\cdot\text{m}$ .  $\kappa_1 = \sigma_0 = 1/\rho_0$ ,  $\kappa_2 = \sigma_0 + j\omega\varepsilon_\infty$ ,  $\kappa_{SL}$  considers Smith-Longmire model, and  $\kappa_{AV}$  considers Alipio-Visacro model.

### 4.3 Discussion

This Chapter presented results regarding the behavior of ground return impedance and admittance (shunt impedance) due to soil resistivity variations, by means of sensitivity analysis. Several cable system configurations were addressed in order to investigate how the soil influence are sensed in each of them. In the following, test cases considering the cable system response to energization were also presented.

In a practical sense, the qualitative results here found in the sensitivity analysis are to be taken as main conclusions. All cases studied have presented similar sensitivity behavior, be it varying frequency with fixed resistivity values or varying resistivity at fixed frequencies. Nevertheless, little differences were found when cables are separated by portions of soil, here represented by configurations flat horizontal and vertical. The latter is the most susceptible configuration to soil resistivity value, because aside phase separation, each cable is buried at a different depth.

For that reason, two different time-domain energization test cases were carried out considering the flat vertical configuration and very interesting results were obtained. For both cases, the low resistivity value of  $100 \Omega\cdot\text{m}$  generated quite similar results, i.e., different soil models had little or non impact on the results. As for the other resistivity values considered, the analysis is presented by each case.

Case 1 considered the energization of the sending-end sheath of one of the cables and the evaluation of the voltage at the receiving-end core of the farthest cable. This energization scheme excites the inter-sheath mode that passes through the ground, therefore, the frequency-dependent soil models may present resonances and higher overvoltages were observed. The exception was the soil with  $\rho_0 = 120 \text{ k}\Omega\cdot\text{m}$ , where  $\kappa_2$  provided greater overvoltage at 200 kHz.

Case 2 considered energization of the sending-end core of one of the cables and the evaluation of the voltage at the receiving-end core of the farthest cable, with all the sending-end sheaths grounded. The grounding of the sheaths put them in a shunt connection with the soil and reduces its impact. Results indicated that for resistivity value above  $3000 \Omega\cdot\text{m}$ , soil models  $\kappa_1$  and  $\kappa_2$  lead to greater overvoltages than  $\kappa_{SL}$  and  $\kappa_{AV}$  at 200 kHz. This is observed for all given frequencies when  $\rho_0 = 120 \text{ k}\Omega\cdot\text{m}$  is considered.

Furthermore, Case 2 also presented very low voltages, being the highest value below 0.004 pu. Therefore, it is possible to say that more complete soil models are not strictly necessary whenever short cable systems with grounded sending-end sheaths are considered.

# Chapter 5

## Conclusions

This doctorate research deals with the interactions between soil parameters and typical underground cable systems configurations. The soil resistivity is often treated as an apparent resistivity, i.e., a single measurement or an estimated quantity  $\rho_0$ , and is frequently considered a deterministic parameter. However, the soil's own geological behavior at a fixed frequency depends on several other parameters and, when frequency dependence is joined in the analysis, uncertainties must be considered.

A probabilistic approach was used as a first attempt to explore these uncertainties and how they might affect the cable system expressions that comprise the soil parameters, namely, ground return impedance and admittance. For a given statistical behavior of one soil, represented by the probability density function associated with a Weibull distribution, it was possible to obtain the PDFs of the ground return impedance and admittance. However, this approach strongly depends on a previous statistical knowledge of the soils in the cable system's path and, therefore, enhances the argument that soil's unknown characteristics should be thoroughly investigated.

Further analysis was necessary as a complete model of the soil itself, regarding all sort of influence such as humidity, seasonal changes etc, can be considered unfeasible. Simulations regarding different formulations and different values had to be considered, so different soil models were reviewed.

In order to include soil's frequency dependence in simulations, it is proposed to represent existing frequency-dependent soil models by means of rational functions obtained via fitting process, such as the Vector Fitting technique here considered. The traditional Smith-Longmire model not only could be fitted with minor RMS-error, but also presented a pattern within its residues and between its poles, which is a fixed ratio regardless of the apparent resistivity considered, confirming its universality. Same approach was applied to Alipio-Visacro model, which is based on measurements that do not confine the soil, but let the electromagnetic fields freely spread. A pole-residue rational model was also obtained with minor RMS-error and a most interesting feature was found that regardless of the soil apparent resistivity,

the same set of poles can be used, correcting the response with new residues. Thus, the universality of Alipio-Visacro model was also proved.

Traditional EMTP-like programs and EMT simulations disregard the ground return admittance, even though recent researches indicate its influence on cable systems performance. Its inclusion, however, usually resorts on infinite integrals calculation, with typical heavy computation burden. Therefore, an important contribution of this Thesis is the novel closed-form expression for the ground return admittance of underground cable systems that was proposed and validated with some frequency- and time-domain test cases.

A sensitivity analysis was carried out to identify the influence of soil resistivity with respect to different models and cable systems configurations. These results showed how the considered configurations are affected and, therefore, how they should respond when submitted to seasonal changes, for example. It was found that regarding the ground return impedance, even though the typical configurations present similar behavior, sensitivity curves of the flat vertical configuration are more susceptible to  $\rho_0$ , because of the different depths and of the distance between phases. Also, the ground return admittance sensitivity, evaluated in terms of shunt impedance, presented a behavior close to constant for frequencies near 1 kHz and with little differences up to 100 kHz.

By using the combined developed tools, it was possible to evaluate the cable system performance due to different energization schemes, considering frequency-dependent soils and ground return admittance. Induced voltages at the core of the deepest buried cable of the vertical configuration were evaluated considering the application of a voltage source: 1) at the sending-end sheath of the less buried cable, with all other terminals opened; and 2) at the sending-end core of the same cable, with all the sending-end sheaths grounded. Case 1 has shown that without grounding the sheaths, the cable system performance is strongly impacted by the soil model considered and frequency-dependent models provide higher overvoltages, some of them in the order of 1 pu. From Case 2, it was possible to conclude that the grounding of the sending-end sheaths brings the overvoltages down to 0.004 pu or less, which allows for the usage of frequency-independent soil models without great losses of accuracy.

Together with the rational models, the development of the closed-form expression for the ground return admittance was of paramount importance because only with these two novel approaches combined it was possible to investigate properly the analyses without resorting to heavy computational burden. Although the soil resistivity value is typically considered as a fixed parameter, it was possible to identify part of the associated impacts by comparing different levels of modeling accuracy.

## 5.1 Future Work

The developed tools and the obtained results of this Thesis are believed to be important and necessary steps towards a greater goal of finding the correct characterization of the impact caused by soils in power systems transient performance. By exploring the methodology and results here presented, one might deal with further studies:

- To apply the proposed methodology on three-conductor SC-cable systems, i.e., the ones with core, sheath and armor and a total of three metallic conductors per phase.
- To investigate numerical modeling on the implementation of the Bessel K functions for the calculations of cable's internal impedances.
- To train neural networks with an enormous set of data, so that it could be able to predict the behavior of several cable system responses to different soils.
- To investigate whether it is possible or not to separate the influence of soil on the nodal admittance matrix, since it was seen that not only the ground return impedance is important for the performance analysis of the cable systems, but also is the ground return admittance.
- To apply the proposed methodology on overhead lines and, then, investigate its transient ground resistance.

# References

- [1] TESCHE, F. “On the modeling and representation of a lossy earth for transient electromagnetic field calculations”, *Theoretical Notes 367*, 2002.
- [2] SALVADOR, J., ALIPIO, R., LIMA, A., CORREIA DE BARROS, M.T. “A Concise Approach of Soil Models for Time-Domain Analysis”, *IEEE Trans. on Electromagnetic Compatibility*, 2019. doi: 10.1109/TEMPC.2019.2927273.
- [3] MAGALHÃES, A. *Metodologia para Representação da Influência de Meios Externos nos Parâmetros Unitários de Cabos Subterrâneos e Submarinos*. Tese de Doutorado, COPPE/UFRJ, 2017.
- [4] LIMA, A., PORTELA, C. “Closed-form expressions for ground return impedances of overhead lines and underground cables”, *Int. J. of Elec. Power & Ener. Sys.*, v. 38, n. 1, pp. 20–26, 2012.
- [5] SALVADOR, J., MAGALHÃES, A., LIMA, A., CORREIA DE BARROS, M.T. “Closed-form Expression for Ground Return Admittance in Underground Cables”, *IEEE Trans. on Power Delivery*, 2019. doi: 10.1109/TPWRD.2019.2897257.
- [6] ARCHIE, G. “The Electrical Resistivity Log as an Aid in Determining Some Reservoir Characteristics”, *Petroleum Trans. of the AIME*, 1942.
- [7] NASCIMENTO, C., PIRES, A., MORAES, R. “Reconhecimento de Solos por meio de Resistividade Elétrica e Radiação Gama”, *Rev. Bras. de Geociências*, 2004.
- [8] JOHANSSON, S., ROSQVIST, H., SVENSSON, M., et al. “An alternative methodology for the analysis of electrical resistivity data from a soil gas study”, *Geophys. J. Int.*, v. 186, pp. 632–640, 2011.
- [9] ROSQVIST, H., LEROUX, V., DAHLIN, T., et al. “Mapping landfill gas migration using resistivity monitoring”, *Proc. of the Institution of Civil En-*

*gineers – Waste and Resource Management*, v. 164, n. WR1, pp. 3–15, fev. 2011.

- [10] DEVRIESE, S. *Detecting and imaging time-lapse conductivity changes using electromagnetic methods*. Tese de Doutorado, The University of British Columbia, 2016.
- [11] DEVRIESE, S., OLDENBURG, D. “Application of sensitivity analysis in DC resistivity monitoring of SAGD steam chambers”. In: *SEG Int. Exp. and 87th Annual Meeting*, 2016.
- [12] KELLER, G., FRISCHKNECHT, F. *Electrical Methods in Geophysical Prospecting*. Oxford, Pergamon Press, 1966.
- [13] WARD, S. “Resistivity and induced polarization methods”, *Investigations in Geophysics No 5: Geotechnical and Environmental Geophysics*, v. I: Review and Tutorial, pp. 147–189, 1990.
- [14] COELHO, V., PIANTINI, A., ALMAGUER, H., et al. “The influence of seasonal soil moisture on the behavior of soil resistivity and power distribution grounding systems”, *Elec. Pwr. Sys. Research*, v. 118, pp. 76 – 82, 2015.
- [15] “ABNT NBR 7117: Medição da resistividade e determinação da estratificação do solo”. , 2012.
- [16] “IEEE Std 81-2012: Guide for Measuring Earth Resistivity, Ground Impedance, and Earth Surface Potentials of a Grounding System”. , 2012.
- [17] FORTIN, S., YANG, Y., MA, J., et al. “Electromagnetic Fields of Energized Conductors in Multilayer Soils”. In: *Asia-Pacific Conf. on Environ. Electromag.*, pp. 893 –899, aug. 2006.
- [18] PATEL, U., TRIVERIO, P. “Accurate Impedance Calculation for Underground and Submarine Power Cables using MoM-SO and a Multilayer Ground Model”, *IEEE Trans. on Power Delivery*, v. 31, n. 3, pp. 1233–1241, 2016.
- [19] WAGNER, C., EVANS, R. “Symmetrical Components”. cap. Constants of Short Transmission Lines Without Ground Wires, McGraw-Hill Book Company, 1933.
- [20] DOS SANTOS, A., CORREIA DE BARROS, M.T. “Transmission Line Zero Sequence Impedance Probabilistic Model – effect of the earth resistivity

- uncertainty.” In: *CIGRÉ, CAGRE’15 - Algerian Large Electrical Net. Conf.*, Algiers, mar. 2015. Paper 015.
- [21] DOS SANTOS, A., CORREIA DE BARROS, M.T. “Probabilistic model of the distance protection error due to the earth resistivity uncertainty.” In: *CIGRÉ, XVI ERIAC Encuentro Regional Iberoamericano*, Puerto Iguazú, May 2015.
- [22] EDP-LABELEC. *Continental Portugal soil resistivity map – geoelectric characterization from main geologic forms (in Portuguese)*. Relatório técnico, 2008.
- [23] SIMÕES ALVES, M., CORREIA DE BARROS, M.T. “Soil Resistivity Probabilistic Modelling”. In: *GROUND’2016 and 7th LPE*, Porto de Galinhas, Brazil, June 2016.
- [24] PISHRO-NIK, H. *Introduction to probability, statistics, and random processes*. Kappa Research, 2014.
- [25] SALVADOR, J., LIMA, A., CORREIA DE BARROS, M.T. “Underground cable systems ground return impedance sensitivity to soil resistivity uncertainties”. In: *PSCC’2018 – Power Systems Computation Conference*, Dublin, Ireland, 2018.
- [26] AMETANI, A. “A general formulation of impedance and admittance of cables”, *IEEE Trans. on Power Apparatus and Systems*, v. PAS-99, n. 3, pp. 902–910, 1980.
- [27] JACKSON, J. *Classical Electrodynamics*. John Wiley & Sons, 1999.
- [28] RAMO, S., WHINNERY, J., VAN DUZER, T. *Fields and waves in communication electronics*. John Wiley & Sons, 2008.
- [29] BALANIS, C. *Advanced Engineering Electromagnetics*. John Wiley & Sons, 2012.
- [30] PORTELA, C. “Frequency and Transient Behavior of Grounding Systems – Part I: Physical and Methodological Aspects”. In: *IEEE Int. Symp. Electromag. Comp.*, pp. 379–384, ago. 1997.
- [31] SMITH, K., LONGMIRE, C. *A universal impedance for soils*. Defense Nuclear Agency, Alexandria, VA, USA, jul. 1975. Topical Report for Period, 1 July 1975 - 30 September 1975.

- [32] ALIPIO, R., VISACRO, S. “Modeling the frequency dependence of electrical parameters of soil”, *IEEE Trans. on Electromagnetic Compatibility*, v. 56, n. 5, pp. 1163–1171, 2014.
- [33] ALIPIO, R. *Dependência da Frequência dos Parâmetros do Solo: Efeito no Comportamento Impulsivo de Aterramentos Elétricos*. Tese de Doutorado, UFMG, 2013.
- [34] CAVKA, D., MORA, N., RACHIDI, F. “A Comparison of Frequency-Dependent Soil Models: Application to the Analysis of Grounding Systems”, *IEEE Trans. on Electromagnetic Compatibility*, v. 56, n. 1, pp. 177–187, Feb 2014.
- [35] MESSIER, M. *The propagation of an electromagnetic impulse through soil: Influence of frequency dependent parameters*. Relatório técnico, Mission Res. Corp., Santa Barbara, CA, USA, 1985.
- [36] MESSIER, M. *Another soil conductivity model*. Relatório técnico, JAYCOR, Santa Barbara, CA, USA, 1985.
- [37] PORTELA, C. “Measurement and modeling of soil electromagnetic behavior”. In: *IEEE Int. Symp. Electromag. Comp.*, v. 2, pp. 1004–1009, 1999.
- [38] ALIPIO, R., VISACRO, S. “Time-Domain Analysis of Frequency-Dependent Electrical Parameters of Soil”, *IEEE Trans. on Electromagnetic Compatibility*, v. 59, n. 3, pp. 873–878, 2017.
- [39] BAÑUELOS-CABRAL, E., GUTIÉRREZ-ROBLES, J., GUSTAVSEN, B. *Rational Fitting Techniques for the Modeling of Electric Power Components and Systems Using MATLAB Environment*. INTECH, 2017.
- [40] WILCOX, D. “Numerical Laplace Transformation and Inversion”, *Int. J. Elect. Eng.*, v. 15, pp. 247–265, 1978.
- [41] MORENO, P., RAMIREZ, A. “Implementation of the Numerical Laplace Transform: A review task force on frequency domain methods for EMT studies”, *IEEE Trans. on Power Delivery*, v. 23, n. 4, pp. 2599–2609, out. 2008.
- [42] GÓMEZ, P., URIBE, F. “The numerical Laplace transform: An accurate technique for analyzing electromagnetic transients on power system devices”, *Int. J. of Elec. Pwr. & Ener. Sys.*, v. 31, n. 2, pp. 116–123, 2009.

- [43] HUA, Y., SARKAR, T. “Matrix pencil method for estimating parameters of exponentially damped/undamped sinusoids in noise”, *IEEE Trans. on Acoustics, Speech, and Signal Processing*, v. 38, n. 5, pp. 814–824, 1990.
- [44] SARKAR, T., PEREIRA, O. “Using the matrix pencil method to estimate the parameters of a sum of complex exponentials”, *IEEE Anten. and Propag. Magaz.*, v. 37, n. 1, pp. 48–55, 1995.
- [45] SHESHYEKANI, K., KARAMI, H., DEHKHODA, P., et al. “Application of the matrix pencil method to rational fitting of frequency-domain responses”, *IEEE Trans. on Power Delivery*, v. 27, n. 4, pp. 2399–2408, 2012.
- [46] GUSTAVSEN, B., SEMLYEN, A. “Rational approximation of frequency domain responses by vector fitting”, *IEEE Trans. on Power Delivery*, v. 14, n. 3, pp. 1052–1061, jul. 1999.
- [47] GUSTAVSEN, B. “Improving the pole relocating properties of vector fitting”, *IEEE Trans. on Power Delivery*, v. 21, n. 3, pp. 1587–1592, jul. 2006.
- [48] DESCHRIJVER, D., MROZOWSKI, M., DHAENE, T., et al. “Macromodeling of Multiport Systems Using a Fast Implementation of the Vector Fitting Method”, *IEEE Microwave and Wireless Components Letters*, v. 18, n. 6, pp. 383–385, jun. 2008.
- [49] GUSTAVSEN, B. “Computer Code for Rational Approximation of Frequency Dependent Admittance Matrices”, *IEEE Trans. on Power Delivery*, v. 17, n. 4, pp. 1093–1098, Oct. 2002.
- [50] POLLACZEK, F. “Über das Feld einer unendlich langen wechsel stromdurchflossenen Einfachleitung”, *Elekt. Nachrichten Technik*, v. 3, pp. 339–360, 1926.
- [51] CARSON, J. “Ground Return Impedance: Underground Wire with Earth Return”, *Bell Sys. Tech. J.*, v. 8, n. 1, pp. 94–98, 1929.
- [52] SCHELKUNOFF, S. “The Electromagnetic Theory of Coaxial Transmission Lines and Cylindrical Shields”, *Bell Sys. Tech. J.*, , n. 13, 1934.
- [53] WEDEPOHL, L., WILCOX, D. “Transient analysis of underground power-transmission systems. System-model and wave-propagation characteristics”, *Proc. of the IEE*, v. 120, n. 2, pp. 253–260, 1973.
- [54] CIGRE WG B1.30, . *Cable Systems Electrical Characteristics*. Technical brochure, CIGRE, 2013.

- [55] SUNDE, E. *Earth Conduction Effects in Transmission Systems*. New York, Dover, 1968.
- [56] PAPADOPOULOS, T., TSIAMITROS, D., PAPAGIANNIS, G. “Impedances and admittances of underground cables for the homogeneous earth case”, *IEEE Trans. on Power Delivery*, v. 25, n. 2, pp. 961–969, 2010.
- [57] PAPADOPOULOS, T., TSIAMITROS, D., PAPAGIANNIS, G. “Earth return admittances and impedances of underground cables in non-homogeneous earth”, *IET Gen., Trans. & Dist.*, v. 5, n. 2, pp. 161–171, 2011.
- [58] MAGALHÃES, A., SILVA, J., LIMA, A., CORREIA DE BARROS, M.T. “Validation Limits of Quasi-TEM Approximation for Buried Bare and Insulated Cables”, *IEEE Trans. on Electromagnetic Compatibility*, v. 57, n. 6, pp. 1690–1697, 2015.
- [59] MAGALHÃES, A., CORREIA DE BARROS, M. T., LIMA, A. “Earth Return Admittance Effect on Underground Cable System Modeling”, *IEEE Trans. on Power Delivery*, v. 33, n. 2, pp. 662–670, April 2018.
- [60] XUE, H., AMETANI, A., MAHSEREDJIAN, J., et al. “Generalized Formulation of Earth-Return Impedance/Admittance and Surge Analysis on Underground Cables”, *IEEE Trans. on Power Delivery*, 2018.
- [61] HO, C., RUEHLI, A., BRENNAN, P. “The Modified Nodal Approach to Network Analysis”, *IEEE Transactions on Circuits and Systems*, v. CAS-22, pp. 504–509, 1975.
- [62] MARTINS, T., LIMA, A., CARNEIRO JR., S. “Effect of approximate impedance formulae on the accuracy of transmission line modelling”, *IET Gen., Transm. & Dist.*, v. 1, n. 4, pp. 534–539, July 2007.
- [63] PETTERSSON, P. “Propagation of waves on a wire above a lossy ground - Different formulations with approximations”, *IEEE Trans. on Power Delivery*, v. 14, n. 3, pp. 1173–1180, jul. 1999.
- [64] SAAD, O., GABA, G., GIROUX, M. “A closed-form approximation for ground return impedance of underground cables”, *IEEE Trans. on Power Delivery*, v. 11, n. 3, pp. 1536–1545, Jul. 1996.
- [65] ERDÉLYI, A. *Asymptotic expansions*. N. 3. Courier Corporation, 1956.
- [66] COPSON, E. T., COPSON, E. T. *Asymptotic expansions*. N. 55. Cambridge University Press, 2004.

- [67] WEDEPOHL, L., MOHAMED, S. “Multiconductor transmission lines. Theory of natural modes and Fourier integral applied to transient analysis”, *Proc. of the IEE*, v. 116, n. 9, pp. 1553–1563, 1969.
- [68] SILVA, J. *Estimação dos Parâmetros Elétricos de Cabos de Potência Submarinos Considerando Meios Dispersivos*. Tese de Doutorado, COPPE/UFRJ, 2016.
- [69] MANHÃES, R. *Formulação e Cálculo dos Parâmetros Elétricos de um Sistema de Cabos em Função da Frequência*. Tese de Mestrado, UNIFEI, 1992.
- [70] SEMLYEN, A. “Accuracy limits in the computed transients on overhead lines due to inaccurate ground return modeling”, *IEEE Trans. on Power Delivery*, v. 17, n. 3, pp. 872–878, 2002.
- [71] MARTINEZ-VELASCO, J. *Power System Transients Parameter Determination*. CRC Press, 2010.

# Appendix A

## Review on Smith-Longmire and Alipio-Visacro Models

### A.1 Smith-Longmire

Soil as admittance:

$$Y(\omega) = \sigma(\omega) + j\omega\varepsilon(\omega) \quad (\text{A.1})$$

Soil as RC network:

$$Y(\omega) = \frac{1}{R_0} + j\omega C_\infty + \sum_{n=1}^N \underbrace{\frac{1}{R_n + \frac{1}{j\omega C_n}}}_{(\#)} \quad (\text{A.2})$$

Rearranging (#):

$$\begin{aligned} \frac{1}{R_n + \frac{1}{j\omega C_n}} &= \frac{j\omega C_n}{1 + j\omega R_n C_n} \cdot \frac{1 - j\omega R_n C_n}{1 - j\omega R_n C_n} \\ &= \frac{\omega^2 R_n C_n^2 + j\omega C_n}{1 + \omega^2 R_n^2 C_n^2} \end{aligned} \quad (\text{A.3})$$

Back to (A.2) and considering  $\sigma = \Re\{Y\}$  and  $\varepsilon = \Im\{Y\}$ :

$$\begin{aligned} \sigma(\omega) &= \frac{1}{R_0} + \sum_{n=1}^N \frac{\omega^2 R_n C_n^2}{1 + \omega^2 R_n^2 C_n^2} \\ \varepsilon_r(\omega) &= \frac{C_\infty}{\varepsilon_0} + \sum_{n=1}^N \frac{C_n/\varepsilon_0}{1 + \omega^2 R_n^2 C_n^2} \end{aligned} \quad (\text{A.4})$$

Thus,  $C_\infty = \varepsilon_0 \varepsilon_\infty$  and  $R_0 = \sigma_0^{-1}$ .

By considering  $C_n = \varepsilon_0 a_n$  and  $\beta_n = 1/R_n C_n$ , we get:

$$\sigma(\omega) = \sigma_0 + \varepsilon_0 \sum_{n=1}^N \beta_n a_n \frac{(\omega/\beta_n)^2}{1 + (\omega/\beta_n)^2} \quad (\text{A.5})$$

$$\varepsilon_r(\omega) = \varepsilon_\infty + \sum_{n=1}^N \frac{a_n}{1 + (\omega/\beta_n)^2} \quad (\text{A.6})$$

where  $a_n$  are given in Table A.1:

Table A.1: Coefficients for Smith-Longmire Model.

| n | $\alpha_n$         | n  | $\alpha_n$         | n  | $\alpha_n$            |
|---|--------------------|----|--------------------|----|-----------------------|
| 1 | $3.40 \times 10^6$ | 6  | $1.33 \times 10^2$ | 11 | $9.80 \times 10^{-1}$ |
| 2 | $2.74 \times 10^5$ | 7  | $2.72 \times 10^1$ | 12 | $3.92 \times 10^{-1}$ |
| 3 | $2.58 \times 10^4$ | 8  | $1.25 \times 10^1$ | 13 | $1.73 \times 10^{-1}$ |
| 4 | $3.38 \times 10^3$ | 9  | $4.80 \times 10^0$ |    |                       |
| 5 | $5.26 \times 10^2$ | 10 | $2.17 \times 10^0$ |    |                       |

Also, considering  $\beta_n = 2\pi f_n$ , we get

$$\sigma(f) = \sigma_0 + \varepsilon_0 \sum_{n=1}^N 2\pi f_n a_n \frac{(2\pi f/2\pi f_n)^2}{1 + (2\pi f/2\pi f_n)^2} \quad (\text{A.7})$$

$$\varepsilon_r(f) = \varepsilon_\infty + \sum_{n=1}^N \frac{a_n}{1 + (2\pi f/2\pi f_n)^2} \quad (\text{A.8})$$

or, simply

$$\sigma(f) = \sigma_0 + 2\pi\varepsilon_0 \sum_{n=1}^N f_n a_n \frac{(f/f_n)^2}{1 + (f/f_n)^2} \quad (\text{A.9})$$

and

$$\varepsilon_r(f) = \varepsilon_\infty + \sum_{n=1}^N \frac{a_n}{1 + (f/f_n)^2} \quad (\text{A.10})$$

It should be noted that SL model relates soil conductivity and its water content by the expressions

$$\begin{aligned}\sigma_0 &= 8 \times 10^{-3}(w/10)^{1.54} \implies w = 10(125\sigma_0)^{1/1.54} \\ \text{and} \\ f_n &= \left(\frac{w}{10}\right)^{1.28} 10^{n-1} \text{ or } \beta_n = 2\pi \left(\frac{w}{10}\right)^{1.28} 10^{n-1}\end{aligned}\tag{A.11}$$

Hence,  $f_n$  can be written as

$$f_n = (125\sigma_0)^{1.28/1.54} 10^{n-1} \implies f_n \approx (125\sigma_0)^{0.8312} 10^{n-1}\tag{A.12}$$

## A.2 Alipio-Visacro

Initially,

$$\kappa = \sigma + j\omega\varepsilon\tag{A.13}$$

$$\sigma(f) = \sigma_0 + K_\sigma f^\gamma\tag{A.14}$$

$$\varepsilon(f) = \varepsilon_r \varepsilon_0 + K_\varepsilon f^{\gamma-1}\tag{A.15}$$

with

$$K_\sigma = \sigma_0 \frac{h(\sigma_0)}{(10^6)^\gamma},\tag{A.16}$$

with  $\sigma_0$  in [S/m] and

$$K_\varepsilon = \frac{K_\sigma}{2\pi} \tan\left(\frac{\pi}{2}\gamma\right).\tag{A.17}$$

Parameter  $h(\sigma_0)$  represents a fitting function for taking into account the inherent statistical dispersion of the frequency dependent variation of  $\sigma$ . It is defined as

$$h(\sigma_0) = \xi \sigma_0^{-0.73}, \text{ with } \xi = \begin{cases} 1.26 & , \text{ for mean results} \\ 0.95 & , \text{ for relatively conservative results} \\ 0.70 & , \text{ for conservative results} \end{cases}\tag{A.18}$$

with  $\sigma_0$  in [mS/m] only for calculating  $h(\sigma_0)$ .

Rewriting (A.14) as  $\sigma(\omega)$ :

$$\sigma(\omega) = \sigma_0 + K_\sigma \left(\frac{\omega}{2\pi}\right)^\gamma.\tag{A.19}$$

Rewriting (A.15) as  $\varepsilon(\omega)$  and using (A.16) and (A.17):

$$\varepsilon(\omega) = \varepsilon_r \varepsilon_0 + \frac{K_\sigma}{2\pi} \tan\left(\frac{\pi}{2}\gamma\right) \left(\frac{\omega}{2\pi}\right)^{\gamma-1} . \quad (\text{A.20})$$

Gathering all in (A.13):

$$\begin{aligned} \kappa &= \sigma_0 + K_\sigma \left(\frac{\omega}{2\pi}\right)^\gamma + j\omega \left[ \varepsilon_r \varepsilon_0 + \frac{K_\sigma}{2\pi} \tan\left(\frac{\pi}{2}\gamma\right) \left(\frac{\omega}{2\pi}\right)^{\gamma-1} \right] \\ \kappa &= \sigma_0 + j\omega \varepsilon_r \varepsilon_0 + K_\sigma \left[ \left(\frac{\omega}{2\pi}\right)^\gamma + j \left(\frac{\omega}{2\pi}\right) \tan\left(\frac{\pi}{2}\gamma\right) \left(\frac{\omega}{2\pi}\right)^{\gamma-1} \right] \end{aligned}$$

hence,

$$\boxed{\kappa = \sigma_0 + j\omega \varepsilon_r \varepsilon_0 + K_\sigma \left(\frac{\omega}{2\pi}\right)^\gamma \left[ 1 + j \tan\left(\frac{\pi}{2}\gamma\right) \right]} \quad (\text{A.21})$$

# Appendix B

## Further Expressions for $\mathbf{Z}$ and $\mathbf{Y}$

In this Appendix, further details on the expressions for impedances and admittances that assemble the matrices  $\mathbf{Z}$  and  $\mathbf{Y}$  are presented.

### B.1 Impedances per-unit-length

$z_1$ : the inner impedance of the core.

$$z_1 = \frac{\rho_c \gamma_c I_0(\gamma_c r_1)}{2\pi r_1 I_1(\gamma_c r_1)} \quad (\text{B.1})$$

where  $\rho_c$  is the core resistivity,  $\gamma_c = \sqrt{j\omega\mu_0/\rho_c}$  is the core propagation factor, and  $I_0$  and  $I_1$  are Bessel functions.

$z_2$ : the impedance due to time-varying magnetic field in insulation 1, i.e., between core and sheath.

$$z_2 = \frac{j\omega\mu_1}{2} \ln\left(\frac{r_2}{r_1}\right) \quad (\text{B.2})$$

where  $\mu_1$  is the permeability of insulation 1.

$z_3$ : the inner sheath internal impedance.

$$z_3 = \frac{\rho_s \gamma_s I_0(\gamma_s r_2)K_1(\gamma_s r_3) + K_0(\gamma_s r_2)I_1(\gamma_s r_3)}{2\pi r_2 I_1(\gamma_s r_3)K_1(\gamma_s r_2) - I_1(\gamma_s r_2)K_1(\gamma_s r_3)} \quad (\text{B.3})$$

where  $\rho_s$  is the sheath resistivity,  $\gamma_s = \sqrt{j\omega\mu_0/\rho_s}$  is the sheath propagation factor, and  $I_0$ ,  $I_1$ ,  $K_0$  and  $K_1$  are Bessel functions.

$z_4$ : the sheath mutual impedance.

$$z_4 = \frac{\rho_s/2\pi r_2 r_3}{I_1(\gamma_s r_3)K_1(\gamma_s r_2) + I_1(\gamma_s r_2)K_1(\gamma_s r_3)} \quad (\text{B.4})$$

$z_5$ : the outer sheath internal impedance.

$$z_5 = \frac{\rho_s \gamma_s}{2\pi r_3} \frac{I_0(\gamma_s r_3)K_1(\gamma_s r_2) + K_0(\gamma_s r_3)I_1(\gamma_s r_2)}{I_1(\gamma_s r_3)K_1(\gamma_s r_2) - I_1(\gamma_s r_2)K_1(\gamma_s r_3)} \quad (\text{B.5})$$

$z_6$ : the impedance due to time-varying flux in insulation 2, i.e., between sheath and the earth.

$$z_6 = \frac{j\omega\mu_2}{2} \ln\left(\frac{r_4}{r_3}\right) \quad (\text{B.6})$$

where  $\mu_2$  is the permeability of insulation 2.

### Brief review on the closed-form expression for $Z_g$ proposed in [4]

The mutual impedance per-unit-length is given by

$$Z_{ij} = \frac{j\omega\mu_0}{2\pi} [K_0(\gamma_1 d) - K_1(\gamma_1 D) + 2J_m] \quad (\text{B.7})$$

where  $d$ ,  $D$ ,  $\gamma_1$  and  $K(\cdot)$  are the same as before, and  $J_m$  is given by (B.8).

$$J_m = \int_0^\infty \frac{\exp\left(-\ell\sqrt{\xi^2 + \gamma_1^2}\right)}{\xi + \sqrt{\xi^2 + \gamma_1^2}} \cos(x\xi) d\xi \quad (\text{B.8})$$

which can be rewritten as

$$J_m = \frac{1}{\gamma_1^2} [I_3 - I_4] \quad (\text{B.9})$$

where

$$\begin{aligned} I_3 &= \int_0^\infty \sqrt{\xi^2 + \gamma_1^2} \exp(-\ell\sqrt{\xi^2 + \gamma_1^2}) \cos(x\xi) d\xi \\ I_4 &= \int_0^\infty \xi \exp(-\ell\sqrt{\xi^2 + \gamma_1^2}) \cos(x\xi) d\xi \end{aligned} \quad (\text{B.10})$$

The solution for  $I_3$  is obtained from the integral definition of the Bessel Function of Second Kind  $K_\nu(\cdot)$ . As  $I_4$  have no closed-form solution,  $J_m$  can be written as

$$J_m = \frac{\ell^2}{D} K_0(\eta D) + \frac{\ell^2 - x^2}{\eta D} K_1(\eta D) - \int_0^\infty \xi \exp(-\ell \sqrt{\xi^2 + \eta^2}) \cos(x\xi) d\xi \quad (\text{B.11})$$

This simplification is interesting once the numerical integration of (B.11) is simpler than of (B.8) as the integrand is less oscillatory. Thus, we can use an asymptotic expansion [65, 66], i.e., divergent series expansion, of the infinite integral in (B.11), which after some manipulation gives the closed-form expression:

$$Z_{ij} = \frac{j\omega\mu}{2\pi} \left[ K_0(\gamma_1 d) + \frac{\ell^2 - x^2}{D^2} K_2(\gamma_1 D) - 2 \frac{\ell^2 - x^2}{\gamma_1^2 D^4} (1 + \ell\gamma_1) \exp(-\ell\gamma_1) \right] \quad (\text{B.12})$$

## B.2 Admittance per-unit-length

$y_1$ : the admittance due to the capacitance of insulation 1.

$$y_1 = g_1 + j\omega \frac{2\pi\epsilon_{r_1}\epsilon_0}{\ln(r_2/r_1)} \quad (\text{B.13})$$

where  $\epsilon_{r_1}$  is the relative permittivity of insulation 1 and  $g_1$  is typically neglected.

$y_2$ : the admittance due to the capacitance of insulation 2.

$$y_2 = g_2 + j\omega \frac{2\pi\epsilon_{r_2}}{\ln(r_4/r_3)} \quad (\text{B.14})$$

where  $\epsilon_{r_2}$  is the relative permittivity of insulation 2 and  $g_2$  is typically neglected.

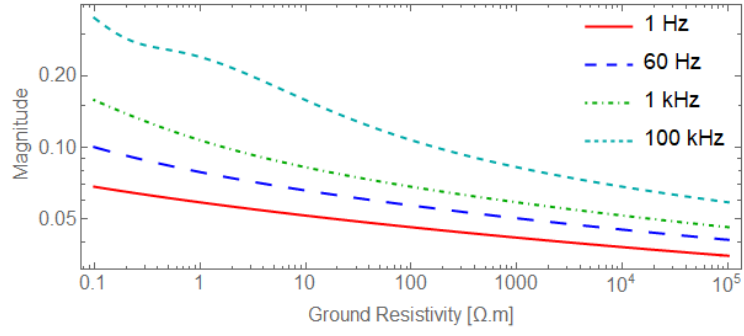
# Appendix C

## Additional Graphics: Sensitivity of Ground Return Series Impedance

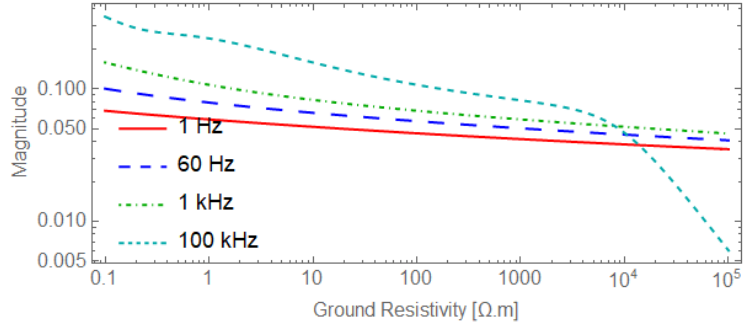
This appendix complements the results of the sensitivity analysis of ground return series impedances addressed in Section ???. Here they are presented with fixed frequencies – 1 Hz, 60 Hz, 1 kHz and 100 kHz – for a soil resistivity variation from  $0.1 \Omega\cdot\text{m}$  to  $100 \text{ k}\Omega\cdot\text{m}$ , and are organized in Tables C.1.

Table C.1: Results for sensitivity analysis plotted against ground resistivity.

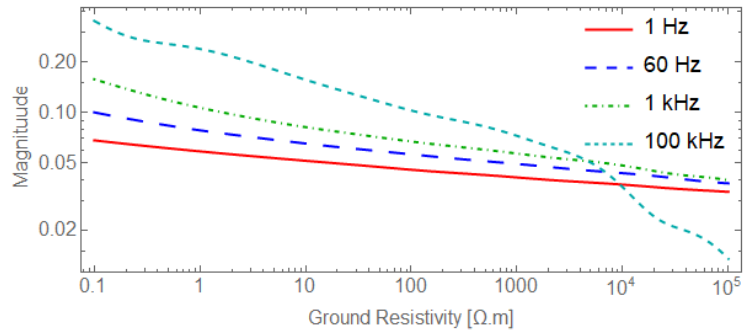
| $S_z$ | Cases    |            |          |                       |
|-------|----------|------------|----------|-----------------------|
|       | Pipe     | Horizontal | Trefoil  | Vertical              |
|       | Fig. C.1 | Fig. C.2   | Fig. C.3 | Fig. C.4 and Fig. C.5 |



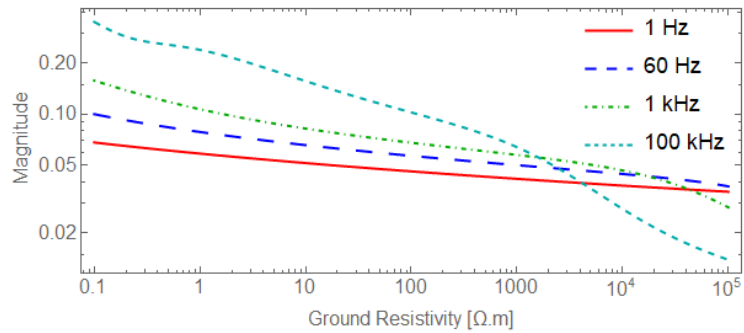
(a)  $\kappa = \sigma_0 = 1/\rho_0$



(b)  $\kappa = \sigma_0 + j\omega\epsilon_r\epsilon_0$



(c) Smith-Longmire



(d) Alipio-Visacro

Figure C.1: Sensitivities of series impedance for pipe-type cable configuration. Figures (a):  $\kappa = \sigma_0 = 1/\rho_0$ ; (b):  $\kappa = \sigma_0 + j\omega\epsilon_r\epsilon_0$ ; (c): Smith-Longmire; and (d): Alipio-Visacro.

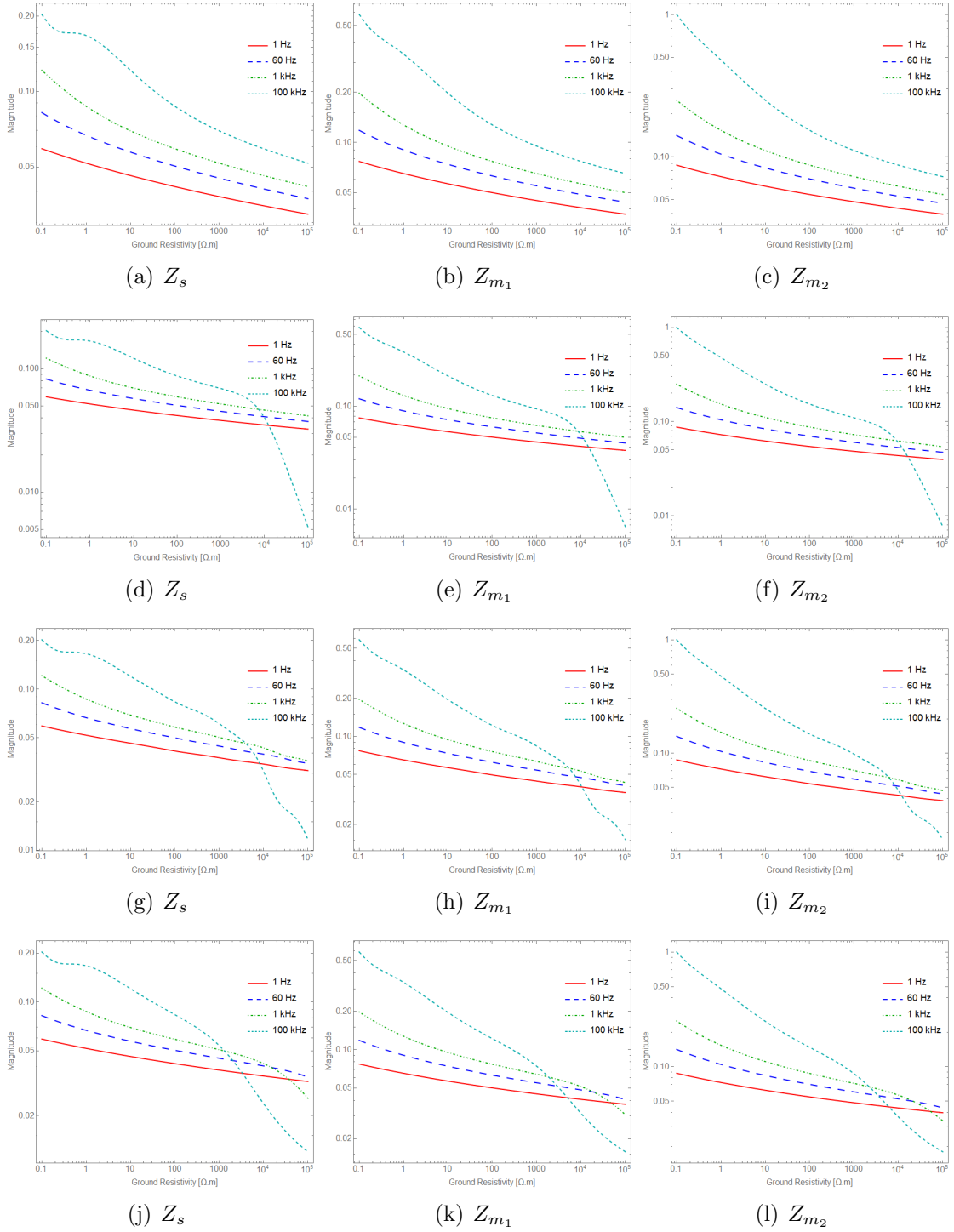


Figure C.2: Sensitivities of series impedance for flat horizontal configuration. Figures (a)–(c):  $\kappa = \sigma_0 = 1/\rho_0$ ; (d)–(f):  $\kappa = \sigma_0 + j\omega\epsilon_r\epsilon_0$ ; (g)–(i): Smith-Longmire; and (j)–(l): Alipio-Visacro.

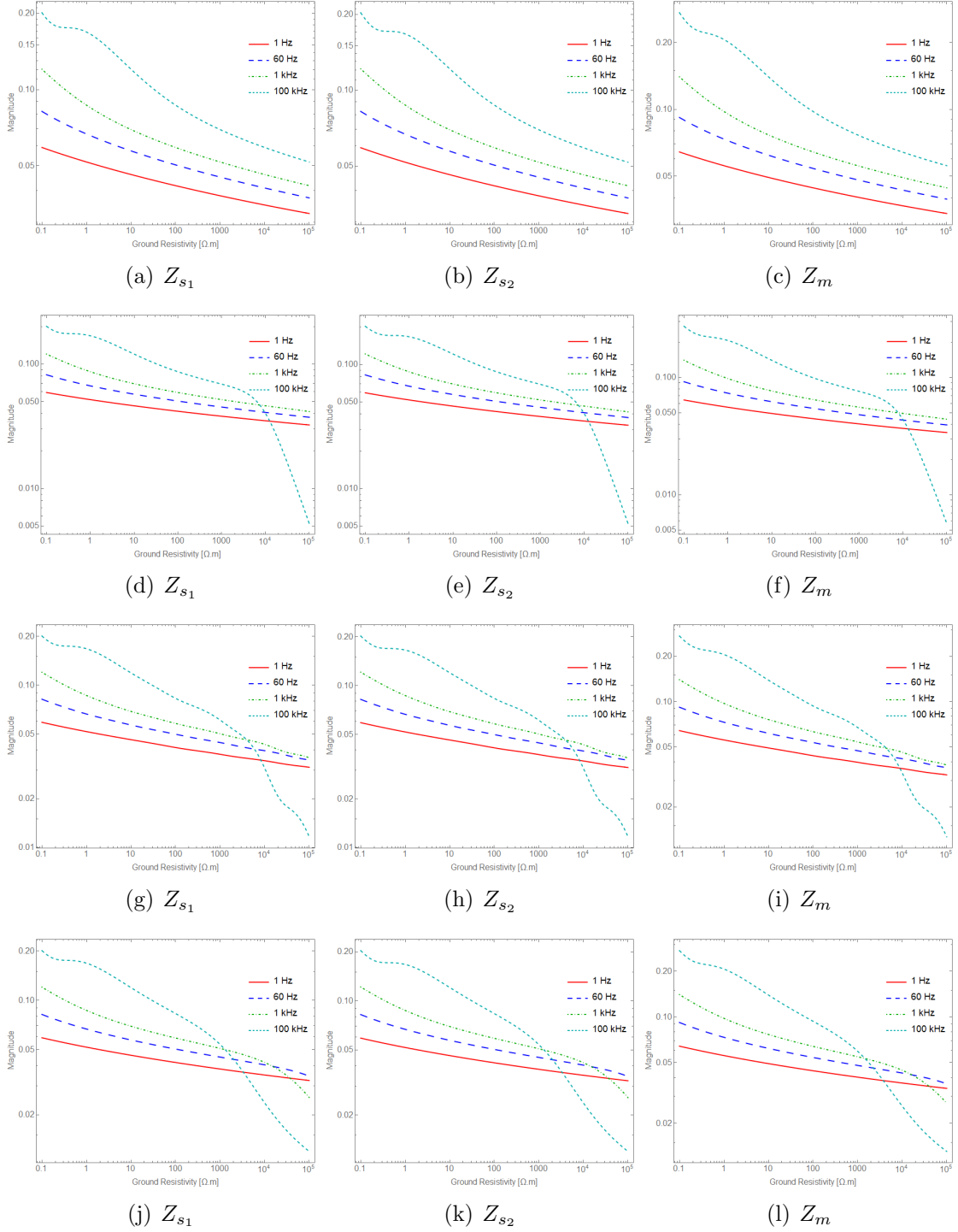


Figure C.3: Sensitivities of series impedance for trefoil configuration. Figures (a)–(c):  $\kappa = \sigma_0 = 1/\rho_0$ ; (d)–(f):  $\kappa = \sigma_0 + j\omega\epsilon_r\epsilon_0$ ; (g)–(i): Smith-Longmire; and (j)–(l): Alipio-Visacro.

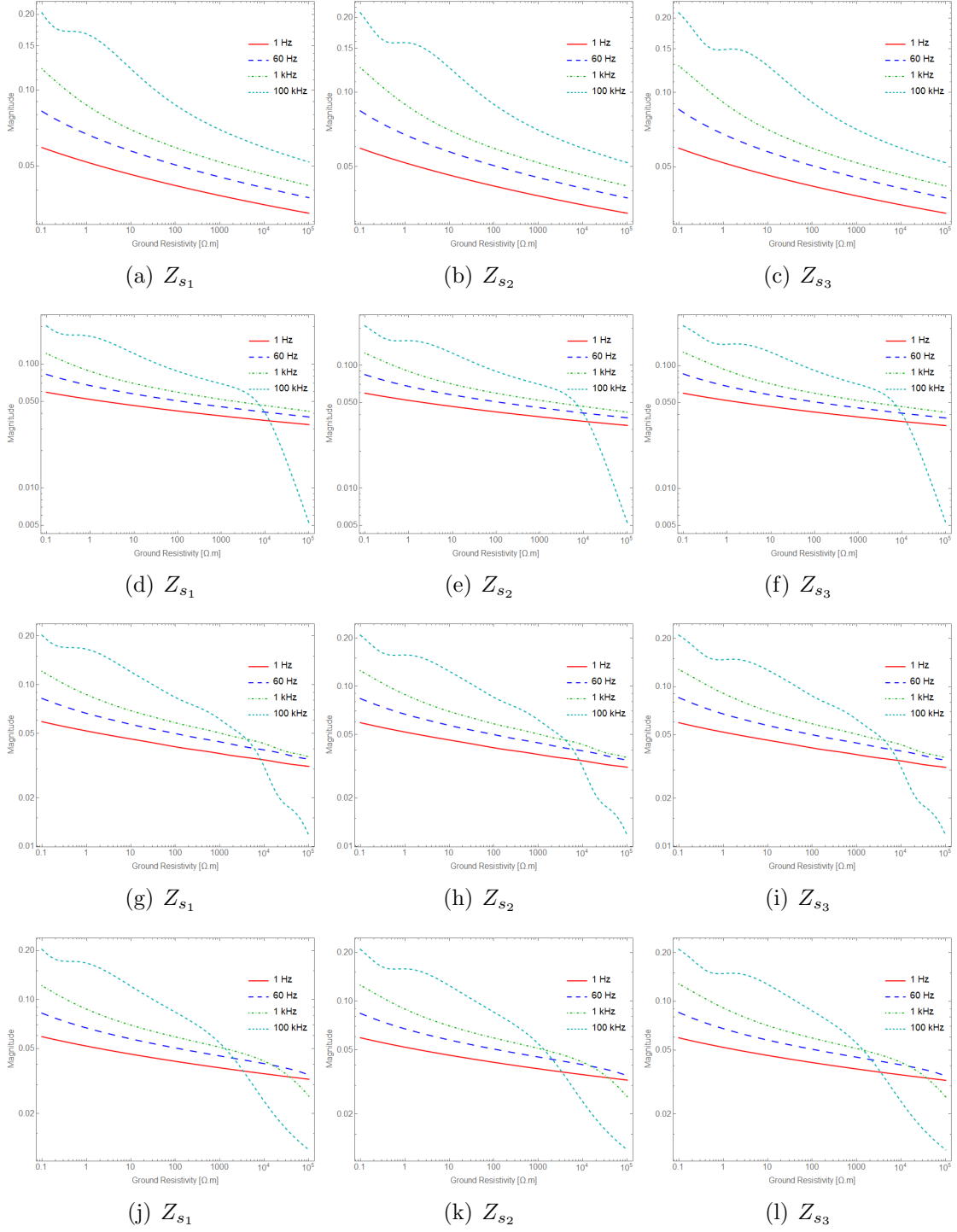


Figure C.4: Sensitivities of series self impedance for flat vertical configuration. Figures (a)–(c):  $\kappa = \sigma_0 = 1/\rho_0$ ; (d)–(f):  $\kappa = \sigma_0 + j\omega\epsilon_r\epsilon_0$ ; (g)–(i): Smith-Longmire; and (j)–(l): Alipio-Visacro.

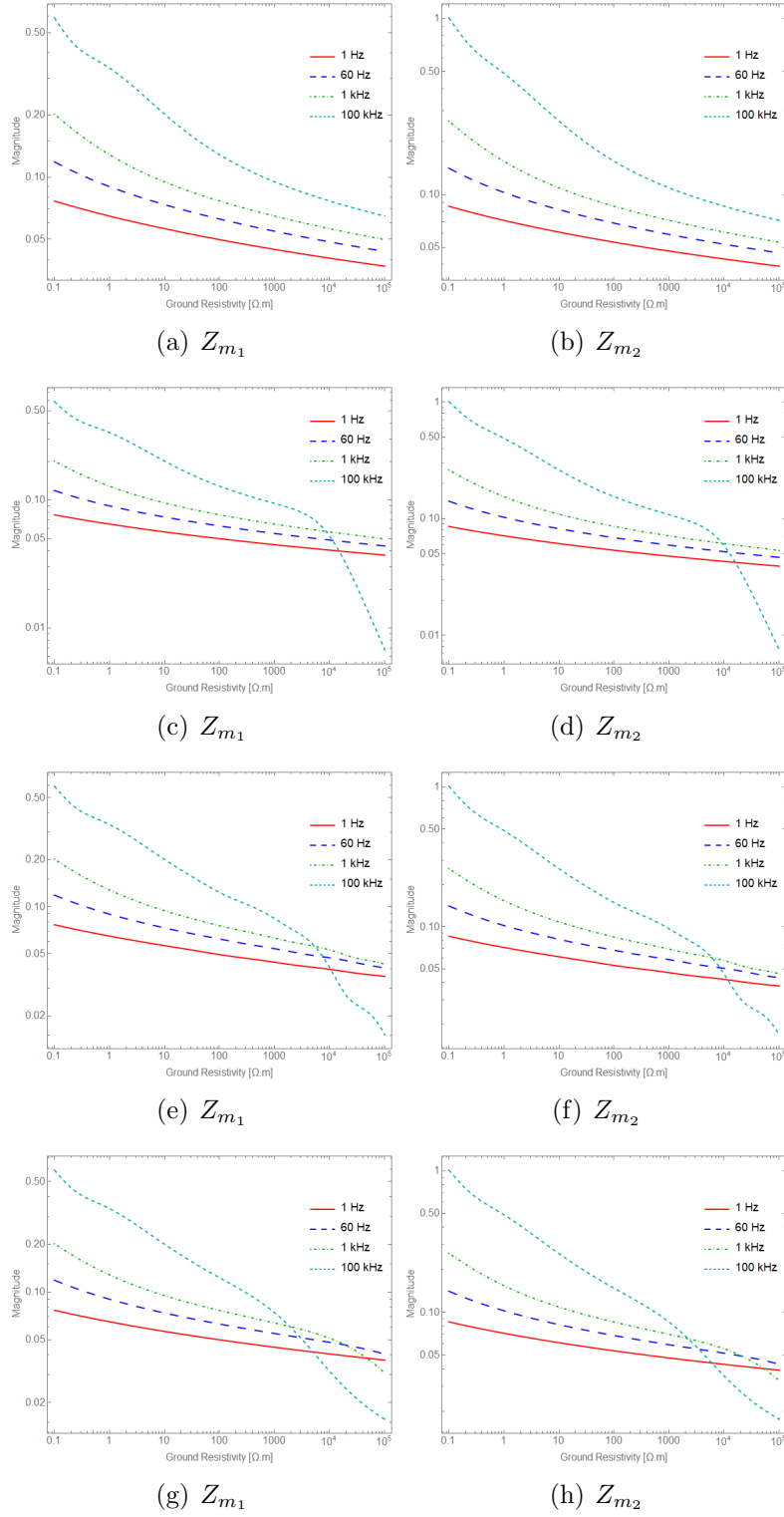


Figure C.5: Sensitivities of series mutual impedance for flat vertical configuration. Figures (a) and (b):  $\kappa = \sigma_0 = 1/\rho_0$ ; (c) and (d):  $\kappa = \sigma_0 + j\omega\epsilon_r\epsilon_0$ ; (e) and (f): Smith-Longmire; and (g) and (h): Alipio-Visacro.

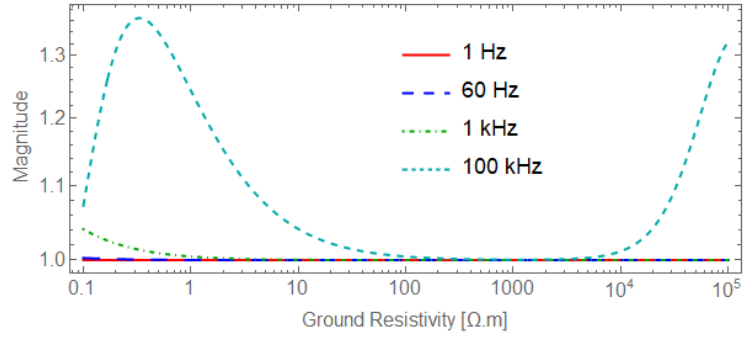
# Appendix D

## Additional Graphics: Sensitivity of Ground Return Shunt Impedance

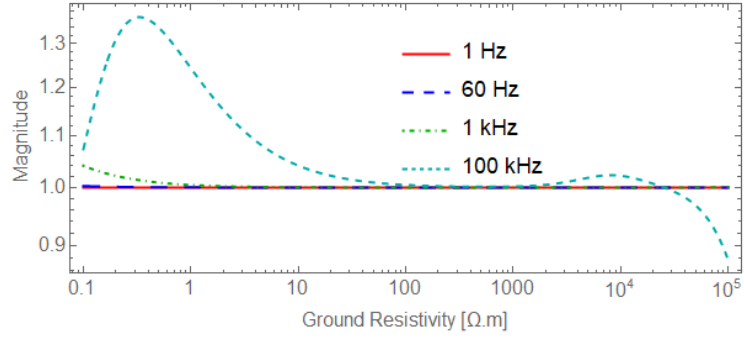
This appendix complements the results of the sensitivity analysis of ground return shunt impedances addressed in Section ???. Here they are presented with fixed frequencies – 1 Hz, 60 Hz, 1 kHz and 100 kHz – for a soil resistivity variation from  $0.1 \Omega\cdot\text{m}$  to  $100 \text{ k}\Omega\cdot\text{m}$ , as organized in Tables D.1.

Table D.1: Results for sensitivity analysis plotted against ground resistivity.

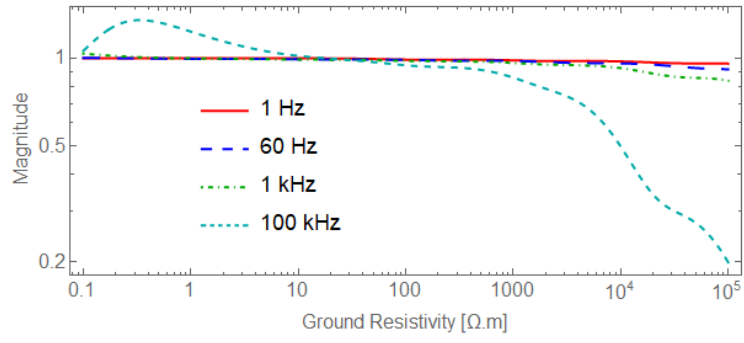
| $S_Z$ | Cases    |            |          |                       |
|-------|----------|------------|----------|-----------------------|
|       | Pipe     | Horizontal | Trefoil  | Vertical              |
|       | Fig. D.1 | Fig. D.2   | Fig. D.3 | Fig. D.4 and Fig. D.5 |



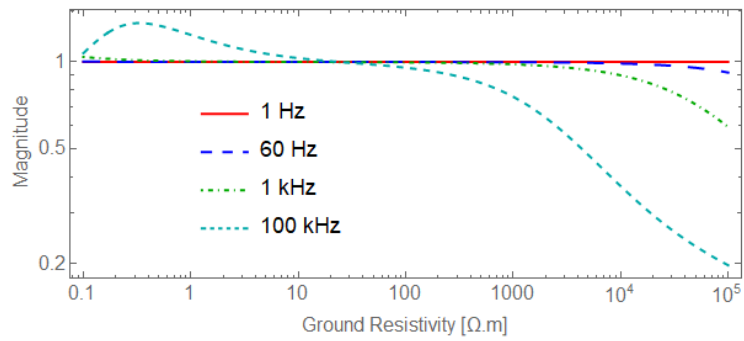
(a)  $\kappa = \sigma_0 = 1/\rho_0$



(b)  $\kappa = \sigma_0 + j\omega\epsilon_r\epsilon_0$



(c) Smith-Longmire



(d) Alipio-Visacro

Figure D.1: Sensitivities of shunt impedance for pipe-type cable configuration. Figures (a):  $\kappa = \sigma_0 = 1/\rho_0$ ; (b):  $\kappa = \sigma_0 + j\omega\epsilon_r\epsilon_0$ ; (c): Smith-Longmire; and (d): Alipio-Visacro.

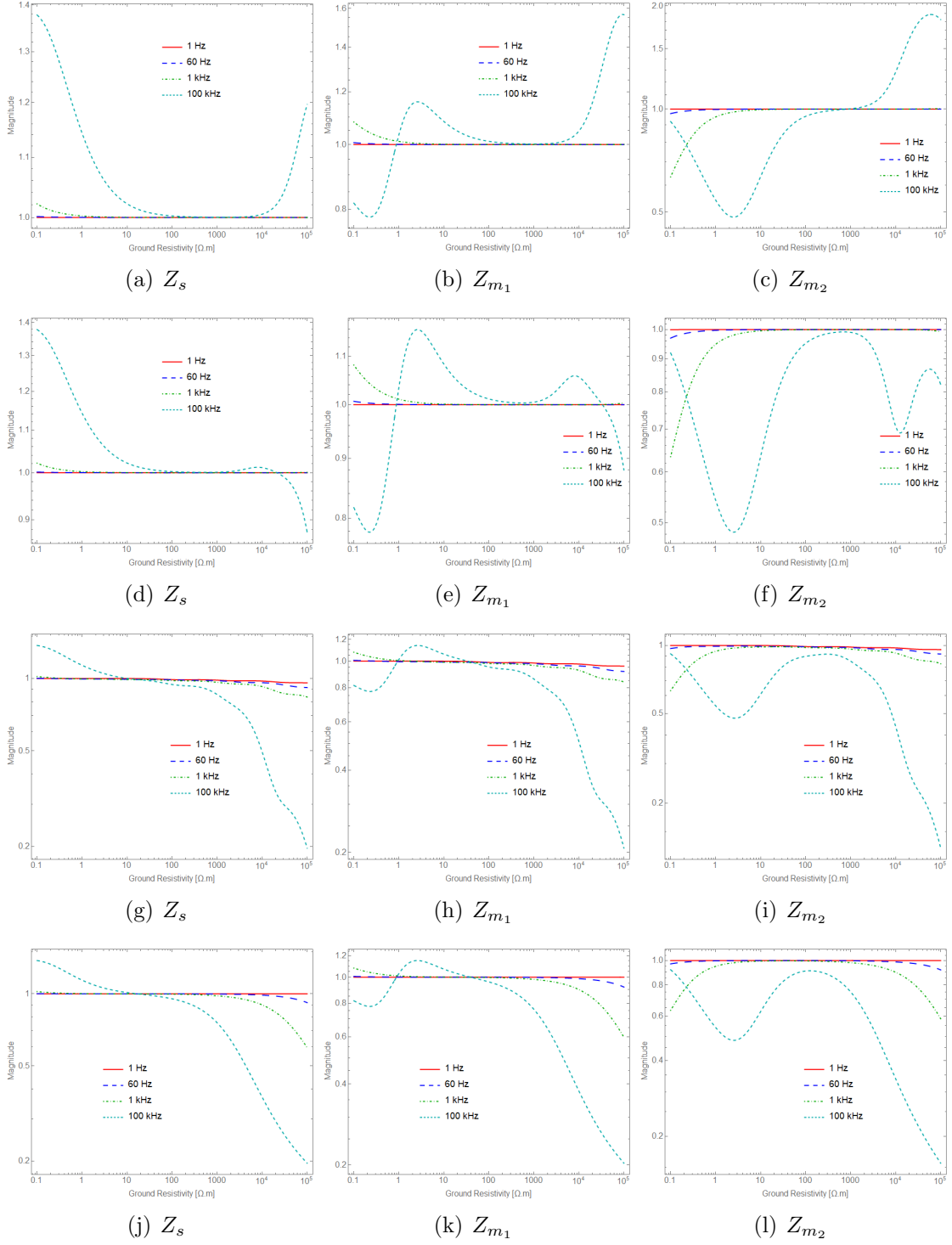


Figure D.2: Sensitivities of shunt impedance for flat horizontal configuration. Figures (a)–(c):  $\kappa = \sigma_0 = 1/\rho_0$ ; (d)–(f):  $\kappa = \sigma_0 + j\omega\epsilon_r\epsilon_0$ ; (g)–(i): Smith-Longmire; and (j)–(l): Alipio-Visacro.

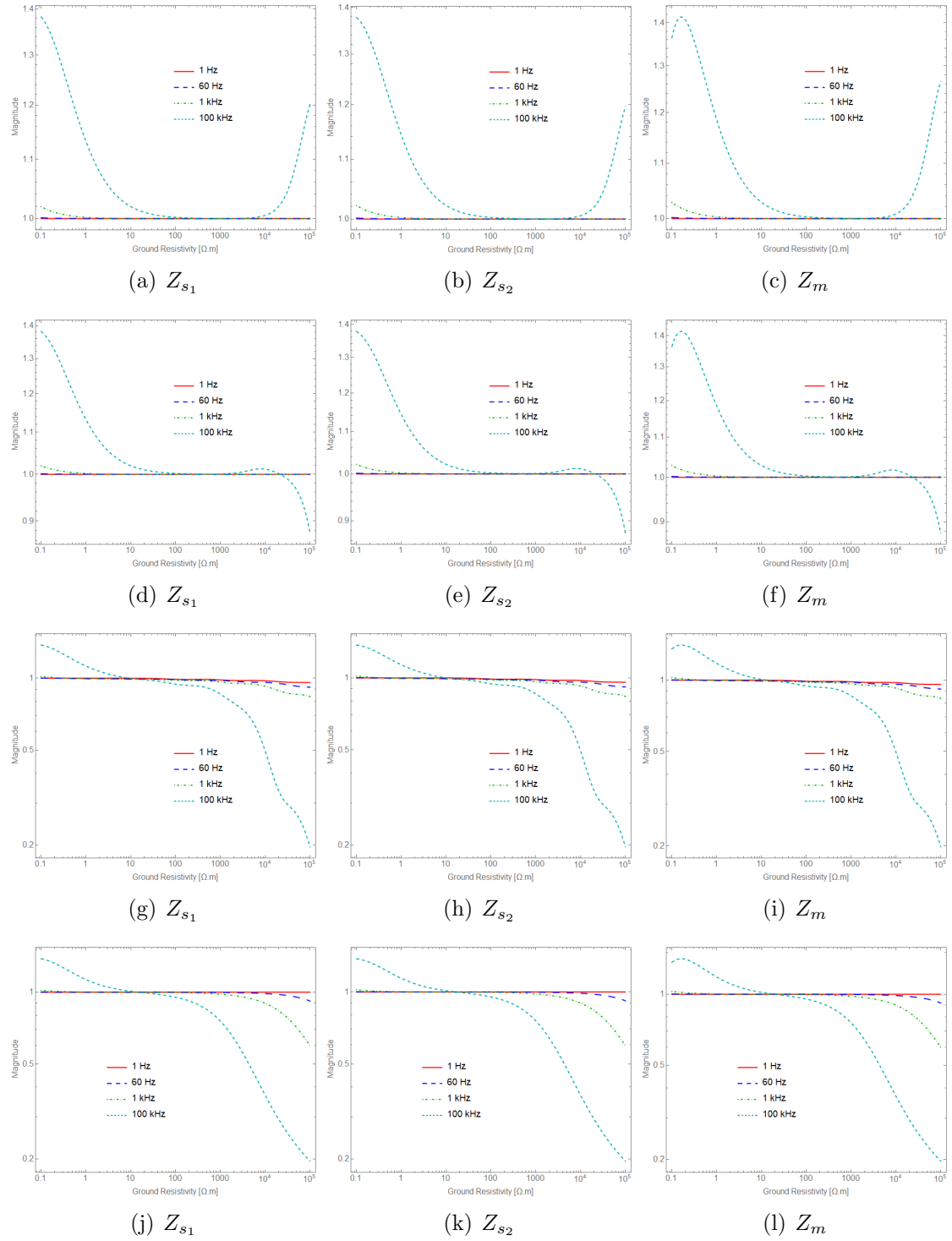


Figure D.3: Sensitivities of shunt impedance for trefoil configuration. Figures (a)–(c):  $\kappa = \sigma_0 = 1/\rho_0$ ; (d)–(f):  $\kappa = \sigma_0 + j\omega\epsilon_r\epsilon_0$ ; (g)–(i): Smith-Longmire; and (j)–(l): Alipio-Visacro.

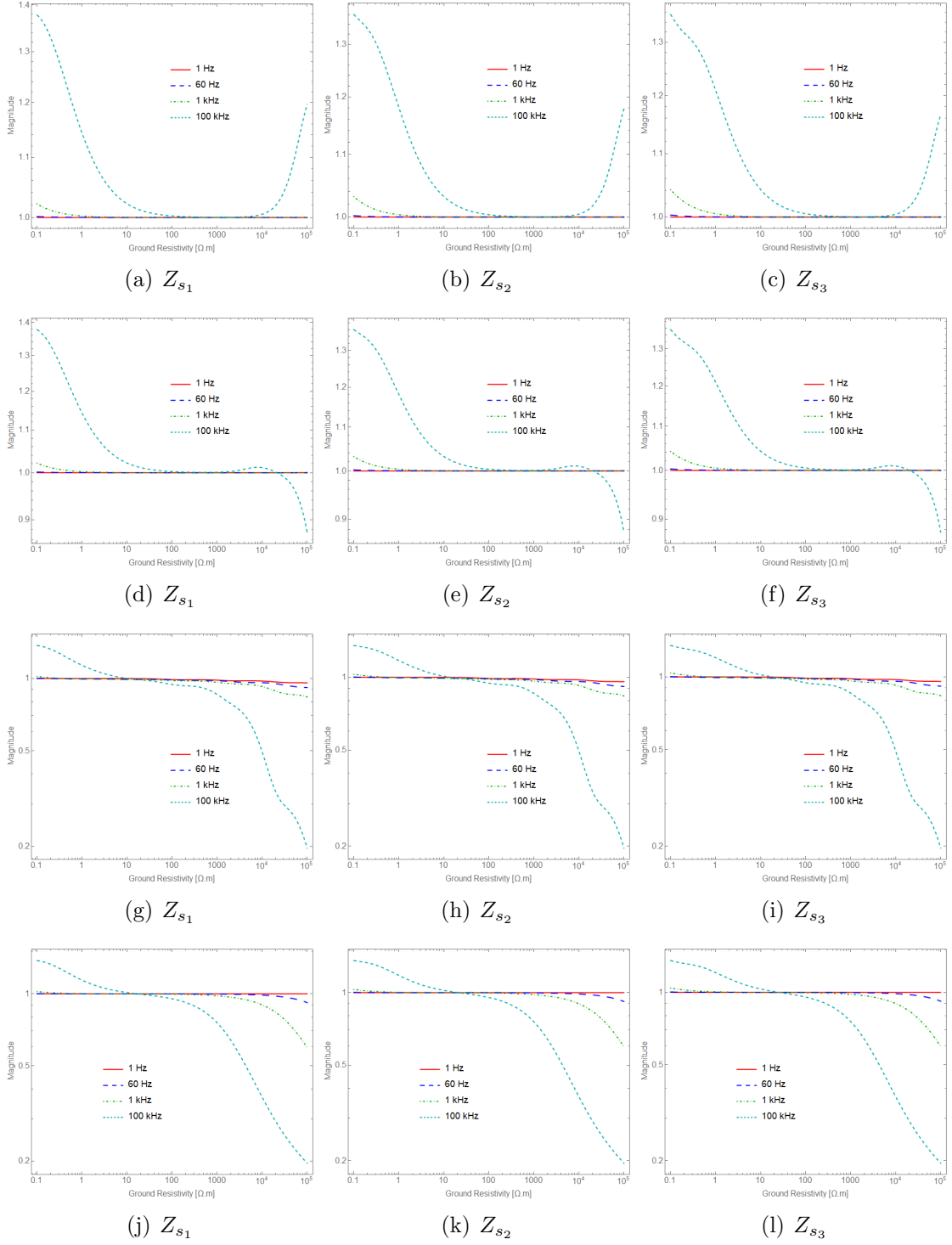


Figure D.4: Sensitivities of shunt self impedance for flat vertical configuration. Figures (a)–(c):  $\kappa = \sigma_0 = 1/\rho_0$ ; (d)–(f):  $\kappa = \sigma_0 + j\omega\epsilon_r\epsilon_0$ ; (g)–(i): Smith-Longmire; and (j)–(l): Alipio-Visacro.

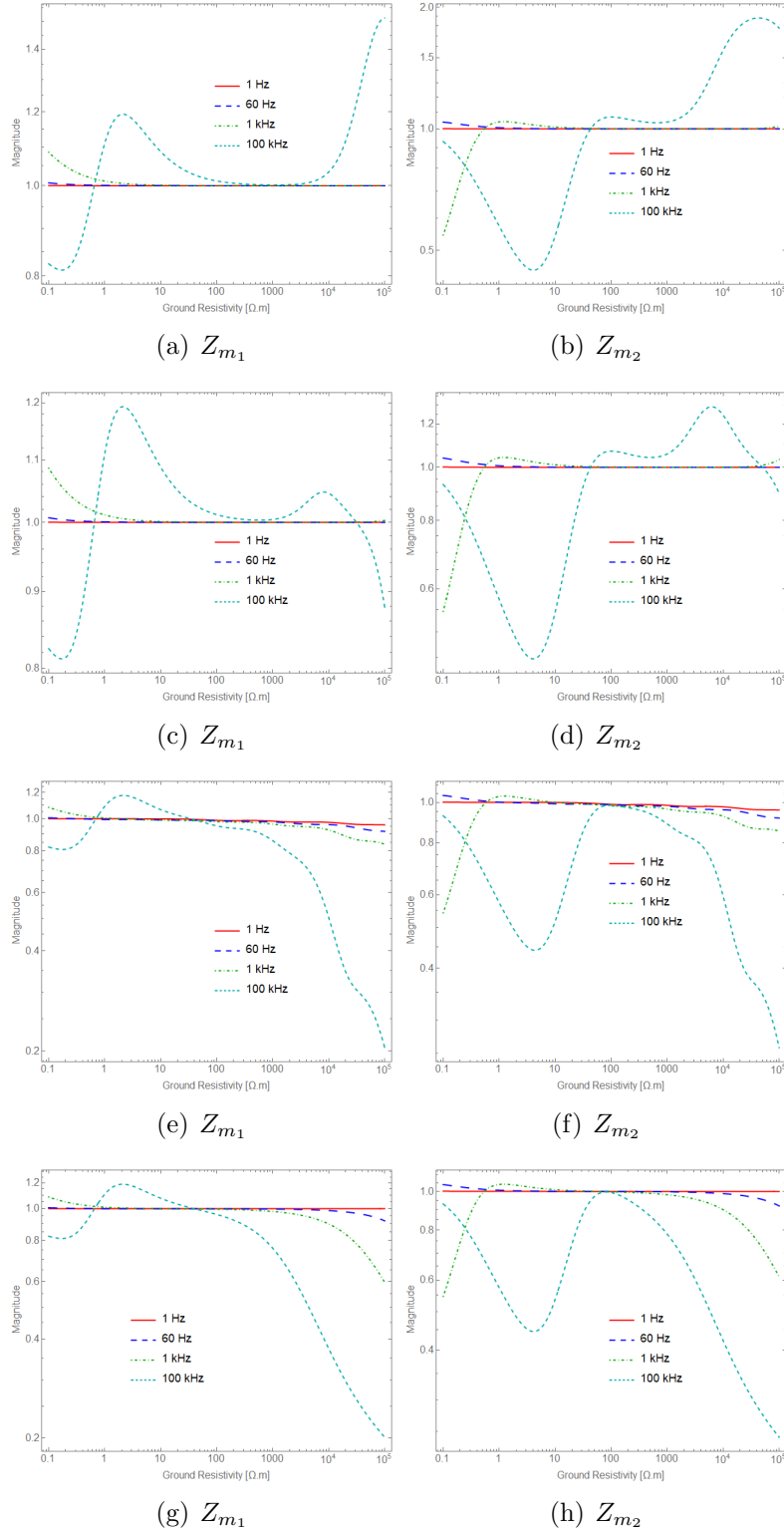


Figure D.5: Sensitivities of shunt mutual impedance for flat vertical configuration. Figures (a) and (b):  $\kappa = \sigma_0 = 1/\rho_0$ ; (c) and (d):  $\kappa = \sigma_0 + j\omega\epsilon_r\epsilon_0$ ; (e) and (f): Smith-Longmire; and (g) and (h): Alipio-Visacro.